A GUIDE TO MAKING CLIMATE QUALITY METEOROLOGICAL AND FLUX MEASUREMENTS AT SEA

Frank Bradley
CSIRO Land and Water, PO Box 1666, Canberra 2601, Australia

Chris Fairall
NOAA/PSD, 325 Broadway, Boulder, CO 30305, USA

DRAFT
May 31, 2006

A GUIDE TO MAKING CLIMATE QUALITY METEOROLOGICAL AND FLUX MEASUREMENTS AT SEA

BACKGROUND

The importance of accurate fluxes of heat and momentum in the coupled ocean-atmosphere system has been acknowledged since the mid-1980s. Arbitrary adjustment to the air-sea fluxes when coupling ocean and atmospheric models was common practice as a means of keeping sea surface temperatures within realistic bounds. In response to this demonstrated sensitivity of coupled air-sea models to small changes in values of air-sea fluxes, the World Ocean Circulation Experiment (WOCE) observing program (WCRP 1989) and process studies such as the Tropical Ocean Global Atmosphere – Coupled Ocean-Atmosphere Response Experiment (TOGA-COARE) (Webster and Lukas 1992) set accuracy goals for the measurement of net heat exchange across the ocean-atmosphere interface of $\pm 10 Wm^{-2}$ over short to medium timescales. However, the comparison of observations from several research ships during TOGA-COARE revealed that raw measurements fell short of this goal. In the subsequent analysis, the reasons for these disagreements were examined and identified, and in most cases corrections could be made.

Problems were traced to interference of the measurement by the ship including: poor location of sensors; inadequate knowledge of how an instrument designed for use over land performed on an unstable platform and in the marine environment; and inappropriate calibration procedures. Overall, it became apparent that, if the requirements of climate research were to be met, more care must be taken to ensure the accuracy of measurement of basic meteorological variables used for the calculation of turbulent and radiative air-sea fluxes (Weller et al. 2004). Such careful observations may be referred to as of "climate-quality".

Following the publication of its report on the status of air-sea flux datasets and observational methods (WCRP 2000), the WCRP/SCOR Air-Sea Fluxes Working Group convened an international workshop to discuss its findings, and to consider the implications for future air-sea flux measurement for climate research generally, and for validation of satellite observations and initialization of models (WCRP 2001). The Workshop noted that "the techniques to obtain high quality data for flux estimation at sea are very demanding" and recommended "the assembly of a Technical Manual on air-sea flux measurement methods".

In March 2003, Florida State University hosted the 1st High-Resolution Marine Meteorology (HRMM) workshop, under the auspices of NOAA/OGP Ocean Observing Initiative. The quality of basic measurements needed to ensure accurate air-sea fluxes was discussed, as was the fact that valuable data could be obtained when research ships operate in rarely visited regions. Often these ships have the necessary sensors on board, and technicians capable of maintaining them, but no mechanism or protocol exists to ensure that flux-relevant data are collected even when meteorological conditions are not important for the objectives of that particular cruise.

To improve this situation and ensure good data return from as many ships as possible, the first step is to make those who would be involved aware of the difficulties in collecting high-quality meteorological data at sea. Recommendation 5 from the report of that meeting (COAPS 2003) was to "Produce a reference manual of best procedures and practices for the observation and documentation of meteorological parameters, including radiative and turbulent fluxes, in the marine environment. The manual will be maintained online and will be a resource for marine weather system standards."

This manual is intended for a wide readership. Primarily it is a guide for scientists and technicians who are responsible for installing and/or maintaining meteorological equipment on board ships, whether research vessels specifically engaged in air-sea studies, ships able to provide relevant data of opportunity, or commercial vessels recruited as part of the Voluntary Observing Ship network (the same general principles apply to meteorological sensors installed on surface buoys). It is also intended to provide background for PI's on oceanographic research cruises who need air-sea flux information from the research vessel as auxiliary data for their study. A quick perusal of this document should allow the PI to ask the right questions about the particular measurements for the cruise. Importantly, this manual should also serve as background material for students interested in ship-based meteorological and air-sea flux measurements.

The second workshop of the HRMM in April 2004 (COAPS 2004) decided that equipment existing or subsequently installed on ships and maintained according to these principles be identified as part of the Shipboard Automated Meteorological and Oceanographic System (SAMOS) Initiative, which will collect and distribute climate-quality data via an assigned Data Acquisition Centre (DAC) and ensure the data are archived at appropriate world data centers. This handbook will be a guide to SAMOS and similar projects. In prescribing costly equipment and calibration standards, and exacting installation procedures, we also presume that technical attention is available each day for the associated routine maintenance, monitoring and data archiving tasks. Reasonable time must also be committed to trouble-shooting in event of instrument failure.

The organisation of the manual is as follows. We first provide a Summary of the most critical information and procedures, intended as a "stand-alone" practical reference. The main body of the handbook describes the nature of the environmental variables which need to be measured, and why this is so much more exacting at sea than over land. It deals with the practical issues of coping with these difficulties on board a ship or mooring, to ensure the data are as reliable as possible. We also refer to procedures such as calibration before and after the deployment, and comparison with other instruments, which help ensure the quality of the data. Emphasis is also given to the critical importance of documentation, particularly of the location and state of the measuring instruments (nowadays easily captured with digital photos), and notes of any occurrence, e.g. roosting birds, which may impair data quality.

There are several specialized Appendices; physical formulae, constants and conversion factors used in the analysis of atmospheric data and the calculation of air-sea fluxes (which you can never find when you need them); a description of the TOGA-COARE bulk flux algorithm; an analysis of thermal radiative flux errors; examples of shipboard observations; a list of links to relevant web sites; and details of the SAMOS DAC with specifications for standardization of data formats, and metadata requirements.

Acknowledgments

Many colleagues contributed to this handbook with careful reviews and writings. We are indebted to Liz Kent, Bob Weller, Ed Andreas, Peter Taylor, Shawn Smith, Ben Moat, Mark Bourassa, Mike Reynolds, Eric Schulz, Will Drennan, and Steven Hartz.

This work was supported by the NOAA Office of Climate Observation. Frank Bradley thanks the CSIRO Division of Land and Water for continuing support by way of a post-retirement Fellowship.

QUICK REFERENCE

The body of this handbook describes in detail the factors to be considered in equipping a vessel to obtain climate-quality meteorological and flux data. It discusses the nature of the basic quantities to be measured, the relevant instruments, and special considerations because the measuring site is a ship at sea. This Summary is a practical reference for the benefit of the scientist or technician assigned the task of installing and maintaining a package of instruments on a ship, without needing too much detail or rationale. It follows roughly the order of the various procedures involved.

S1. Instruments and Calibration

The meteorological measurements required for determination of air-sea fluxes comprise:

- Wind speed
- Wind direction
- Air temperature
- Air humidity
- Atmospheric pressure
- Downward shortwave radiation
- Downward longwave radiation
- Rainfall
- Sea surface temperature (not strictly meteorology, but a vital measurement)

Table 1 lists the required accuracy for each of these quantities; the suite of instruments provided should have been assembled to meet these specifications. Whether or not the accuracy is achieved will depend on installation and maintenance. In general, there will be more than one sensor of each type available. If possible, two sets of instruments should be deployed to ensure good exposure for any ship-relative wind or sun direction. At least one spare instrument of each type should be set aside as replacement should its operational counterpart fail. Spare instruments may be stored on the vessel if the operator feels that replacements at sea are feasible.

Each instrument comes with a calibration from a certified facility to which it should be returned for re-calibration as necessary, and at least once a year. It is important to record the **calibration** and **deployment** history of each sensor, so that the correct calibration can be applied should instruments be exchanged or replaced. This metadata (see section 9) is critical when the raw data is re-analysed during post-processing.

The data record will also include input from the ship's navigation system:

a) Latitude and longitude from GPS
b) The ship's true heading, and the ship's course and speed over the ground, and speed through the water. these are required to convert relative wind speed and direction to true values.
c) Although the instrument package to be installed may include a separate sea temperature measurement, if a built-in ship thermo-salinograph exists, its data should be recorded.
d) Likewise, if the ship's bridge meteorological measurements are available on the vessel's computer network, they should be recorded, and their location included in the metadata.
e) A copy of the bridge event log; this is particularly useful when investigating anomalous data, revealing if the ship was hove to (e.g. for a CTD) or maneuvering and creating flow distortion, stack exhaust problems etc.

Table 1: Accuracy, precision and random error targets for SAMOS. Accuracy estimates are currently based on time scales for climate studies (i.e., ±10 W/m^2 for Q_{net} on monthly to seasonal timescales). If this target accuracy is apportioned equally between radiative and turbulent fluxes, a caveat applies to the latter. Biases in calculated surface turbulent heat fluxes, due to biases in temperature and wind speed measurements, are likely to exceed the $5Wm^{-2}$ limit if the actual values of (SST – air temperature) > 3°C or wind speed $>15ms^{-1}$.

Parameter	Accuracy of Mean (bias)	Data Precision	Random Error (uncertainty)
Latitude and Longitude	0.001°	0.001°	
Heading	2°	0.1°	
Course over ground	2°	0.1°	
Speed over ground	Larger of 2% or 0.2 m/s	0.1 m/s	Greater of 10% or 0.5 m/s
Speed over water	Larger of 2% or 0.2 m/s	0.1 m/s	Greater of 10% or 0.5 m/s
Wind direction	3°	1°	
Wind speed	Larger of 2% or 0.2 m/s	0.1 m/s	Greater of 10% or 0.5 m/s
Atmospheric Pressure	0.1 hPa (mb)	0.01 hPa (mb)	
Air Temperature	0.2 °C	0.05 °C	
Dewpoint Temperature	0.2 °C	0.1 °C	
Wet-bulb Temperature	0.2 °C	0.1 °C	
Relative Humidity	2%	0.5 %	
Specific Humidity	0.3 g/kg	0.1 g/kg	
Precipitation	~0.4 mm/day	0.25 mm	
Radiation (SW in, LW in)	5 W/m^2	1 W/m^2	
Sea Temperature	0.1 °C	0.05 °C	
Salinity	0.1 psu	0.05 psu	
Surface Current	0.1 m/s	0.05 m/s	

The accuracy guidelines given in this table are nominal values appropriate for typical marine operations. The reader should recognize that some specifications may not make sense when applied from the equator to the Arctic. For example, if the air temperature is -40 C, there is no need to measure relative humidity to 2%. Furthermore, observations acquired in extreme conditions (say, a 50-kt gale in the Labrador Sea in January) will likely not meet the 5 Wm^{-2} accuracy window. However, very strong wind and/or extremely large sea-air temperature or humidity differences are sufficiently rare that long term averages of the fluxes should fall within, or close to, the desired window.

S2. Installation (Location and exposure)

On an otherwise uniform and relatively flat ocean, the ship is an obstacle which distorts the wind flow and air temperature, and shadows radiometers and raingauges. Thoughtful location of sensors on the ship can minimize errors due to ship influence.

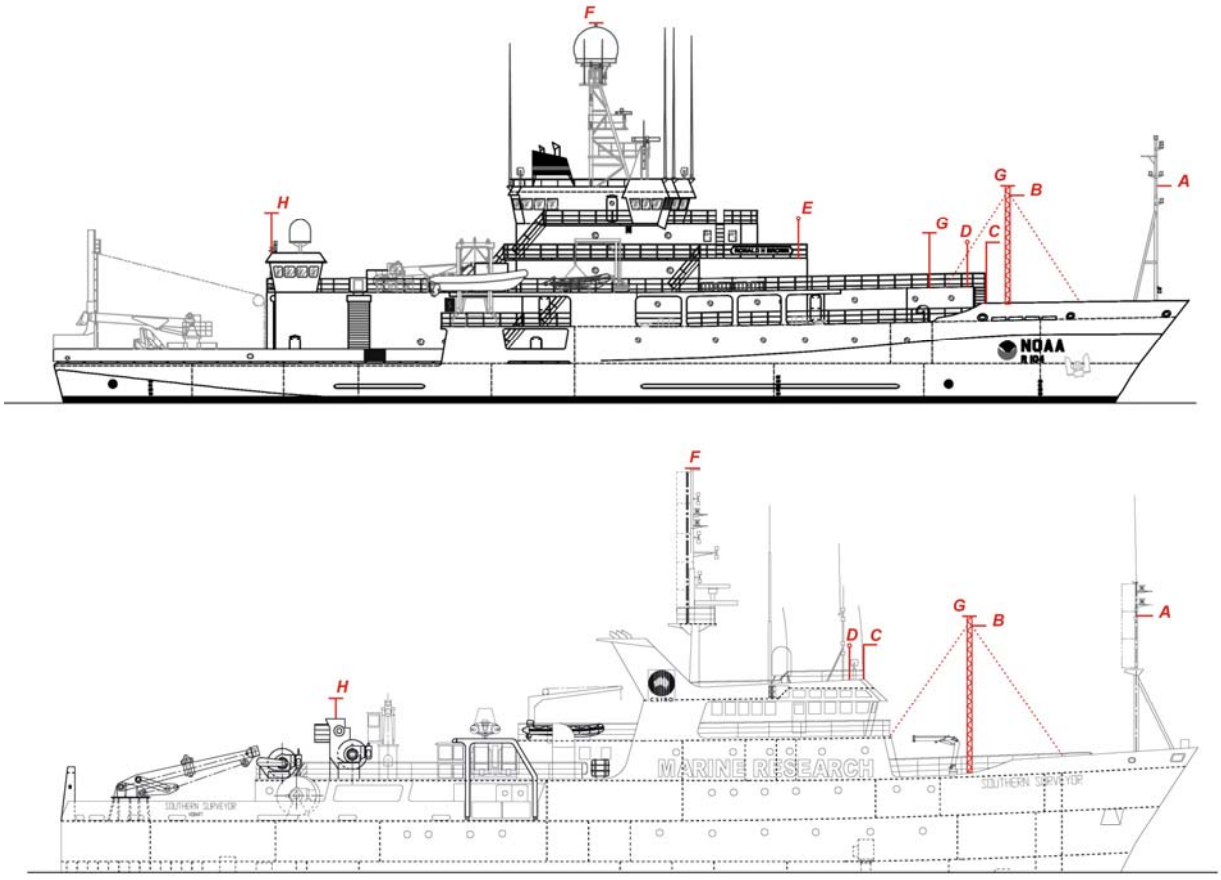

Figure S1. Examples of ships with good foremast locations for instruments: *R/V Ronald H. Brown* (NOAA) and *R/V Southern Surveyor* (CSIRO). Locations A, B, etc. are described in the text.

Ideally, sensors should be exposed to the air before it has blown across the decks and superstructure. In Figure S1, position A on a foremast is usually the best place for meteorological instruments. However, a tall enough mast may not exist or be unsuitable for regular climbing; on smaller ships such a mast may be swamped by seas over the bow. If practical and acceptable to the ship (operators, officers, technicians and crew), a guyed lattice mast could be specially installed on the foredeck for the instruments at B (See figures S1 and S2).

A final option may be a pole above the wheelhouse at C in figure S1.This position will suffer from flow distortion and some thermal contamination from the foredeck, both of which will vary with relative wind direction. On the other hand, it provides better accessibility to instruments for maintenance, should this be an important issue. Location of instruments often entails trade-offs and matters of judgment. If only one set of instruments is available, a forward

facing support arm from A, B, or C will provide the best all-round exposure to relative wind. If two sets are provided, they should be installed either side of the ship, at D or E for example, to improve exposure.

Figure S2. Guyed mast installed on foredeck for good exposure of meteorological instruments.

In principle, radiation instruments need to be mounted so that surrounding objects don't cast shadows on them. On the restricted domain of a ship, this requirement is virtually impossible to achieve. For the two ships in Figure S1 location F would serve, but such elevated sites are usually unsuitable because of prohibited access in rough weather, and proximity to RF antennae. Radiation instruments need careful leveling and regular attention to clean the domes. Compromise sites would be at G in the Figure. At low view angles errors in the measurement are less important. Long and shortwave instruments would normally be mounted as a pair on a rigid plate at the top of a pole attached, for example, to the rail around the wheelhouse roof. A gimball mount would benefit the shortwave radiometer, but would need to very carefully designed. If two sets of instruments are available, they should be widely separated to avoid coincident shadows.

For radiation instruments, but *not* those for wind speed or air temperature, a position well aft such as H may be used as a last resort, recognizing that the longwave signal may be significantly in error whenever the exhaust plume is above the pyrgeometer. More frequent washing of the domes may also be necessary to remove soot.

Barometers can be located within the bridge, a science lab, or can be mounted on a mast with other instruments. Whether inside or outside it is important to ensure that the port for the barometer is located so as to avoid dynamic pressure fluctuations due to the wind, or if inside free from a space which may be pressurised by, for example, air conditioning.

Raingauges are susceptible to wind effects which cause optical gauges to overestimate and funnel gauges to underestimate. The wind is deflected upwards when it encounters the ship, and carries raindrops away from the funnel instead of falling in. The loss can be corrected to

some extent providing the **relative** wind speed at or near the sensor is known. Thus, a location on the same mast as the anemometer is best.

If sea temperature is to be measured with a floating sensor, it should be trailed from the end of a light boom (or pole) as far forward and as far out as practicable, to try and avoid the bow wave.

Nearly all meteorological sensors, and particularly those for radiation, are susceptible to interference from the many sources of RF transmission aboard a ship. This should be borne in mind when locating the instruments, as noise in the signals can often be attributed to RF interference.

S3. Documentation and event logging

The importance of documenting the location and serial numbers of all instruments deployed, and the date and time of any changes cannot be overstated. Ideally, this should be an electronic document accompanied by digital photographs of the installation. The most useful photos are taken at sufficient distance to show the sensor in its environment, and possible obstacles to wind flow around it. A photograph from the wharf can also be helpful. This is also an opportunity to record the height of all instruments above the water, and above some ship datum (e.g. the deck below). Knowledge of instrument height is crucial for calculating bulk fluxes.

In addition, significant events which may affect the quality of the data should be recorded with the time in a daily log (e.g. cleaning radiometer domes, power failure, bird on anemometer). Information about the ship's speed, heading, position, etc. can be extracted from the link to the ship's network, but such eyewitness accounts are invaluable, particularly when trying to explain anomalous data.

S4. Monitoring and maintenance

The computer recording software should permit real-time display, in physical units, of the variables being logged. This may be as a list, a graphic display of time series, or both. This display should be monitored as part of a daily routine, and also from time to time as convenient. If paired sensors are installed, their values can be compared – if different by more than some amount (e.g. twice the specified instrumental accuracy), the reason should be sought. Whether a single or pair of sensors is installed, it is also useful to compare them daily with a hand-held standard (e.g. an Assman psychrometer or portable barometer).

It is worth checking that the ship's navigation data are being recorded properly. A graphic display will also reveal anomalies in the measurements, such as spikes, noise, unreasonable values (e.g. air temperature (T) 75ºC, relative humidity (RH) 150%!). Such information should be logged and, as time permits, investigated. The first approach is usually to replace the sensor with a spare. If that doesn't solve the problem, replace the original and troubleshoot in the usual way.

The marine environment is hard on instruments mostly designed for use over land. Regular maintenance includes washing salt from radiometer domes, replacing the Gortex filter around humidity sensors, checking that the aspirator fan on the temperature/humidity instrument is working, that the raingauge funnel is not blocked (e.g. bird droppings). An expensive factory calibration intended to be valid for a year is useless if the sensor is crusted with guano! Often, the simple application of upward facing cable ties can discourage birds from roosting on sensors.

S5. Recording and securing the data

The computer date and time will be set to GMT (UTC) and the event log should also be referenced to GMT.

The recorded data will normally consist of the raw time series at the logger sampling speed, and a conversion to physical units via the instrument calibrations and transfer functions. This processing will often involve some computation involving several signals and sensors; for example, combining the three pyrgeometer signals for downward longwave radiation; or obtaining true wind from the measured relative wind and the ship's speed, course, and heading.

In many cases (SAMOS, for example), the meteorological data collected automatically by computer on the ship will be destined for use by scientists engaged in climate research elsewhere - modelers and analysts for example. The role of the shipboard operator is to maintain the quality of the data by monitoring the performance of the sensors, and making sure that all detail (e.g. time of radiometer dome cleaning, or a faulty instrument) is noted in the daily log. She/he should be provided with training to enable recovery of the system in the event of a computer crash; since extended time series are most valuable.

The capacity of the computer hard disc will be sufficient to hold several weeks' data, which should be backed up regularly according to normal computing practice. Every few days both raw and derived data should be written onto CD or DVD together with a copy of the metadata. If possible, an electronic copy should be made of the event log (e.g. in Word) and saved with the data and metadata.

Each vessel operator should establish a protocol for long term archival of the meteorological observations with a national or international archive center. Data residing on a disk or tape in someone's desk drawer will not aid climate science and the media will degrade with time. Archive centers are equipped, in most cases, to ensure the long term viability of the data, event logs, and metadata on digital media. On a regular schedule, (at the end of each cruise, quarterly, etc.) all data and metadata should be forwarded to a national or international archive center.

FLUX MEASUREMENTS FROM SHIPS AND BUOYS

1. The air-sea fluxes

1.1 *Introduction*

The dynamic coupling between the ocean and the atmosphere depends on the transfer across the interface of energy, momentum and freshwater. It is the fluxes of these quantities which we seek to determine experimentally from global networks of ships and moorings, to provide constraints on coupled models of the climate system and for validation of similar observations from satellites. Producing these flux estimates will require measurements of traditional near-surface meteorological variables (wind speed, air temperature, humidity, water temperature) with more than sufficient accuracy to make them useful for numerous other applications.

The basic set of fluxes we consider are those of sensible and latent heat, of momentum (or wind stress), the shortwave and longwave radiative fluxes, and the freshwater flux.

1.2 *Turbulent fluxes*

Air-sea exchange of sensible heat (H_s), latent heat (H_l), and momentum (τ) occur predominantly by turbulent transport processes in the atmosphere. They are described by turbulence theory and may be obtained directly by measuring the fluctuating quantities and applying the covariance (or eddy-correlation) technique. This is a research tool, as yet unsuitable for routine use, so will not be discussed in this manual; rather, we will consider the bulk flux parameterization of the turbulent fluxes. When the situation changes the manual will be updated accordingly.

1.3 *Radiative fluxes*

Shortwave fluxes are in the wavelength band 0.3 to 3 μm. Downwelling shortwave radiation at the surface ($R_{s\downarrow}$) has a component due to the direct solar beam, and a diffuse component scattered from atmospheric constituents and reflected from clouds. Upwelling shortwave radiation ($R_{s\uparrow}$) comes from reflection at the surface and the re-emergence of radiation back-scattered from the upper ocean. In clear water shortwave radiation penetrates to a depth of several tens of meters, influencing the thermal structure of the ocean surface layer. The ratio of downwelling to upwelling shortwave is the surface albedo (α), which depends on solar elevation, cloudiness and wavelength. For use in bulk algorithms, a single value of 0.058 for *broadband* albedo, based on the ratio of daily averaged upwelling and downwelling shortwave flux, has been found to be satisfactory.

Longwave fluxes range from 3 to around 50 μm wavelength. Downwelling longwave radiation ($R_{l\downarrow}$) originates from the emission by atmospheric gases (mainly water vapour, carbon dioxide and ozone), aerosols and cloud droplets. It is thus linked quite closely to the particular regional climate conditions. Upwelling longwave from the sea surface $R_{l\uparrow}$ depends on the ocean skin temperature and surface emissivity (ε), with a small contribution due to reflection of the downwelling component. Emissivity is wavelength-dependant, and a spectrally integrated value of 0.97 is commonly used. Longwave absorption and emission take place in about the top 0.5 mm of water.

1.4 *Freshwater flux*

The vertical density structure of the ocean surface layer determines its stability and mixing, which in turn has consequences for the transport of heat to and from the interface. Density is a function of both temperature and salinity, so that the freshwater exchange through evaporation (E) or precipitation (P) is an important component of the coupled system.

1.5 *Net surface fluxes*

The fluxes described above are illustrated in Figure 1.1. They are measured individually, and required separately to study various atmospheric processes. The *net* surface heat and freshwater fluxes are important quantities which prescribe the evolution of the coupled ocean/atmosphere system for use in climate models. The net heat flux **into** the ocean surface is given by,

$$H_{net} = -(H_s+H_l) + (R_{s\downarrow} - R_{s\uparrow}) + (R_{l\downarrow} - R_{l\uparrow}) - H_{rain} \qquad (1.1)\ ,$$

where the second and third terms on the right are the net shortwave and longwave radiative fluxes, and the fourth term is the small heat contribution from rainfall (see section 2.8). H_{net} is the quantity for which the WOCE and TOGA-COARE accuracy goals of $\pm 10 \mathrm{Wm}^{-2}$ were proposed, on monthly to seasonal time-scales.

The net freshwater exchange (P-E) is usually expressed as mm of water in unit time. Note that E is H_l divided by the latent heat of water (see Appendix A).

2. Basic variables input to bulk flux algorithms

2.1 *Introduction*

Bulk air-sea flux algorithms are generally of the form $F_x = C_x u(\delta_s - \delta_z)$, where F_x is the vertical flux of entity x (heat, moisture, momentum), u the wind speed, δ the value of the corresponding meteorological variable (temperature, humidity, wind speed). Subscripts s and z refer to the value at the sea surface and at height z, so the quantity in parentheses is a sea-air difference of the particular variable, which depends upon the height of measurement. It is therefore common practice to refer all measurements to a "standard height" (usually 10m above the sea surface), using knowledge of the vertical profile of the particular variable. C_x is an empirical transfer coefficient for entity x, determined from direct measurement (e.g. by the covariance method) and specified at the standard height. More detailed information on this subject is given in Section 11.

Given a reliable value or functional form for C_x, the accuracy of F_x depends on the other quantities on the right hand side of the equation. In modern algorithms these will not necessarily be the values as measured; as discussed below, they may have been corrected for known error, reduced to standard height, or combined with other physical quantities. The required data set will consist of the state variables (temperature, humidity, and pressure), wind speed and direction, the radiative fluxes, and sea temperature at some specified depth.

The target net heat flux accuracy of $\pm 10\ \mathrm{Wm}^{-2}$ implies certain accuracies for the measured variables, as shown in Table 1. Recent experience has demonstrated that, even for the research-quality instruments installed on survey vessels, these accuracies are only achievable with very careful attention to instrument location and performance, calibration and post-cruise scrutiny (details and references can be found in WCRP 2000). We consider some issues with the measurement of each variable:

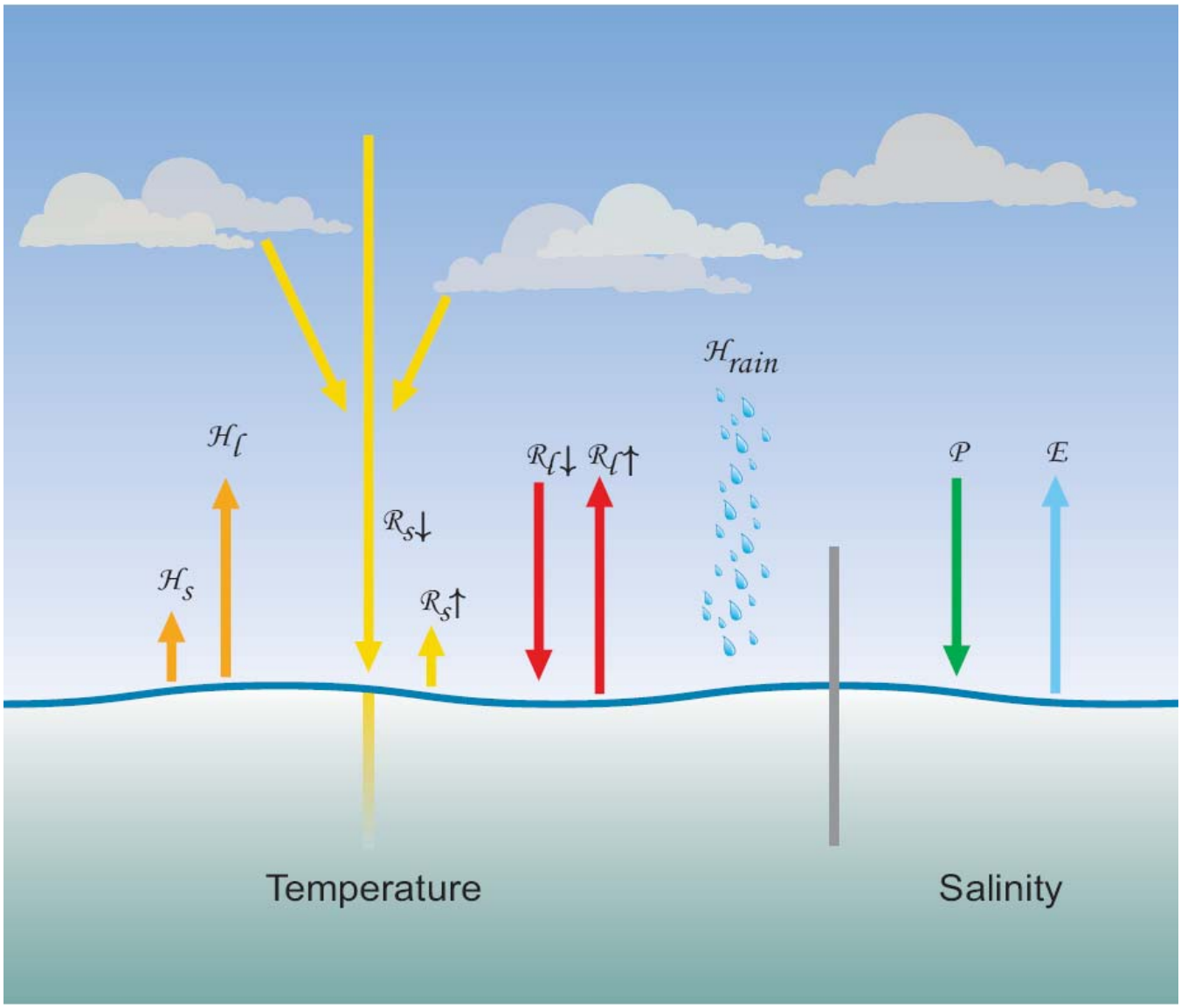

Figure 1.1. Schematic showing the net surface energy balance at the sea-air interface. H_s and H_l are the turbulent sensible and latent heat flux, R_s and R_l the shortwave and longwave radiative fluxes (upward or downward according to the arrows), H_{rain} the sensible heat contributed by rain, P precipitation and E evaporation. The gray bar separates heat and freshwater components

2.2 *Air temperature*

The most usual causes of error in air temperature measurement are sources of anomalous heating; the sun and the ship. The temperature sensor is often installed within an enclosure which shades it from the sun but which relies on natural ventilation, i.e. through slots in the sides of the enclosure, as shown in Figure 2.1(left). These may be effective in overcast conditions or strong winds; but in light winds and strong sun, the temperature in such a simple housing has been shown to rise several degrees above the true air temperature. To achieve the accuracy cited in Table 1, the sensor element must be within a specially designed, shielded and ventilated enclosure such as the one illustrated in Figure 2.1(right). Even such an arrangement is ineffective if the system is poorly located. The ship itself is a massive source of heat, and almost any

location aft of the bow will measure air which has passed over some area of warm steel. Usually the best location is high on a foremast (e.g., A in Figure S1), if one exists. Experiments which rely on continuous and accurate measurement of air temperature (and other meteorological quantities) will often duplicate instrument packages on port and starboard, taking data from the most favourably exposed instruments. Even so, the wind will sometimes be directly over the stern of the ship and the data will have to be discarded. Thus, relative wind direction is a critical part of the data record.

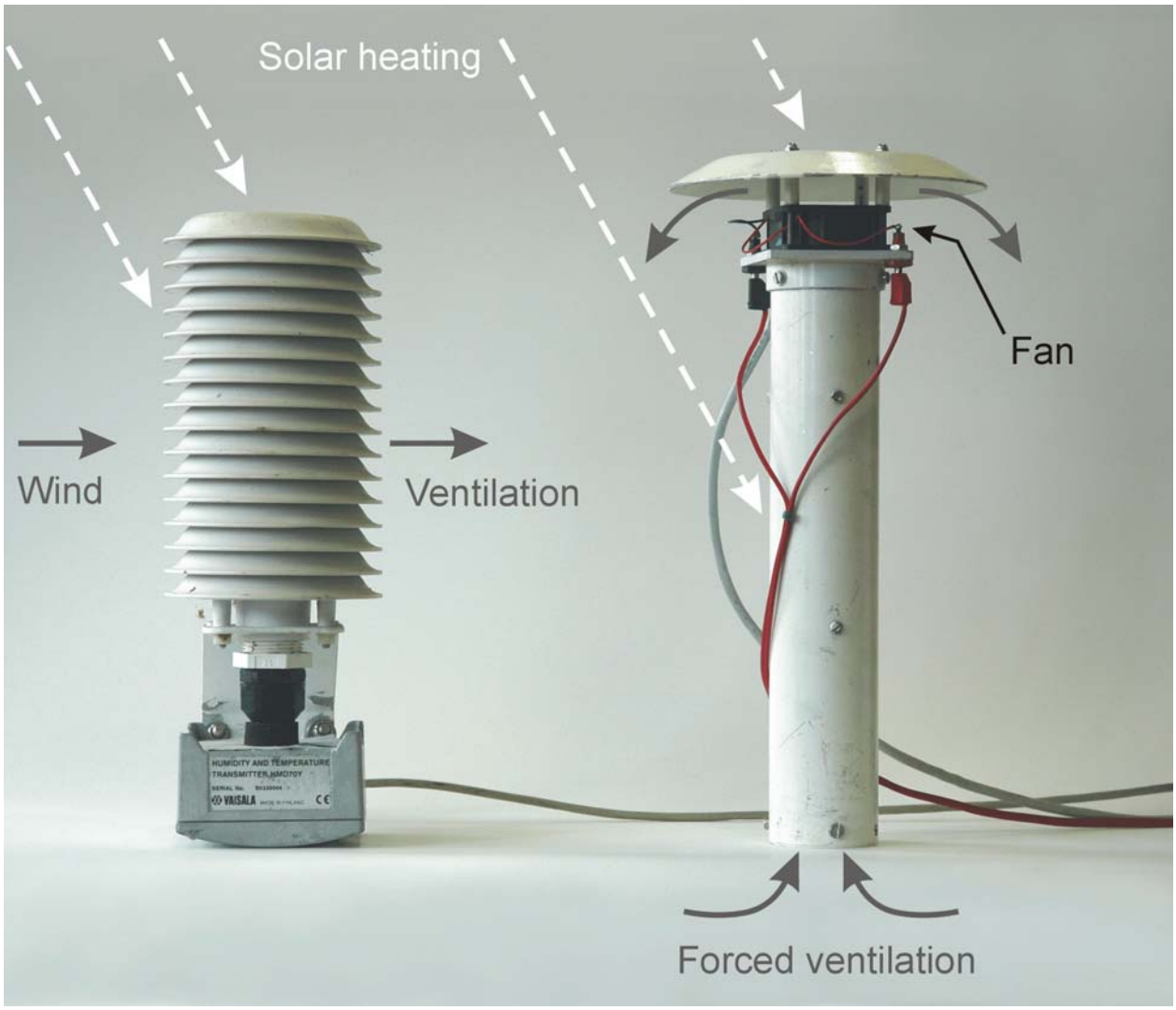

Figure 2.1 Temperature/humidity screens; left with natural ventilation; right with double screening and forced ventilation.

2.3 *Humidity*

Atmospheric humidity is variously specified by the partial pressure of water vapour (e, mbar or equivalently hPa), vapour density (ρ_v, gm^{-3}), specific humidity (q, g/g of moist air), mixing ratio (r_v, g/g) or relative humidity (RH=100e/e_s) where e_s is the saturation vapour pressure at air temperature T_a. At a particular ambient humidity, reducing air temperature reaches the point where e equals e_s. This is known as the dew-point T_d. Formulae to convert between

these various definitions of humidity are given in Appendix A, as are empirical equations for e_s as a function of T_a.

Humidity sensors in common use are described in Section 3.3. Depending on the particular measuring principle the output may be any one of the above definitions of humidity. Some sensors are more suited to use at sea than others, and most need periodic maintenance to remove salt deposited on the sensor or the filter provided to protect some sensors. Some systems combine air temperature and humidity sensors in the same package, so they are subject to the same conditions of ventilation and screening from solar heating. Conversion between some forms of humidity, for example from *RH*, requires the temperature of the air surrounding the humidity sensor. Since water vapour is a conservative quantity, the corresponding error in the water vapour measurement is less severe than an error in temperature when the latter is obtained from the co-located sensor.

2.4 *Atmospheric pressure*

Pressure is one of the state variables which define the thermodynamic properties of the atmosphere. It varies with elevation above sea level and slowly with synoptic weather changes. The WMO target accuracy for pressure measurement is ±0.1 mb. In boundary layer and climate studies, pressure most commonly appears in the calculation of dry and moist air density (needed for air-sea flux calculation), and in humidity conversions; it also appears in the psychrometer equation (see Appendix A). Under "normal" synoptic conditions (i.e. no hurricanes or severe storms) pressure at sea level lies between about 990 and 1030 mb, with a diurnal variation (the atmospheric tide) of around ±3mb in the tropics, less at higher latitudes. Relative to "standard" sea level pressure of 1013.25 mb, the above range typically represents a ±2% difference in air density or specific humidity. Pressure near the surface varies with height by roughly 0.1mb per metre, so overall it's seldom the most severe source of error in flux calculation, providing the barometer is installed in such a way as to avoid the effects of dynamic pressure. With increasing demands for accuracy in climate applications, it is wise to include the measurement of pressure and to document the actual location of the barometer.

2.5 *Wind speed and direction*

Accurate wind data are important because, as shown above, the fluxes calculated using a bulk algorithm are directly proportional to the wind speed. Thus any error in wind speed will carry through to the latent and sensible heat fluxes. For momentum flux (or wind stress), the difference term ($\delta_s - \delta_z$) represents the wind speed *relative to the surface*, so the flux is proportional to u^2. In fact, it increases rather faster than the square of the wind speed, because the exchange coefficient for momentum also increases with wind speed. Wind stress is also an important factor in determining the atmospheric stability, again affecting both scalar and momentum fluxes. The need for care in determining true ambient wind cannot be emphasized too strongly. As indicated in section 5.2, the location of the wind/direction sensors is critical to minimise errors caused by wind flow distortion around the ship.

Wind speed and direction are taken together, partly because they are often both obtained from a single instrument, but also because they are measured relative to the ship and must be combined with the ship's heading, course, and speed to arrive at the true wind vector (the correct equations with which to combine these vectors are given in Appendix A). The demands on accuracy of the ship's velocity are therefore equivalent to those of the anemometer measurement, a fact not always appreciated. It is thus necessary to record the ship's navigational data stream

together with the meteorological data, and to document whatever information is available on the accuracy of the various components. The appropriate wind speed to use in bulk flux algorithms is that relative to the ocean surface; i.e. taking account of the surface current. This introduces another source of uncertainty, because the water velocity at the interface itself is very seldom measured. There are two ways in which conversion from relative to true wind can take some account of the surface velocity: by combining the ship motion in earth coordinates (e.g. from GPS) with currents from the ship's ADCP; or by using the Döppler-log/gyro which measures the ship's motion through the water. Data reports should indicate which method has been used; both incur additional sources of instrumental error, and furthermore the measured currents are at considerable depth (of order 10m). Fortunately, in many cases current is a small fraction of the wind speed, so its contribution to the error is also small, but in light winds it can be significant.

2.6 *Sea surface temperature*

Historically, sea surface temperature was understood to be the temperature measured from a ship by whatever means available, and reported as SST irrespective of the depth of measurement. We now know that temperature in the ocean surface layer can vary with depth by an amount which is significant in the context of accurate bulk flux determination. It is the temperature of the sea-air interface itself which physically determines the magnitude of the turbulent heat fluxes and also the outward flux of longwave radiation. At the same time, these fluxes produce a cooling at the interface, the so-called "cool skin" of order 1mm thick and typically a few tenths °C.

In moderate to strong winds the water below the skin will be well mixed, and its "bulk" temperature will vary little in the vertical. During the day, however, penetration of solar radiation can produce a diurnal warm layer below the cool skin. Under clear skies and with light winds, as found in tropical oceans, this layer may be a few °C higher than in the bulk below. "Sea surface temperature" may thus vary with depth, as shown in Figure 2.2, and for the purposes of flux calculation the temperature value should always be accompanied by the depth at which it was measured (e.g. $SST_{(d)} = 18.3°_{(4.5m)}$). As indicated in section 3.6, this depth can be ambiguous. The characteristics of the ocean surface mixed layer are discussed in Price et al. (1986), and the physics of the cool skin and diurnal warm layer is given in Fairall et al. (1996a).

Traditional bulk transfer coefficients have usually been determined using a bulk sea temperature. However, newer algorithms use transfer coefficients determined with respect to the interface value. The true interface temperature cannot be measured with present technology, but the measurement of an infrared radiometer (at a few μm depth) comes close; and is sometimes available from shipboard or satellite sensors. Also, models of both the cool skin and diurnal warm layer, which enable skin temperature to be estimated from a bulk measurement at known depth, are becoming more reliable.

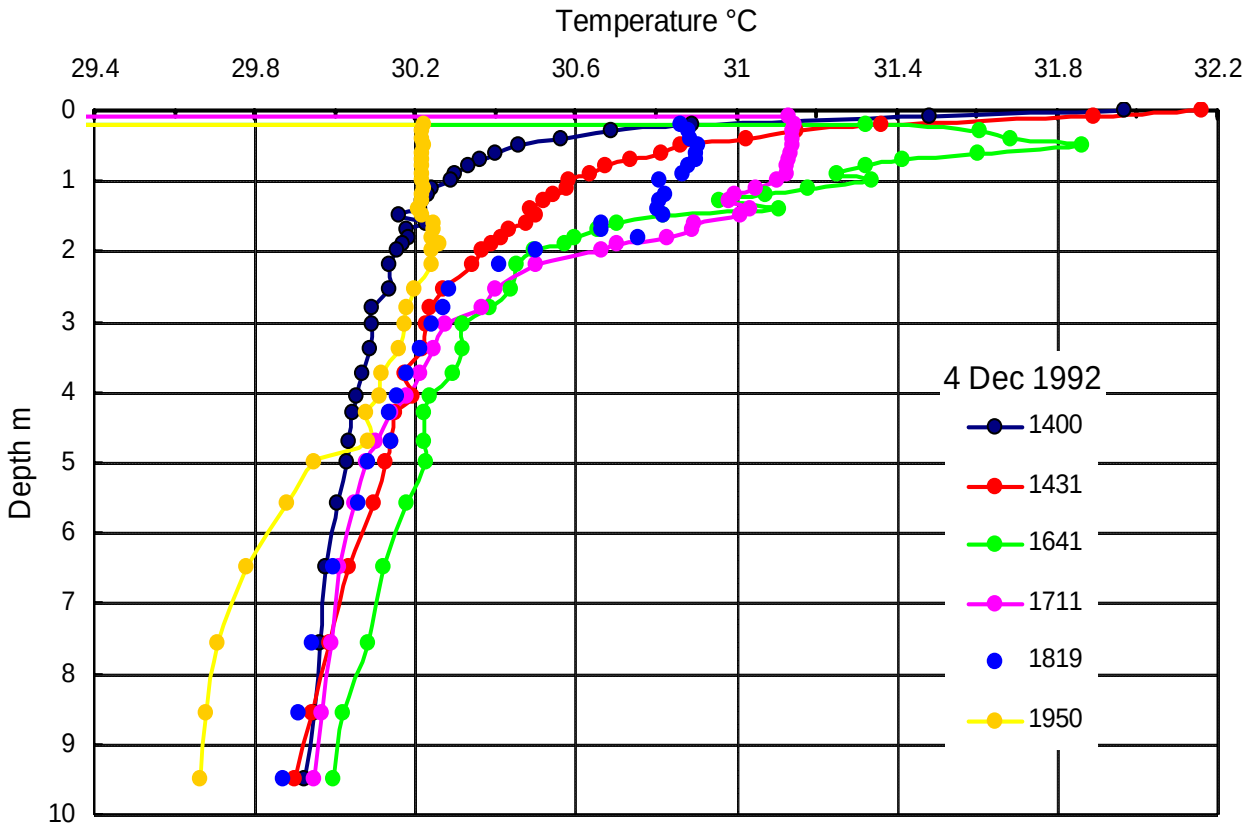

Figure 2.2 Profiles of sea water temperature measured during the TOGA COARE program with a near-surface undulating towed sensor, known as Seasoar. The different symbols denote the (local) time of the profile. The strong increase near the surface is caused by solar heating. Later in the afternoon, the surface mixing is eroding the warm layer.

The TOGA program specified an accuracy of ±0.3ºC for SST over a 2 x 2 degree region as a target for validation of space-borne radiometers (WCRP 1985). An error of 0.3ºC changes sensible and latent heat fluxes calculated with a bulk flux algorithm by 2Wm^{-2} and 10 Wm^{-2} respectively, for typical climatic conditions in the tropics. The past decade has seen the development of several high-resolution infra-red radiometers for shipboard deployment which achieve 0.1ºC accuracy.

2.7 *Radiation*

Besides direct application in equation (1.1), the net radiative fluxes ($R_{s\downarrow}$- $R_{s\uparrow}$) and ($R_{l\downarrow}$- $R_{l\uparrow}$) are also used in bulk algorithms for models of the oceanic mixed layer temperature profile and to estimate SST. For these reasons they are increasingly being measured routinely aboard ships and moorings.

On a clear day at low and middle latitudes, $R_{s\downarrow}$ is the dominant component of surface heating, peaking in the vicinity of 1000 Wm^{-2}. Thus any deterioration in performance of the measuring instrument can lead to significant error in determining the net flux, and the thermal and density structure of the ocean mixed layer. Studies of cloud-radiation interaction, currently in their infancy, will need to distinguish between the direct and diffuse components of $R_{s\downarrow}$.

Over tropical oceans $R_{l\downarrow}$ is determined largely by very high humidity in the boundary layer, with little diurnal variability or effect from clouds (typically $R_{l\downarrow}$ ~350-400 Wm^{-2}); at higher latitudes and under clear skies $R_{l\downarrow}$ is significantly lower. The warm water of the tropics can emit 450 Wm^{-2} of thermal energy, cooler waters of higher latitudes correspondingly less. ($R_{l\downarrow}$- $R_{l\uparrow}$) is therefore the difference of two fairly large quantities, and typically of order 50 Wm^{-2}.

Accurate measurement of both $R_{s\downarrow}$ and $R_{l\downarrow}$ requires an unobstructed hemispheric view of the sky, which is virtually impossible to achieve on board ship while retaining access to the instruments for maintenance. In the case of $R_{s\downarrow}$, shadowing by the highest parts of the ship, masts, funnel, antennae and the like, is the main difficulty. Instrumental problems have plagued the measurement of $R_{l\downarrow}$ for some years, partly associated with the fact that sources of thermal radiant energy are ubiquitous. These issues are dealt with in detail in Sections 3.7, 6.6, and Appendix C.

2.8 *Precipitation*

Rainfall, particularly during convective storms, is perhaps the "patchiest" of all meteorological variables. Single point measurements from ships and buoys are generally less relevant for climate models than area averaged values or spatial characteristics. Nevertheless, accurate point measurements over the ocean are invaluable for validating satellites and radar which *do* obtain spatial rainfall patterns, but must be calibrated against ground truth. Currently such validation is mostly obtained from rain-gauges located on islands and atolls, which have been found to distort the rainfall field.

The main problem in measuring rainfall from ships (and to a lesser extent from buoys) using the traditional funnel gauge is error due to wind flow distortion which can lead to under-estimation depending on the location of the gauge. The problem has been studied, using an array of gauges distributed around the ship, and correction schemes devised which can improve the accuracy of rain measurement, to within 10-15%, as shown in Figure 2.3. Operationally it is important to ensure the raingauge is well-exposed and near the location where relative wind speed and direction are recorded. A well-positioned gauge adjacent to a wind instrument is better than several gauges scattered around the ship.

The range of rainrates observed, from drizzle registering less than 1 $mmhr^{-1}$ to tropical storms producing 200mmh^{-1} (often accompanied by strong winds) also presents challenges for rain-gauge design. As shown in equation 1.1, the net air-sea heat flux includes a component of sensible heat from rainfall. It has been found that this should be calculated assuming that raindrops are 0.2ºC cooler than the wet-bulb temperature at the surface. Over extended periods the contribution is small, but during heavy storms it can be several hundred Wm^{-2} and a significant component of a daily average net flux (Figure D2). Note that the momentum flux imparted to the ocean by raindrops may also be non-negligible.

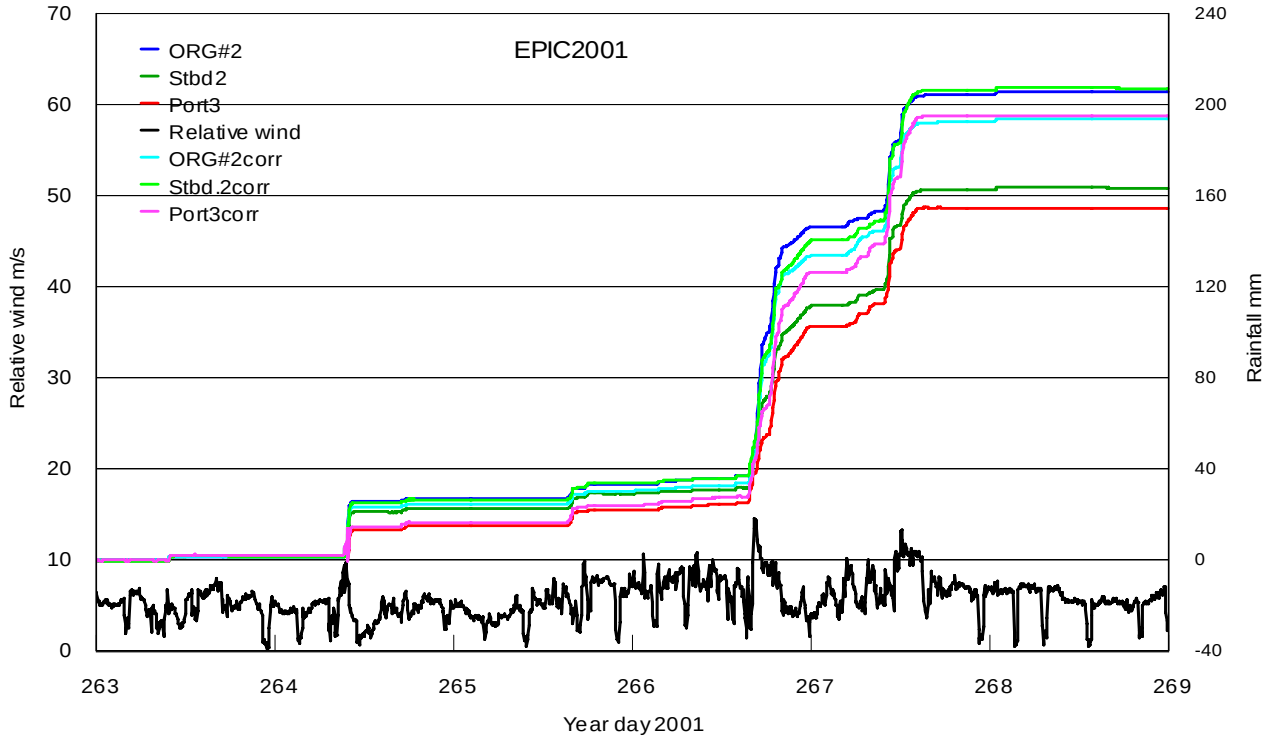

Figure 2.3. Cumulative rainfall measured by optical and funnel raingauges on a ship, before and after wind correction. The ORGs overestimate slightly when the raindrops are blown through the optical path at an angle to the vertical (dark and light blue traces). Siphon gauges underestimate when strong winds are distorted up over the ship and deflect raindrops away from the funnel (dark and light pairs of red and green traces). The black curve is the relative wind speed. Rainfall events started around day 264.4, 265.7, 266.6, and 267.3.

3. Bulk-flux meteorological sensors

3.1 *Introduction*

In this section we consider the types of sensor in common use at sea for measuring atmospheric temperature, humidity, wind speed, pressure, and sea temperature. The sensor is the part of a measuring instrument which is directly exposed to the entity being measured, and whose characteristics respond in a predictable way to changes in that entity (e.g. resistance of a platinum wire to temperature). Other important components of the measuring system are the sensor housing, and any associated electronics or recording equipment. Mostly these sensors have been developed for observations over land, and their use on ships and buoys has required some adaptation. At the very least they need protection from the highly corrosive environment of salt air and spray, which usually means that the housing has to be specially designed for marine applications. It may also be important to take account of platform motion, and systems on long-term moorings may need modification for low power consumption. Sensors evolve continuously in the research and commercial environment; either testing new physical principles of measurement or to quantify some newly significant entity (e.g. a trace gas transferred across the air-sea interface), and with the advance of measurement technology.

There are often several choices of sensor for each variable, the most suitable for a particular application depending on several factors, including the accuracy and resolution required, frequency response, and overall convenience of operation. Atmospheric variables fluctuate on time scales from below 0.1 seconds to several hours. Rapid sampling, typically at 20Hz or more, is required to obtain the turbulent fluctuations of wind, temperature and humidity for eddy-correlation or inertial dissipation determination of the fluxes. These methods are not considered in this handbook, in which we focus on the observations required to calculate *bulk* fluxes. A sensor responds to a step change exponentially, the time taken to reach ($1-1/e$; ≈ 0.632) of the final value being its *time response*. By virtue of their mass, most bulk sensors have a time response of many seconds and to avoid aliasing are sampled at about once per second. The resulting data are then time-averaged over suitable periods from a few minutes to one hour to reduce unsteadiness. We note however, that some fast-response instruments (e.g. sonic anemometers) have become sufficiently stable that, if deployed for other purposes, they can also provide reliable long time-averages.

3.2 *Temperature*

Sensors commonly used to measure atmospheric temperature are thermocouples, platinum resistance thermometers (PRTs), thermistors, and mercury-in-glass thermometers. The latter are still used operationally in hand-held instruments such as Assman psychrometers and the sling thermometers used by observers who file ships' weather reports, as well as in some fixed thermometer screens. Accuracy depends on the quality of the thermometer and the care with which the observer reads it. High quality Assman thermometers can be read to 0.1°C. Being free from instrumental errors, their value in the present context is to verify data from the electronic measuring systems installed on the ship by taking careful "spot" readings at a location free from ship influence (Figures 3.1 and 3.2).

The other three types of sensor lend themselves to automatic, continuous data-logging. Thermocouple systems have the disadvantage of low output voltage, and for absolute measurement require a reference "cold" junction. Good quality PRTs are very stable and with careful calibration accuracy of about 0.01°C can be achieved, although their typical resistance of 100 ohms requires a high resolution resistance bridge. PRTs are the temperature sensors most commonly used in high-quality commercial instruments. Both thermocouples and PRTs can be easily configured for differential measurement, which can improve the measurement accuracy of the wet bulb depression when they are used in a psychrometer (see next Section).

Thermistors are semi-conductor devices with much higher resistance values (typically 3000 ohms) than PRTs, making the measurement of resistance changes easier. Unlike the linear response of PRTs, the larger signal comes at the expense of non-linearity. Formerly, they were prone to uncertainties of stability and calibration, but guaranteed interchangeability of ±0.1°C is now available from some manufacturers, and micro-processor technology enables their logarithmic response to be linearized.

3.3 *Humidity*

The traditional instrument for atmospheric humidity measurement is the psychrometer, consisting of a pair of thermometers, one being covered with a moist wick. Air drawn over the thermometers evaporates the moisture, cooling the wick until the evaporation rate is in equilibrium with the atmospheric water vapour. This *wet bulb depression* is understood from thermodynamic theory, and described by the psychrometer equation given in Appendix A. Hand-

held sling or Assman psychrometers use mercury-in-glass thermometers, the former achieving ventilation by rapid movement through the air, while the Assman is equipped with a spring-wound or electrically driven fan which draws air over the thermometer bulbs. The basic accuracy of 0.1ºC for both wet and dry bulb thermometers leads to an uncertainty of 0.20 g kg^{-1} in specific humidity or about 1% in *RH*. To achieve this, the wick must be moistened (but not flooded) with distilled water, washed from time to time to remove salt, and changed after a period of use.

Figure 3.1 Measuring wet and dry bulb temperatures with an Assman ventilated psychrometer. The use of the forward chock as a sampling location ensures good exposure and some shielding from the sun.

For automatic data logging, psychrometers can be constructed using either PRTs or thermocouples as the sensing elements. Accurate measurement requires adequate airflow over the thermometers to ensure full wet bulb depression, and that they be well shielded from solar radiation. This is best achieved by using a double heat-reflecting shield, as illustrated in Figure 2.1 right, with the air drawn over it *and* through the space between the shields at a rate of at least 4 ms^{-1} . With PRTs in a differential bridge, temperature resolution of ±0.01°C is possible, and with care specific humidity accuracy of 0.05 g kg^{-1}.

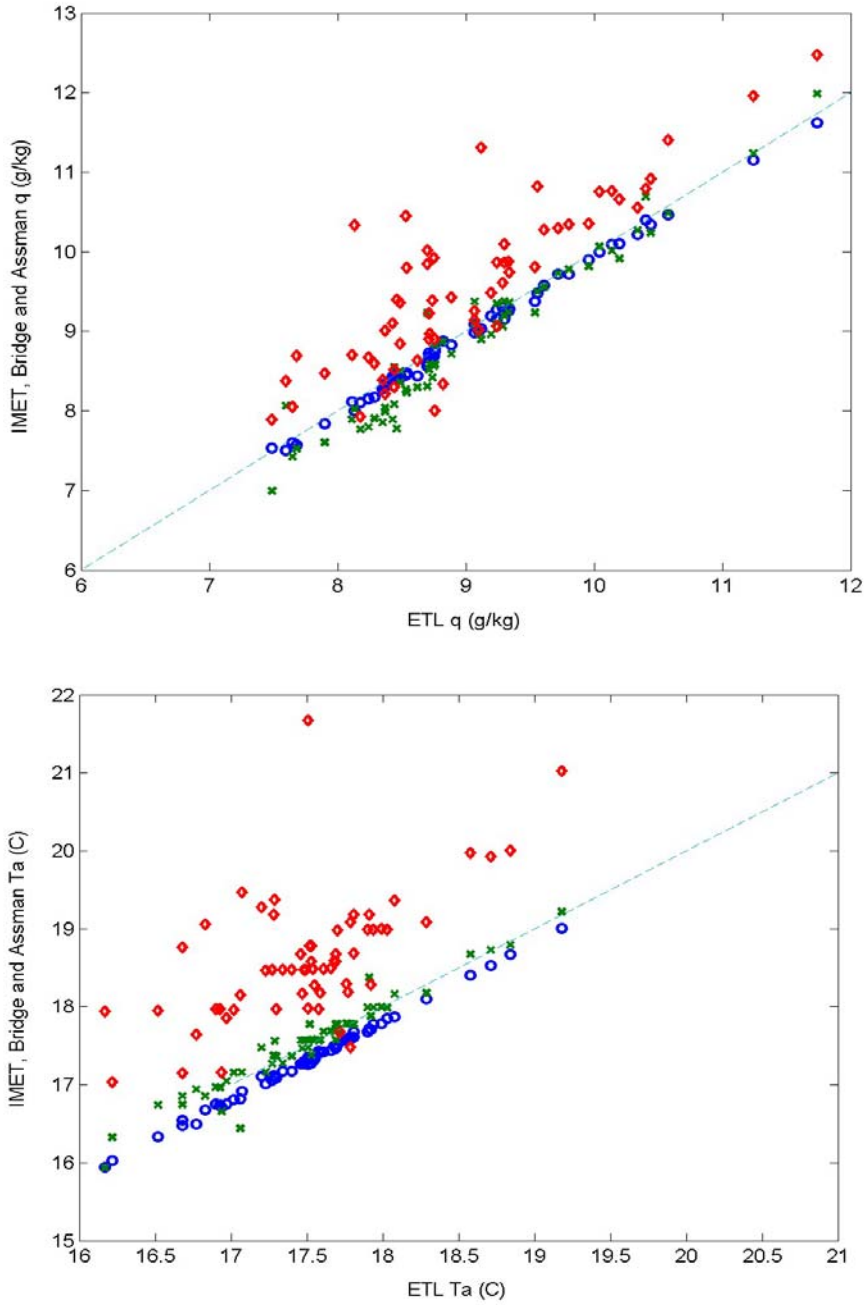

Figure 3.2. Comparison between a high quality T/RH sensor used by ETL and: (green symbols) an Assman psychrometer; (blue) the ship's IMET system; (red) the wet and dry bulb thermometers read by the bridge officers hourly for their weather reports.

Figure 3.3. Example of the installation of wet and dry bulb thermometers used for the hourly weather observations transmitted to shore by ships participating in the Voluntary Observing Ships (VOS) program. This screen is in a well-exposed location, but the screen design is poor leading to inadequate ventilation of the wet and dry-bulb thermometers. In sunny conditions the temperature inside the box could be several degrees above ambient and the air-flow through the box is not sufficient for accurate measurement of the web-bulb depression. Observations from this unit during mostly overcast conditions are given in Figure 3.2.

Figure 3.4. A more usual type of screen to house the wet and dry bulb thermometers read hourly by the bridge officers. It is also well-exposed, but all four sides are louvered to allow free air flow to the thermometers.

Nowadays, thin-film polymers which absorb or desorb water as the relative humidity changes are the most common humidity sensors used on research vessels at sea. Early versions of these sensors often failed at very high humidity, but recent developments have largely overcome this problem, and improved their accuracy and stability of calibration. The polymer usually forms the dielectric of a capacitance in a circuit which provides an electrical output proportional to relative humidity. Conversion to mixing ratio, specific or absolute humidity requires the temperature of the air surrounding the dielectric, often using a co-located PRT. The best quoted accuracy is ±2% *RH* (or ±0.3 g kg^{-1} at 20°C and 70% *RH*). For accurate measurement these temperature/RH sensors are ventilated and screened as for the psychrometer. There is also a Gortex filter around the sensing element which must be changed or washed to remove salt.

Radiometric air temperature sensors are just starting to be used (Minnett et al. 2005) and are likely to become more common in the future. Being non-invasive, they have some advantages over traditional methods but validation against high-quality *in situ* air temperature measurements have yet to take place.

The dew-point hygrometer incorporates a mirror which is maintained, by optical and electronic feedback, at the temperature, T_d , where moisture or ice just condense on its surface. Using the relationships in Appendix A, this dew-point can be converted to any of the other units. It is an absolute instrument, not well suited for operational use at sea, but often carried as a secondary standard to calibrate other sensors. Best quoted accuracy for a dew-point instrument is ±0.2°C which converts into an uncertainty in *RH* of ±1%.

Humidiometers which measure the absorption of ultra-violet (Lyman-α) or infra-red radiation by water vapour, respond to rapid changes in humidity and are used for eddy-correlation flux measurement. Currently they are not sufficiently stable to be suitable for routine measurement of long time-series.

3.4 *Atmospheric pressure*

Ships monitor atmospheric pressure routinely to include in their daily weather reports, transmitted on the Global Telecommunication System (GTS) for use by national weather forecasting institutions. The barometer is normally located on the bridge. The proper installation and operation of mercury barometers at sea has proved very difficult, and they are now rarely used aboard ships. Modern aneroid barometers with a digital readout have a resolution of 0.1mb and are relatively stable, but require checking against standard instruments from time to time. However, for applications requiring continuous time series of pressure to be recorded, solid state sensors with high resolution and long-term stability of 0.1mb are now available. Whether inside the wheelhouse or outside it is important to ensure that the port for the barometer is located so as to avoid dynamic pressure fluctuations due to the wind, or if inside free from a space which may be pressurised by, for example, the ship's air conditioning. Special inlet ports designed to overcome dynamic pressure fluctuations from the wind are available, to be connected to the barometer via a plastic tube.

3.5 *Wind speed and direction*

For average wind speed and/or direction over some time period, cup (or propeller) anemometers and wind vanes are usually the most convenient. Some operational designs will withstand continuous exposure to stormy conditions, but there are also more sensitive instruments intended for research work. Apart from mechanical strength, the difference is reflected in their starting speed and distance constant (response time converted to run of wind). A sensitive cup anemometer will start from rest in a breeze of 0.3 ms^{-1} and have a distance constant less than 1 metre.

For best accuracy (typically 1%) cups must be calibrated individually, although calibration in the steady horizontal flow of a wind tunnel can be misleading when the instrument is exposed to the natural fluctuating wind. In such a situation, cup anemometers usually overestimate for two reasons; the rotor responds more quickly to an increasing wind than to the reverse; and in a wind gust with a vertical component shielding by the upwind cup is reduced. Numerous studies have been made of these effects. Propellers have poor response to off-axis wind direction, but this is normally overcome by mounting them on the front of a wind vane. The one instrument thus measures both wind speed and direction. Otherwise, a cup anemometer/wind vane pair is often mounted at opposite ends of a horizontal bar. Ideally the wind direction sensor should have a complete 0 to 360˚ response. However some instruments use a potentiometer which has a finite deadband (≤10°), in which case care must be taken to ensure that readings in this deadband are infrequent and do not corrupt the average reading.

As noted above, sonic anemometers, which are commonly used for fast-response applications in the research environment, have become sufficiently stable to enable observation of long time-series. They have many advantages; no moving parts, less distortion to the wind flow than cups or propellers, they obtain the total wind vector, and some have an air temperature output. Sonic anemometers are likely to become more widely used at sea as the more robust, and less costly, models appearing on the market prove their suitability and gain acceptance.

3.6 *Sea temperature*

The so-called "bucket" sea temperature is aptly named. An open cylindrical container, usually insulated and equipped with a mercury-in-glass thermometer, is attached to a line and cast from the after deck to collect a sample of water. Allowing for some change during the time it takes to read the thermometer, this procedure produces spot values of a well mixed sample of surface water every hour or so, probably to an accuracy of 0.5ºC depending on atmospheric conditions. As described in Section 2.6, this frequency and accuracy are no longer adequate for the calculation of research quality air-sea heat fluxes; furthermore, disturbance by the ship makes it uncertain what depth the sample represents. Some of the errors in bucket measurements of sea temperature are predictable and can be corrected, and routine bucket temperatures from VOS still form an important part of the climate record.

On some research vessels, a thermosalinograph measures the temperature of engine cooling water near the intake port. The basic accuracy of the instrument is a few 0.001ºC and the flow sufficiently large that spurious heating from inside the ship is not significant. The depth of the intake is known but it is usually well aft. It has been found that, because of the pattern of flow along the hull, the water entering the intake may have originated from some shallower depth ahead of the ship. With a well-mixed surface layer, at night for example, the difference may be small, but in daytime if there is a significant vertical temperature gradient near the surface due to light winds and solar heating it can be several tenths of a degree.

A better arrangement is when the thermosalinograph has its own intake port and pump near the bow of the ship. There is still some uncertainty about the effective depth of measurement particularly with the ship pitching in heavy seas when there is also the danger of the intake breaking the surface. Often the thermosalinograph is turned off in port and in some coastal conditions to prevent fouling of the sensors by oil and other contaminants.

Another class of sensors are attached inside the hull of the ship and measure some sort of average temperature over the surface layer, providing they are located well below the water line.

Some research cruises measure sea temperature close to the surface by trailing a sensor (usually a thermistor) mounted at the end of a length of plastic hose, or a rope with an internal conductor. One type is known as a "Seasnake". It is towed from a light boom near the bow of the ship and extending as far out as practicable, preferably outside the bow wave. Underway in slight seas the hose will follow the surface at a depth of 5-10cm, but in heavier seas will often become airborne. This can be overcome to some extent using streamlined weights. Comparisons with ships' thermosalinographs at night, and when the surface layer is well mixed to a considerable depth, indicates that the Seasnake is capable of 0.1ºC accuracy. During the day it captures nearly all the daytime surface warming, but is below the cool skin regime. In persistent stormy conditions it may have to be brought inboard and stowed to prevent its destruction. When the ship stops it normally sinks, even if not weighted, but under these conditions the water temperature is contaminated by the ship in any case.

During the past decade a number of high-resolution infra-red (IR) radiometers have been developed for use at sea. This instrument is normally mounted forward on a side-rail of the ship, high enough to view the sea surface outside the bow wave. Its view is a narrow cone operating within spectral bands in the range 8-12μm similar to the channels of space-borne IR radiometers. The view angle to the undisturbed surface will depend on the geometry of the ship, and is usually between 30º and 60º to the vertical. SST is obtained from the measured radiance and surface emissivity, which is a function of view angle, and a correction made for reflected sky radiation using a second radiometer pointed skyward at the same angle (which is covered during rain). Depending on sky conditions and atmospheric water vapour content, this correction can vary from near zero to at least 1ºC. Some instruments self-calibrate the radiometer sensor using internal black body targets at different temperatures. The most sophisticated examples of this type of instrument claim SST accuracy of 0.1ºC. However, combined with estimates of the cool skin from recent models, a Seasnake is the more economical option.

3.7 *Radiation*

Because of its dominant role in the earth's energy budget, much attention has been given to the study of solar and terrestrial radiation components, their intensity, spectral characteristics and distribution. In the course of this, accurate instruments and methodology have evolved, often requiring precise directional pointing, meaning that they can only be operated from a completely stable platform. This requirement precludes their routine deployment from ships and moorings. The following describes instruments currently suitable for marine studies.

Downwelling shortwave and longwave radiation are measured with a pyranometer and a pyrgeometer respectively. These instruments are physically similar, both accepting broad-band, whole sky radiation through a hemispherical dome with the relevant spectral transmission characteristics (Figure 3.5). Solar radiation passing through the glass dome of the pyranometer impinges on a flat thermopile with a blackened upper surface. The instrument is so constructed, using two concentric domes to overcome convection within the instrument, that the thermopile output has a linear response to the radiative intensity. Accuracy of the instrument is usually quoted as 2%. The pyrgeometer works by determining its own thermal balance, combining the contributions from dome and case temperatures with longwave radiation through the silicon dome which is detected with a thermopile. There are thus three output signals to be recorded and combined externally using the pyrgeometer formula (Appendix A). An alternative scheme provided by the manufacturer, using an internal compensating circuit to provide just a single output signal, is to be avoided since it severely degrades the potential accuracy of the instrument from about 3% to worse than 20%. Both radiation instruments are vulnerable to the many sources of electromagnetic interference aboard ships, since the domes leave the thermopile unscreened. Pyregeometer domes also suffer from problems of shortwave leakage.

Ideally both instruments should be in a location with an unobstructed horizon-to-horizon view in any direction, but shipboard it is virtually impossible to avoid shadowing of the instruments while still maintaining accessibility for maintenance. At sea, the domes become contaminated with salt and soot and need washing frequently. The shadowing problem means that the pyranometer location is usually a compromise. The instruments shown in Figure 3.4 are quite well exposed at position G (Figure 6.1) and duplicated for increased reliability. In less favourable exposure the pairs could be separated far enough to avoid being covered simultaneously by the same shadow. With their relative locations carefully documented, shadows

can usually be diagnosed and flagged from the data record. In the case of pyrgeometers, the effect of IR flux contamination by objects in the field of view is analysed in Appendix C.

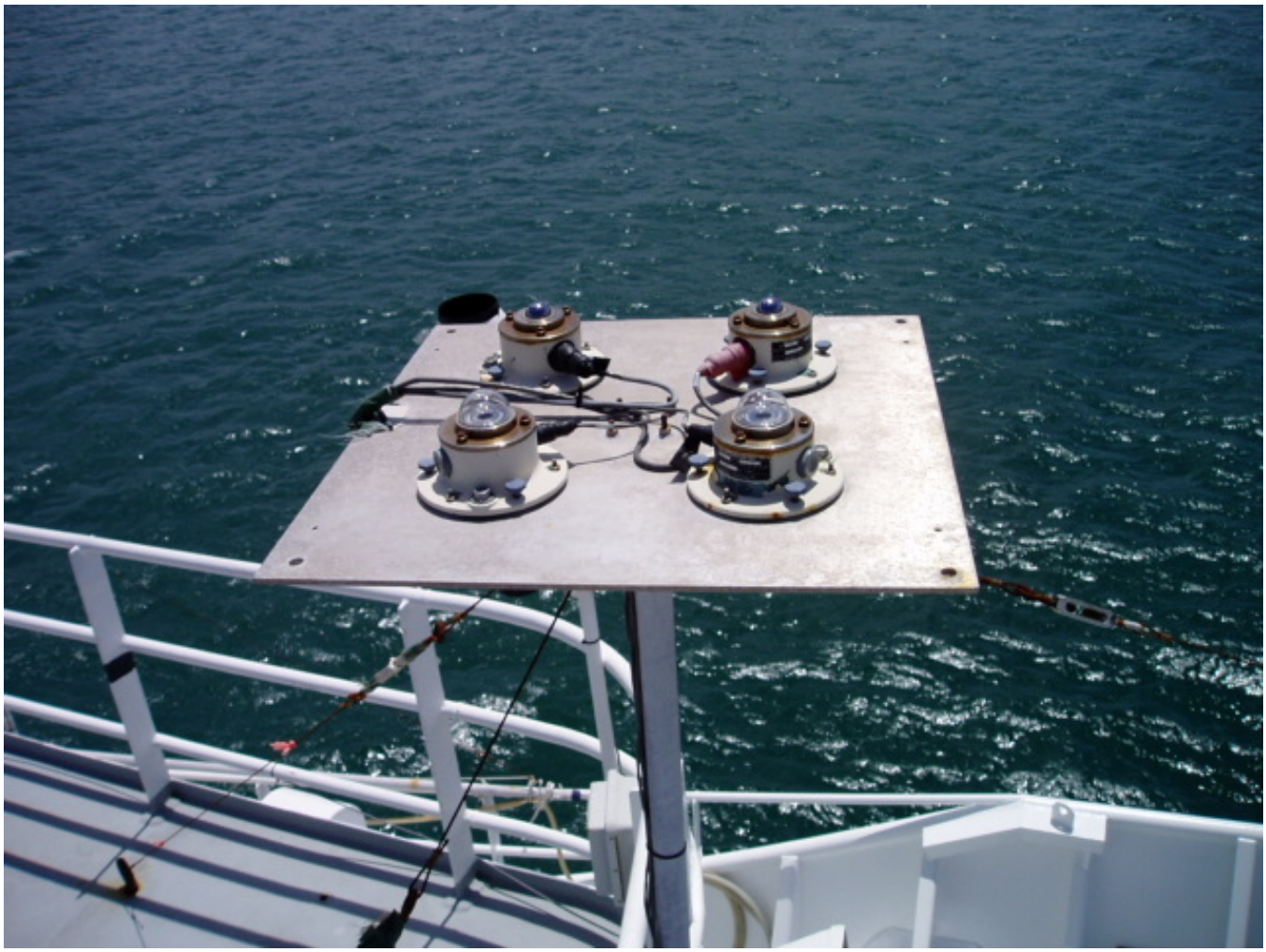

Figure 3.5 Example of duplicated pyranometer and pyrgeometer sensors mounted on a ship

Platform motion is also a potential source of error when radiation instruments are used at sea. For correct measurement the instruments must be horizontal, but both ships and buoys can roll through several degrees or take on a systematic lean caused by wind force or poor trim. The severity of the error depends on the inherent stability of the particular platform, but also on factors such as cloudiness, latitude, season and time of day. It is less severe for the pyrgeometer, since any sea in the field of view would be close to the near-surface air temperature. A possible solution is to set the instruments on gimbals but, unless very carefully designed, gimbals introduce other problems due to damping and phase variations. The better arrangement would be a dynamic system, such as a servo-controlled platform whose stability is achieved by feedback from a motion sensor, but so far such an arrangement is not available.

Regular dome cleaning may not be sufficient to overcome erroneous measurement. A recent observation of condensation on the inside of a pyranometer dome, despite the provision of desiccant within the instrument, was found to reduce the output by about 100 Wm^{-2}. The

probability that this phenomenon would be noticed is small because the instruments are usually mounted well above eye level. This example prompts the question of whether condensation inside the domes of pyrgeometers may be the cause of anomalous signals found with those instruments also. Because of the interference filter deposited inside pyrgeometer domes, condensation would not be seen but perhaps suspected if found in an adjacent pyranometer.

Over land or on a fixed platform at sea, diffuse radiation is measured by fitting the pyranometer with a "shadow-band", set to shield the sensing element from the direct solar beam as it tracks across the sky. Unstable platforms preclude the use of a fixed shadow-band, but measurements of the diffuse component have been made from shipboard using a rotating shadow-band which, whatever the relative position of the sun, casts a shadow on a fast-response radiation sensor once per revolution. The diffuse signal produced by the shadow-band is determined from the time series, and is unambiguous under clear skies but under broken cloud can be difficult to recognise. The fast-response sensor is usually of poor accuracy and stability, so is continuously referenced to a regular pyranometer during the non-shadow periods.

The essential steps that must be taken to ensure the required accuracy from radiation instruments are careful data acquisition, a well exposed location, frequent washing of the domes, regular replacement of desiccant, and calibration before and after each deployment.

3.8 *Precipitation*

Traditional raingauges measure the rain falling into a funnel of known area. For automatic recording either a weighing system is used, or a tipping bucket raingauge in which the funnel discharges to a pair of buckets in a "see-saw" arrangement which flips over at every 0.1 mm of rainfall. Neither of these methods is feasible on the unsteady platform of a ship or buoy. The most usual raingauge in this case is the siphon gauge in which the funnel discharges to a reservoir which fills to its capacity (about 50 mm of rain), when it siphons automatically and starts filling again. An electronic sensor keeps track of the level of water in the reservoir.

Raingauges used at sea must handle rainrates to around 200 mm hr^{-1}, which would be an extreme tropical storm. A heavy rainstorm in mid-latitudes might produce instantaneous rainrates of 50 to 100 mm hr^{-1}, but more commonly rainrates are between 1 and 20 mm hr^{-1}. All funnel gauges lose catch in strong winds, when the gauge deflects airflow so raindrops are carried past the funnel. This phenomenon is exacerbated at sea by wind flow distortion over the entire bulk of the ship. The siphon gauge also misses rain while the instrument is siphoning. A raingauge intended to overcome both of these problems has been developed by the Oceanographic Institute at Kiel, but is not yet fully proven (Hasse et al.1998).

Optical rain gauges (ORGs) measure *rainrate* by detecting raindrops falling through an optical path. One system measures extinction of a light beam by the raindrops; another measures the intensity of scintillations caused by raindrops passing through the semi-coherent infra-red beam from a light-emitting diode. Rainfall amount is obtained by integrating the rainrate. ORGs must be calibrated against a funnel gauge in natural or simulated rainfall. Their main drawback is that the light path has a particular (and arbitrary) direction relative to the rainfall, whose vertical component is thus uncertain. Some indication of errors due to this uncertainty may be obtained by mounting two ORGs orthogonally (Figure 3.6).

Figure 3.6 Example deployment of optical rain gauges. A pair of sensors is mounted with their axes oriented at 90º to each other. This geometry helps with the wind correction procedure.

Disdrometers are primarily intended for the measurement of drop size and drop distribution in rainfall. The most usual is an acoustic device which converts the sound of impact of raindrops hitting the sensor surface into an electrical signal related to the size of the drop. Continuous recording of the size and number of drops provides a time series of rainrate and total rainfall by integration. Disdrometers are still regarded as a research tool and are seldom used operationally on ships.

4. Measurement systems

The sensors described above, their physical shortcomings and potential for poor exposure, represent only one aspect of the possible sources of error in the final dataset. Between the actual sensor and the raw data record there is an hierarchy of stages, each of which is capable of degrading the accuracy of the measurement. Figure 4.1(left) illustrates a typical measurement system, comprising the sensor which is presumed to have an analogue output signal, analogue amplifier/filter unit, multiplexer, analogue to digital converter, data-logger, data processing and archiving system.

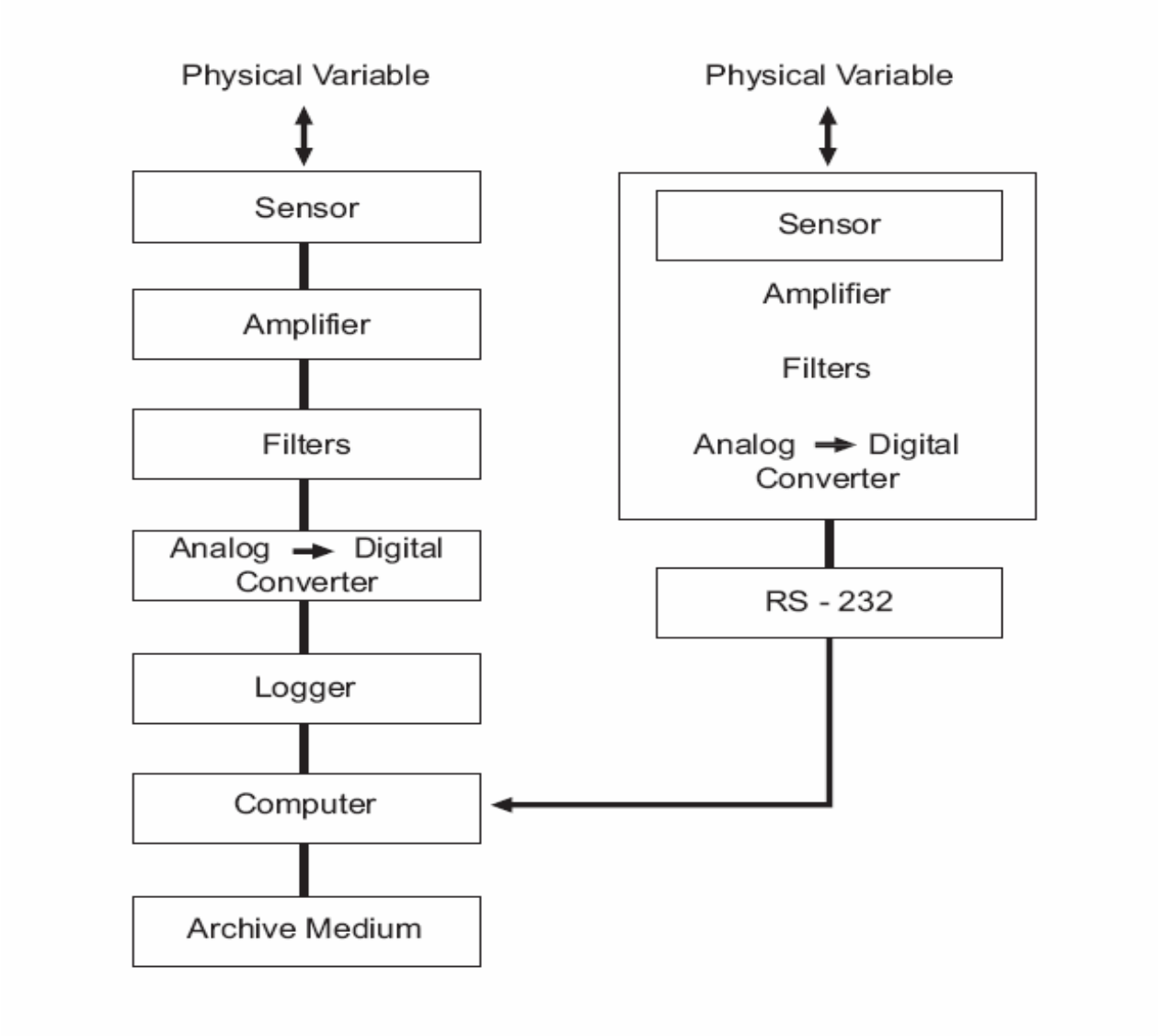

Figure 4.1 Schematic of components of a measurement system. The left part of the diagram shows a conventional sensor-to-acquisition component cascade; the right part shows an example where a fully digital sensor is used.

Whereas each component is a discrete unit with known characteristics (calibration, gain etc.), it should in principle be possible to combine these to determine the overall transfer function of the system. In reality, individual errors, together with electronic noise and offsets produced by connecting the units together, often combine to produce an overall uncertainty which exceeds what is acceptable. The most critical part of the signal processing system is what takes place between the sensor and its conversion to digital form, i.e. the analogue stages and the digitization prior to recording. Providing the bit resolution of the logger and subsequent computer hardware is adequate, the digital record will retain its accuracy through ensuing manipulation.

It is therefore good practice to calibrate the system as a whole from sensor to digital record, and repeat this as often as practical to verify that offsets do not change with time. Ground

loops are easily created when many instruments are distributed around a ship, and may change when the load on the line power changes. Most research vessels provide "clean" power which is isolated from the surges produced by starting large electric motors, and should be used when available. These problems are minimized in some instruments where integrated circuit technology enables the analogue signal processing, and conversion to digital mode, to be packaged together with the sensor (Figure 4.1; right). In this case the instrument output is already in digital format (e.g. RS232) and an overall system calibration is implicit.

If it is not possible to log all information (meteorological sensors, navigation information, etc.) on the same system, particular attention must be paid to synchronising the time stamps. In any case, the time reading used by the logging should be checked periodically.

5. Particular problems on ships and buoys

5.1 *Introduction*

Land-based meteorologists seeking an observing site for research studies or operational use will try to select an area free of local anomalies such as buildings, trees or surface inhomogeneity. They aim to avoid features which may introduce local gradients of the quantities (temperature, humidity, wind speed and direction) which would make the recorded data unrepresentative of the surrounding region. They normally have a choice of candidate locations, and are able to distribute measuring instruments to avoid mutual interference. Furthermore, the land doesn't move around.

A ship represents a challenging measurement platform. It is a local heat island and a bulky obstruction to the ambient wind flow. When the ship is steaming it disturbs the ocean surface layer and when hove to transfers heat to the surrounding water, so that a water temperature measurement close to the hull is always uncertain. A ship is a forest of tall obstacles, masts, funnels, cranes, and communication antennae which severely restrict the exposure of instruments and cast shadows on radiometers. Moored buoys and meteorological stations on pilings can have similar problems

5.2 *Wind flow distortion*

Because of the height dependence of all meteorological variables in the surface layer, and the need to reduce all observations to "standard" height (usually 10m) it is important to know the average height of each sensor above the sea surface. Except in very calm weather this is difficult to determine at sea, and a measurement made at the wharf must be accepted. However, in blowing over the ship the wind is deflected upward, so that the true height from which the air measured by the sensor originates is unknown. There are also consequences for the measurement of rainfall using siphon gauges as described in Section 3.8. Particularly in strong winds, and when the ship speed augments the true wind, the upward flow carries raindrops away from the funnel instead of falling in. As for the wind measurement itself, flow distortion by the ship not only creates uncertainty in the height of origin upwind, but also changes the wind speed (and often direction) by accelerating the wind round the obstacle of the ship. Obviously, errors in both wind speed and direction measurement affect the true wind calculation, and hence the bulk fluxes (Figure 5.1).

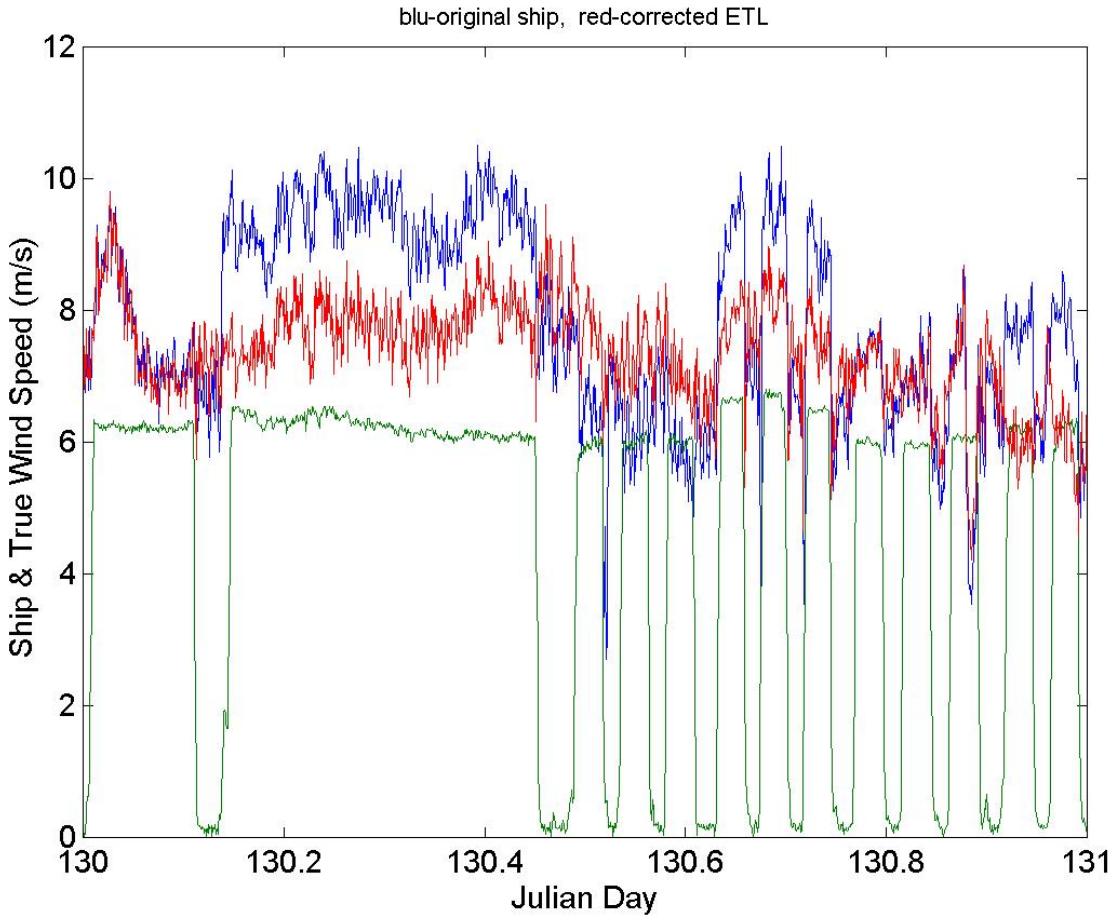

Figure 5.1 Illustrating the effects of flow distortion by the ship's structure on the determination of true wind speed. On this day the ship steamed in a star pattern performing a series of CTDs, which required the ship to stop periodically (ship speed is the green line) and change course at the vertices of the star. Such a course change occurred after the stop at 130.13. The red trace shows true wind speed computed from a research anemometer mounted well forward on the foremast (at A in Fig 6.1). This anemometer has a flow distortion correction applied. The blue trace shows true wind speed computed from the ship's anemometer mounted to port of the foremast, with no flow distortion correction. The course change alters the flow distortion pattern and thus the relative wind; the effect on the uncorrected anemometer is apparent in the blue trace.

Correction for wind distortion is seldom attempted due to lack of knowledge at this stage. From simple aerodynamic considerations, the deflection will be less severe when wind blows directly over the bow than abeam, when the ship represents a larger obstacle. The effect of wind distortion can be quantified with wind tunnel, water flume or computational fluid dynamics (CFD) model experiments. Studies have already been made of the air flow distortion around a number of research vessels. Figure 5.2 is such a CFD simulation of particle trajectories for wind flow head on to NOAA's *R/V Ron Brown*. The effect caused by the central superstructure is particularly dramatic; the upstream wind of about 12ms^{-1} at around standard instrument height is lifted by 2 decks and decelerated to around 5 ms^{-1}.

It is necessary to establish the wind field around various generic ship designs and determine corrections as a function of wind incidence angle to the ship. Meanwhile we emphasize the importance of documenting the location of anemometers (with photographs), and the height of all measuring instruments above some reference level on the ship (e.g. the foredeck). The height of the reference level relative to the sea surface is also needed. The planned flow distortion studies provide the opportunity for retrospective correction providing sensor locations are properly documented.

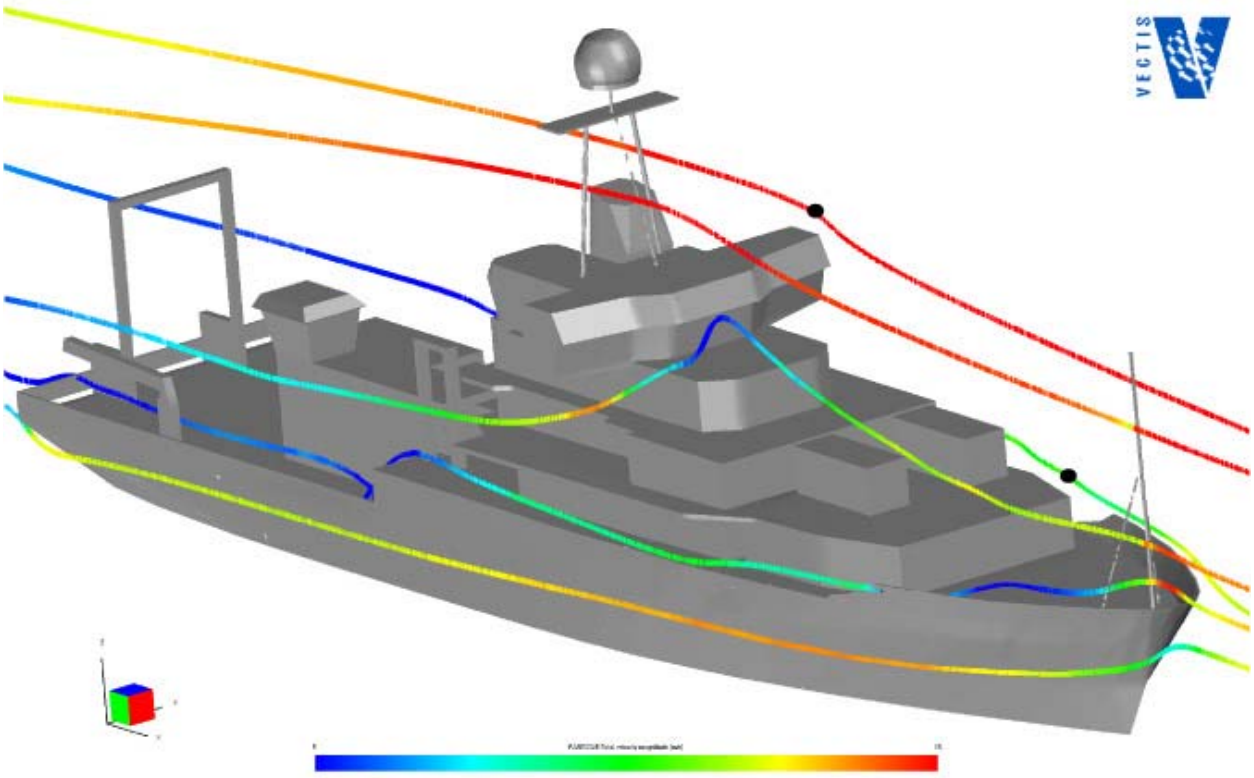

Figure 5.2 CFD simulation of wind flow around *R/V Ron Brown*. Positions of two funnel rain gauges are shown as black dots on particle trajectories which pass through them, showing the flow deflected sideways and upward at each site. Other trajectories originate 100m upwind on the centreline of the ship, at heights of 5, 7, 9, and 15 m above the sea surface. The colours represent wind speed and scale from 5 to 15 ms^{-1}. Courtesy Ben Moat.

5.3 *Sea spray and salt contamination*

Even without strong winds and flying spray, instruments at sea become coated with a layer of salt which needs cleaning periodically, especially from the domes of radiometers. Temperature and humidity sensors must be well shielded from salt contamination, which would directly affect the measurement by absorbing and desorbing water vapour. All electrical connections and electronic instruments outside must be enclosed in sealed boxes. Signal cables have to be protected against damage, due to chafing on sharp edges for example. Cases have

been known where a slight, barely noticeable nick in the jacket of a cable allowed salt to corrode the copper conductor and cause an intermittent fault which was almost impossible to locate.

In rough weather, even the largest research vessels pitching into swell will send spray surprisingly high over the ship. This spray is sometimes detected in rain-gauge records.

5.4 *Ship and buoy motion*

The irregular motion, rolling and pitching, of ships and buoys produce various effects on measuring instruments. There is no such thing as "level" on a ship, unless it is produced by a stabilized platform as is done for some radar installations, or naval guns. Instruments for which orientation is important, such as radiometers and anemometers, must be set up with reference to the axes of the ship.

Except in extreme conditions, a ship will typically pitch through ±3º, and roll through ±10º (Class 2 without stabilizers) or ±5º (Class 1 with stabilizers). The effect of this motion on radiation measurements is less severe for the diffuse shortwave and downwelling longwave than for the direct solar beam. For the latter, providing the motion is symmetrical about zenith, experiments have shown that for rolls of 10º amplitude at a zenith angle of about 50º the largest error was 2%; thus for low latitudes and modest seas the effect of platform roll may not be too serious for radiation measurement. Even at mid-latitudes, more severe seas causing greater roll tend to be associated with bad weather and cloudiness, reducing the absolute radiance which is also mostly diffuse. However, a persistent tilt of only 5º has been found to produce errors much greater than 5%. Such tilt angles may be caused by misalignment of the instrument relative to the ship, or by the ship listing due to poor trim or a strong wind abeam.

The effect of pitching on the meteorological sensors is to move them up and down through a gradient of the quantity they are measuring. The vertical motion at the bow of the ship (the preferred location for many sensors) can be several metres in rough weather. The frequency of pitching motion is irregular, but typically has a period of a few seconds, of the same order as the time-constant of the sensor. Thus, the measurement is some sort of average over the sensor path, assumed to be at an average height close to the one determined at the wharf. The height of measurement is thus subject to yet one more uncertainty. Fortunately, in more moderate conditions the vertical motion is less and at typical instrument height the gradient of most boundary layer variables is relatively small.

Wind sensors are affected directly since the ship motion creates a complicated apparent wind pattern relative to the instrument. In Section 2.5 we discussed determining the mean true wind speed from the relative wind speed (i.e., accounting for the heading and vector motion of the ship). However, pitch and roll may produce second-order errors in true wind speed when non-ideal wind sensors are used. For example, with cup anemometers the motion acts like a continuous sequence of vertical wind gusts on the rotor's imperfect cosine response. Because sonic anemometers measure all three instantaneous components of the wind vector, it is possible to continuously correct for pitch, roll, and other ship motions. This correction produces the most accurate true wind vector measurements but requires an additional system to provide all of the motion information. Such systems are now entering the research vessel fleet in an effort to improve the accuracy of ADCP measurements of current profiles, but have yet to see general application to wind measurements.

5.5 *Exhaust contamination*

On a ship it is unavoidable that periodically the stack exhaust plume will cross the location of the meteorological sensors. The impact of the exhaust is most severe on temperature, humidity, and radiation sensors down wind from the stack. One may also expect contamination problems with any optical sensor (e.g., optical rain gauges, radiometers). The likelihood of exhaust contamination is lessened by locating sensors as far forward of the vessel stack as possible (e.g. in Figures S1 or 6.1, positions A and B for temperature or G for radiation sensors).

The exhaust plume will result in shadowing errors for shortwave radiation sensors. The impact on longwave radiation sensors is caused by the exhaust plume, being a heat anomaly, resulting in overestimated downward longwave readings. Also, the plume will deposit soot on the radiometer domes, so frequent cleaning of the domes is essential if the radiometers are aft of the stacks.

Abrupt changes in temperature and humidity are caused by the exhaust plume. Figure 5.2 shows the abrupt rise in air temperature, and consequent reduction in relative humidity, that occurs when the exhaust plume on the RV Meteor passes these sensors. In this case, although the sensors are forward of the stack, the relative wind is from astern causing sensor contamination. One would expect that similar problems would occur with dew-point or wet-bulb temperature sensors.

For all measurements affected by the stack exhaust, the ship-relative wind can be used to eliminate suspect values. In the case of temperature and humidity sensors positioned forward of the stack, but above the wheelhouse, upwards of 25% of these measurements will be in error when the relative wind is from the stern (typically when the ship is manoeuvring at low speed). Even sensors on a bow mast can be affected by the exhaust when the relative winds are from the stern, but the range of relative wind angles that will result in sensor contamination is reduced as sensors are placed farther forward of the stack.

5.6 *Electrical problems*

Lightning and build up of static electrical charge must be considered as a source of damage and interference. Use of plastic instrument cases that accumulate rather than bleed off static charge is not advised. The ship's own power system may present challenges in the form of uncertain grounding, potential between neutral and ground, and surges and level fluctuations, especially during port call or when generators are shifted on and off line for servicing.

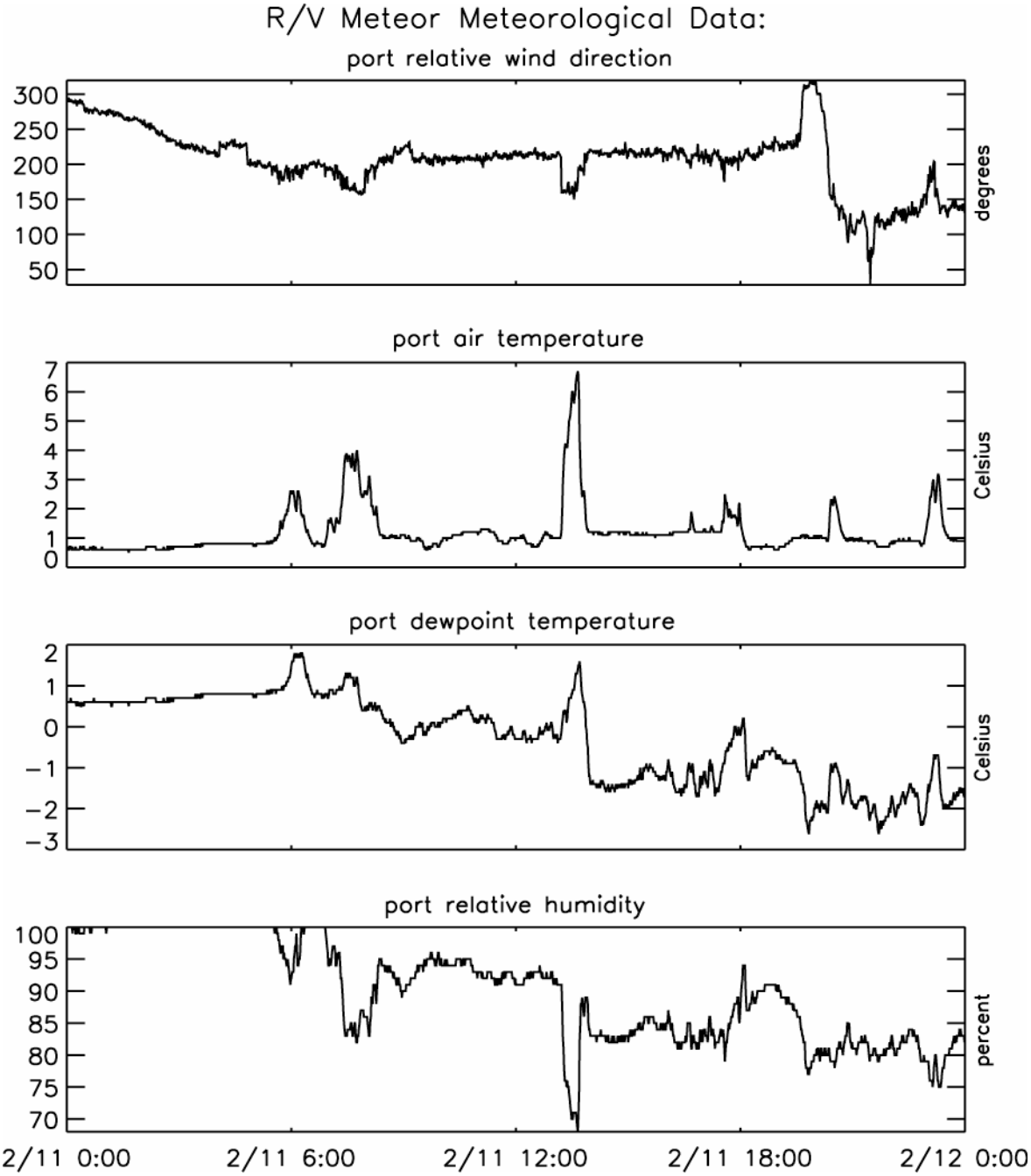

Figure 5.2. One-minute sampled relative wind direction, air and dewpoint temperature, and relative humidity from the scientific instrument system on the RV Meteor. Data are all from the port side sensors collected on 11 February 1990. The increases in air and dewpoint temperature and the decrease in relative humidity occur when the relative winds are from the stern (~160-200˚) indicating contamination of the sensors by the vessel exhaust.

6. Location of instruments

6.1 *Introduction*

Location of the sensors on the ship is the most critical aspect for accurate measurement of the basic meteorological variables, and therefore of the fluxes. The particular difficulties of making these measurements aboard an unstable, bulky obstacle were noted in Sections 3 and 5. In general, meteorological instruments should be located forward on the ship, ahead of the engine and air-conditioner exhausts. The ideal position would be high on a forward mast high enough to be above spray when the ship pitches in heavy seas. Because ships are various shapes, sizes, and have different appendages, such decisions must be made on a ship-by-ship basis. But there are principles, mostly common sense, which can help minimize defective observations. They are illustrated in relation to typical ships in Figure 6.1.

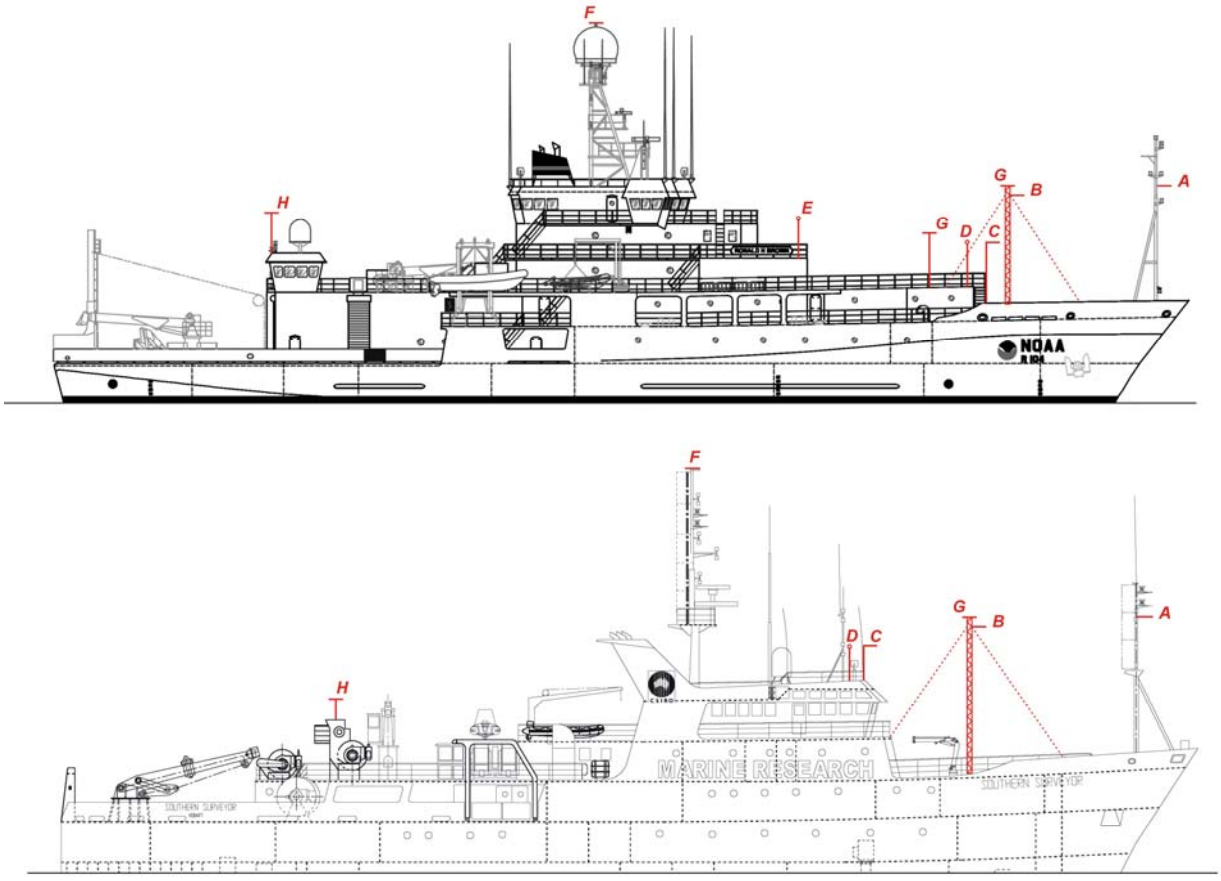

Figure 6.1 Examples of ships with good foremast locations for instruments: *R/V Ronald H. Brown* (NOAA) and *R/V Southern Surveyor* (CSIRO). Locations A, B, etc. are described in the text.

6.2 *Temperature*

The temperature sensor should be as far forward as possible to avoid heat contamination from the ship. Again, this is impossible when the wind is from astern, so duplicate sensors to port and starboard provide better data recovery. The temperature sensor should be shielded and ventilated, but care must be taken to ensure that there is no possibility of sea-spray being drawn into the air inlet. Although the mainmast may have a well-exposed site for wind instruments, and be clear of sea-spray, it is usually a poor location for temperature sensors which can then "see" large areas of the deck.

6.3 *Humidity*

As described above, water vapour measurement is little affected by wind and thermal distortion caused by the ship. It is important that the temperature of air surrounding the sensor is recorded, and since the two measurements are commonly made in the same package the more stringent exposure requirements of the temperature sensor ensure that the humidity sensor is also well exposed. The location must, however, permit access to the humidity element for periodic maintenance. If a psychrometer is being used, it will also be necessary to top up the water reservoir with distilled water from time to time.

6.4 *Wind speed and direction*

The most important requirement of the wind sensors is that they should have no obstruction upwind. A single speed/direction set can be mounted on a forward-facing arm from a foremast, or high on the main mast. With only one set of instruments, there will always be a sector astern over which the relative wind will be in error. If two wind sets are available, it is good practice to mount one each side of the ship, and give preference to whichever has best exposure to the relative wind.

Note that even an object **behind** the anemometer will cause some disturbance to the wind, the error scaling with the size of the object. Thus mounting a sensor high on the top of a mast or pole is a good location. If mounted on an arm facing forward from the mast, it should be at least 5 mast diameters forward. However, a horizontal boom in front of the bow is not a good place because, with the bulk of the ship behind, it is not possible to go far enough forward to measure undisturbed flow.

6.5 *Sea temperature*

The location of a ship's thermosalinograph, and its inlet port, are usually outside control of the investigator. Ideally, as noted above, the port should be in the bow at sufficient depth (e.g. about 5m) that it does not break water. A hull sensor should similarly be mounted inside the bow. A Seasnake type sensor should be towed from a point as far forward and as far out as practical, intending that the sensor will spend much of its time outside the ship's bow wave. For the same reason infra-red radiometers for SST measurement, when available, are mounted as far forward and as high as possible (on the wheelhouse roof for example) so that their view is of an undisturbed ocean surface.

6.6 *Radiation*

Upward facing radiometers need an all-round, horizon-to-horizon view with minimal obstruction by parts of the ship, which would cast shadows on the pyranometer and be a source of thermal radiation for the pyrgeometer. Possible locations are the top of the main mast or

foremast, providing they are accessible at sea under moderate weather conditions so that the domes can by cleaned periodically, and the desiccant replaced. In some cases installing water jets, controlled from a convenient tap on the deck, has been successful in cleaning domes without climbing an instrument mast at sea. The pair of instruments are normally mounted together on a single aluminium plate, and levelled. If the masts prove impractical, the plate can be mounted on the top of a rigid galvanized metal pipe (e.g a scaffolding tube or thick water pipe), clamped in some way to a convenient rail, perhaps above the wheelhouse.

Shadows can often be diagnosed by installing a second pyranometer, separated widely enough from the first that they are not covered by common shadows (see section 3.7). Both pyranometers and pyrgeometers are 'cosine' detectors, so objects near the horizon have a much smaller effect than objects overhead. Appendix C describes the error in a pyrgeometer measurement when it receives thermal radiation from parts of the ship unavoidably in its field of view. In a real-life example, pyrgeometers mounted in position G (Figure 6.1 top ship) "see" an area 6m × 1.5m of the bulkhead 10m aft on deck 3, and 16m × 2.5m of the bridge 16m aft. If the sky and bulkhead temperatures are as given in Figure C1b, by interpolating the upper curve we can estimate that these two barriers would produce errors of 1 Wm^{-2} and 3 Wm^{-2} respectively. According to the middle curve on each diagram, the foremast, 16m forward, has negligible effect.

6.7 *Rainfall*

The difficulties of making accurate measurements of rainfall on ships, and the strong dependence on location of the instruments, have been described above. Funnel gauges should not be mounted in a location of strong upflow, such as on a rail just above the side of the ship or above the wheelhouse, where they will lose catch. Rain-gauges located on the after part of the ship may overestimate by catching water which has accumulated on the superstructure. Once again, the best location is on a foremast. If that becomes too crowded, a position on the foredeck near the centre-line of the ship will help avoid updraughts.

Because wind information is used to correct both funnel and optical raingauges, a location near the wind sensor is preferred.

7. Instrument calibration

While the absolute accuracy of an atmospheric measurement is the result of the cumulation of errors in each step of the measurement/archival process, it is clear that the calibration of the sensor is the starting point. The operator of a ship observation system must establish (and document) a routine for regular replacement and re-calibration of each sensor in use, at least once a year and preferably before and after each cruise. The routine will involve having a stock of pre-calibrated sensors on board to replace those which are away for calibration, or any found to be faulty or poorly-performing while in operation.

The calibration facility used should be traceable to a national standard. The system operator may choose to rely on factory calibrations (i.e., regular maintenance/calibration by the manufacturer of the sensor), a secondary calibration laboratory, or maintain an in-house calibration facility. For institutions with one or two research vessels, an in-house calibration facility is unlikely to be cost effective. Reputable manufacturers of meteorological equipment (e.g., Vaisala, Rotronic, ATI, Gill, RM Young, Eppley, Kipp and Zonen) have large, well-equipped facilities, calibrate thousands of instruments every year, and usually represent a solid

standard. In some cases secondary calibration laboratories provide more comprehensive information that may be useful. For example, the NOAA Climate Monitoring and Diagnostics Laboratory (Boulder, CO) can provide cosine-response curves for pyranometers and dome-heating correction coefficients for pyrgeometers. A pyranometer with a poor cosine response curve could be retired or relegated to the emergency backup shelf.

Regardless of the approach, the process must include keeping a documentation record of the calibration and deployment history of each sensor. It is important to realise that seemingly identical sensors from a production line may differ sufficiently in their calibrations to be significant in the context of the accuracies of Table 1. So when sensors are switched this history will ensure that the correct calibration is associated with the active sensor. In view of the many possible hazards to sensors deployed on ships, which have been described in the above sections, and which may remain undetected particularly on long voyages, it is good practice to calibrate both before and after the deployment. Gradual deterioration of a sensor may thus be detected and corrected, perhaps by simple linear regression to improve data accuracy.

8. Intercomparisons

8.1 *Portable standards*

While it is sometimes justified to equip laboratories which handle large numbers of instruments with standard calibration facilities, or in some cases to carry calibration equipment on board ship, this is usually impractical. In any case, not every ship could be so equipped which would lead to non-uniformity of data quality. With many ships involved in a cooperative project such as SAMOS, it is feasible to verify the operational instruments installed against a common set of portable secondary standards. These are instruments whose calibration is traceable to a recognised standards laboratory. They can be operated alongside the ship instruments in a realistic field situation, on part of a regular cruise for example, and recorded independently of the ship's system. The portable standard can be rotated around several ships, and verify not only the performance of the ship sensors, but the measuring system as a whole, from instrument location to recorded data.

8.2 *Replication of sensors*

It has been noted above that there are benefits in having duplicate sensors on opposite sides of the ship, to deal with the range of relative wind direction or the shielding of radiometers. However, there are times when both sets of instruments might be reasonably well exposed, and expected to agree fairly closely. The ability to compare their measurements, and to analyze any differences between them, is a further advantage. While it is not always feasible to have two sets of instruments in operation, it is good practice to carry a complete set of spare, freshly calibrated sensors, ready to replace the operational ones in the event of failure. However, excepting for trouble-shooting purposes, replication of sensors should not normally be done at the expense of exposing a freshly calibrated spare unit. The intermittent loss of data through unfavourable wind or sun direction, is usually less important than having a data time series cut short by instrument failure on a long cruise.

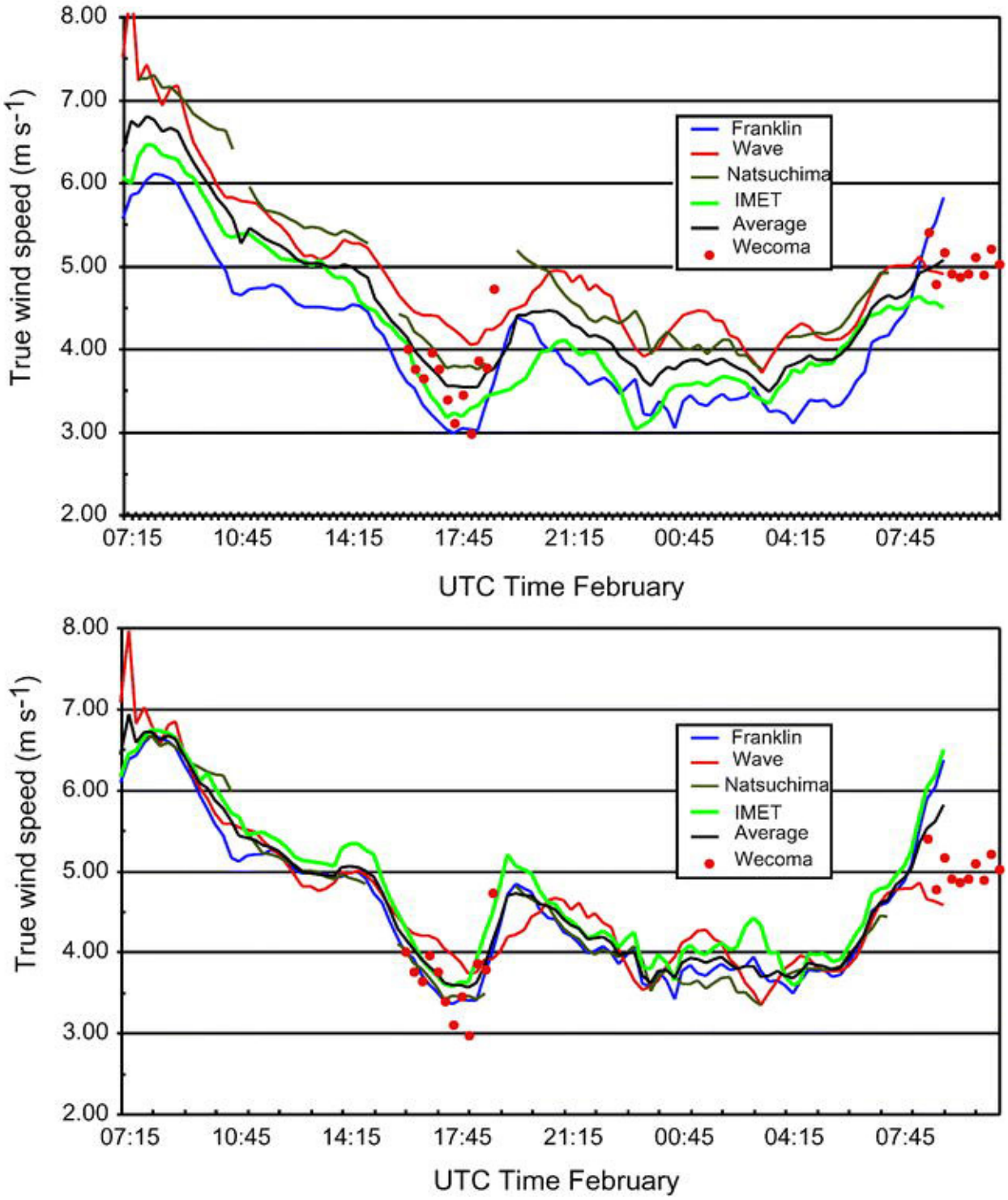

Figure 10.1 Field intercomparison of ship true wind speed measurements from TOGA COARE. Three ships ran side-by-side for about one day in the vicinity of the WHOI IMET mooring; a fourth ship (Wecoma) transited the area on two occasions. The raw comparison (upper panel) showed mean differences between platforms. Each platform was then corrected by that difference with the lower panel showing the new comparison. The corrected wind speeds were used for flux calculations for the entire experiment.

8.3 *Field intercomparisons*

Field intercomparisons between sets of instruments on different platforms should be made whenever the opportunity presents itself. During TOGA-COARE such comparison periods were scheduled as part of the operation plans of ships and aircraft, and there were also other occasions when platforms in the same vicinity could compare measurements. The quality of surface meteorology and flux datasets resulting from COARE is due in large measure to these field intercomparisons, and their careful analysis (Figure 8.1). This alerted participants to several potential sources of measurement error, and has influenced methodology in many subsequent air-sea measurement campaigns. For example, the ship used for deployment and retrieval of the Woods Hole Oceanographic Institution (WHOI) ocean reference moorings is equipped with a set of high quality meteorological instruments, and stands off the mooring for a few days at either end of a deployment while the old and new buoy instruments are compared with those on the ship.

Note that the scheduled intercomparison periods must be long enough, typically 24 hours or more, to give statistically meaningful results

8.4 Manual observations

In the same way that ship's officers preserve their skills in the use of a sextant to check the ship position in case GPS fails, it is prudent for meteorological observers to remain familiar with observation techniques before the days of SAMOS. The reason is not so much to fill in data should the automatic system fail, but as an aid to monitoring the health of the sensor array and signal processing system. There are at least three "traditional" observations that should be made regularly for this purpose.

a) Temperature/humidity. Use of the Assman psychrometer is referred to in sections 3.2 and 3.3, and little needs to be added. The Assman is preferred over the sling psychrometer because it usually has superior thermometers, and they can be read while the instrument is held *in situ*. This has the advantage that short-term fluctuations in temperature (in light wind, convective conditions for example) may be averaged visually. If possible, the instrument should be stored outside air-conditioned space for quicker equilibration with ambient conditions. Along with the precautions described in section 3, the critical thing is to note the time of reading to the minute for comparison with the automatically logged value.

b) Sea temperature. The traditional measurement is of the "bucket" temperature. The nature and probable accuracy of this method is referred to in section 3.6. From very large vessels a bucket measurement may be impossible, but most research ships possess such an insulated bucket. Its size is important; too small, and the water sample will change temperature before it can be read; too large and it will be heavy and awkward to handle. The technique is to throw it forward and out from the ship, and bring it in when level with the observer. Several casts are needed to ensure that the bucket is close to the water temperature. Obviously, the temperature should be read as soon as possible after bringing it on board, but timing is not so critical because sea temperature does not fluctuate as rapidly as air.

c) Wind speed. The traditional estimate of wind speed at sea is by observation of its effect on sea state. Unlike cup and acoustic anemometers, the Beaufort scale (Table E1) does not break, fuse or rust and is independent of ship speed and heading. In recent years the various sea state descriptions have been refined by comparison with careful instrumental wind measurements. As

indicated in sections 2.5 and 5.2 there are several potential sources of error in the true wind measurement, from instruments measuring wind and ship speed, the calculation from relative wind, and flow distortion. It is almost impossible to estimate the true wind by "feel", so the Beaufort scale enables the observer to judge, within a couple of ms^{-1}, whether the logged wind speed is within reasonable limits.

d) Downwelling radiation. Excepting under special conditions, short-term variability in solar and IR radiative fluxes, especially due to cloudiness, make these signals the most difficult to check with spot observations. There are various parameterizations for radiative fluxes, based on surface air temperature and humidity combined with visual observations of cloud fraction, but these are too uncertain to be of use in this context. However, reliable models of these fluxes for a *cloud-free sky* may be used to check the radiation observations for this particular condition. The IR flux (see equation 1.1) may be written $R_{l\downarrow} = \varepsilon_{e0}\sigma T_a^4$, where T_a is the air temperature (Kelvin) and ε_{e0} an effective emissivity for clear skies for which Brunt (1932) proposed a 2-parameter form $\varepsilon_{e0} = A + B\sqrt{q_a}$. From a database of several cruises, Hare et al. (2005) determined A and B as linear functions of latitude φ, such that

$$R_{l\downarrow} = \left[\left(0.52 + \frac{0.13}{60}|\varphi|\right) + \left(0.082 - \frac{0.03}{60}|\varphi|\right)\sqrt{q_a}\right]\sigma T_a^4 \qquad (8.1).$$

The pyrgeometer output, being a combination of 3 temperature signals, is vulnerable to stray thermal contamination, but equation (8.1) can provide a check to within ±10 Wm^{-2}.

Clear-sky parameterizations for solar flux are also available, but require atmospheric profiles of certain constituents, and involve strong dependencies on location and season, making them too complex for checking the pyranometer. However, knowledge that the solar flux falls identically to zero at night (note, a standard pyranometer will normally read a few Wm^{-2} negative at night), and takes a maximum clear-sky value around 1100 Wm^{-2} in the tropics, enables the observer to identify unreasonable values in most situations.

9. Documentation (Metadata)

9.1 *Introduction*

Careful documentation of the sensor installation, calibration practices, and known data faults is an essential task of the person responsible for maintaining a shipboard meteorological system. These metadata are crucial to the future application of the observations; a detailed example of a metadata structure is given in Appendix F. The importance of documenting the calibration and deployment history of each instrument cannot be emphasized too strongly. In the shambles which sometimes accompanies replacement of a faulty sensor it is easy to postpone, and eventually forget to note the circumstances. Down the track, this can lead to puzzling features in the air-sea flux time series which can never be resolved with certainty. Similarly, it is sometimes unavoidable that the location of the sensor is less than optimal. Providing the location is carefully documented, ideally supported by digital photographs, seemingly anomalous data from that sensor can often be explained, and in some cases, corrected. Equally, data from a sensor known to be very badly exposed for a given relative wind direction can be flagged as erroneous without fear that the information is being lost. The following indicates details and incidents which should be recorded (with date and time) in an event log during the cruise, and if

possible transcribed into an electronic document. This, and the digital photos, will be part of the metadata to accompany the measurements.

9.2 *The basics*

- Time convention (preferably GMT [UTC])
- Recorded Units of observations (preferably SI)
- Ship name
- Data sampling rates
- Averaging or calculation methods (e.g., true wind vs. ocean-relative winds)

9.3 *Sensor calibration and history*

- For each instrument, the make, model and serial number.
- The date and source of each calibration (indicates stability of sensor)
- Sensor dates of deployment period
- Incidents during deployment period (maintenance, repairs, mishaps e.g. swamped by wave over bow)

9.4 *Instrument location*

- Description of main support (e.g. foremast, forward rail above wheelhouse)
- Position w.r.t. main support (e.g. 1.2m to port or stbd., 0.8m forward)
- Position w.r.t. ship's centreline (e.g. 2.5m to port or stbd)
- Distance from bow
- Height above the water, and/or height above some ship reference (e.g. 15.3m above foredeck)
- Height above the deck immediately below the sensor
- Any significant object which may affect the exposure of the instrument (e.g. Inmarsat dome on rail 2m to port; after installation large instrument box mounted 1m forward)

9.5 *Digital photographs*

Rough sketches in the log book of the locations of instruments, with heights and salient dimensions with respect to the ship, are extremely helpful. Better still would be digital schematics of the vessel (top and side view) showing instrument locations (similar to fig. 6.1). Together with digital photographs of the installations they enable the analyst to assess the overall quality of the ensuing measurements, and provide valuable information on the likely cause of any suspect data.

Close-up photographs of the instrument itself can sometimes be helpful in detecting instrument faults (e.g. damaged cables), but are most useful when taken at a distance sufficient to show the sensor's environment and possible obstacles to air flow around the sensor; in the case of radiation sensors, objects or installations likely to cast a shadow. If possible, after installation photographs should be taken from the wharf, as in Figure 9.1 of the NOAA research vessel *Ronald H. Brown* on the following page. If written documentation were lost or mislaid, having the plans of the ship (e.g. Figure 6.1), together with such photographs, would enable the heights of the instruments, and their relative positions, to be estimated reasonably well.

Figure 9.1 Meteorological instruments on the foremast of the NOAA ship Ronald H. Brown; a) below the upper crossarm is a covariance package. The sensor of the sonic anemometer is well exposed, although the instrument boxes below and behind it represent a greater obstacle to air flow than is desirable; b) closeup of the bulk flux instrument package. From left to right on crossarm: optical raingauge; T/RH sensor with forced ventilation; second T/RH sensor in naturally ventilated screen; siphon raingauge; propeller anemometer and wind vane unit. Below these instruments can be seen a laser wave-height sensor aimed forward of the bow and a second sonic anemometer.

10. Securing the Data

10.1 *Introduction*

All data and metadata should be stored in a manner that will preserve the information for current and future scientists. This requires each operator to establish a protocol for managing the output from their sensor system. A detailed data protocol should include plans to store the observations, metadata, and event log on digital media during each cruise and to ensure the long term availability of the observations at a national or international archive center.

10.2 *Data storage*

The computer date and time should be set to GMT (UTC). The event log should also be written in GMT, although some relationships (cloud-radiation forcing for example) make more sense when analysed in local solar time. It is often helpful if the difference between local time and GMT is noted (but note that ship time, i.e. the time that the ship's clocks are set to, may differ from local solar time).

The recorded data will normally consist of the raw time series at the logger sampling speed, and a conversion to physical units via the instrument calibrations and transfer functions. This will often involve some computation involving several signals and sensors, for example combining the 3 pyrgeometer signals for downward longwave radiation, or obtaining true wind from the measured relative wind and the ship's speed/course.

In many cases (SAMOS for example) the meteorological data collected automatically by computer on the ship will be destined for use by scientists (e.g. modelers and analysts) engaged in climate research elsewhere. The role of the shipboard operator is to maintain the quality of the data by monitoring the performance of the sensors, and making sure that all detail (e.g. roosting birds, or a faulty instrument) is noted in the daily log. She/he should be provided with training to enable recovery of the system in the event of a computer crash, since extended time series are most valuable.

The capacity of the computer hard disc will be sufficient to hold several weeks' data, which should be backed up regularly according to normal computing practice. Every few days both raw and derived data should be written onto CD or DVD together with a copy of the metadata. If possible an electronic copy should be made of the event log (e.g. in Word) and saved with the data and metadata.

10.3 *Data Archival*

Archiving is a term that is rather poorly utilized in the climate community. Simply storing the observations collected on a cruise on a DVD or other digital media and placing this on a shelf does not constitute archival of the data.

As part of an ocean observing system, the mission of a national or international archive center is "to acquire, preserve, and provide access to data in perpetuity. High-priority objectives include integrity and completeness of the archives. Essential functions include constant monitoring of data streams, accounting for all files and records, and frequent checks of accuracy. Metadata are equally important since they ensure that the maximum information can be derived from the data. Archive centers must have maintenance strategies that protect the data as storage media and systems change. Data stewards must constantly guard against changes in formats and software that could make accessing the data more difficult, more costly, or even impossible.

Since important collections are seldom static, a significant effort is required to integrate new metadata, add improvements and corrections to the data, and make additional related historical archives easier to access" (Hankin et al. 2005). This effort goes beyond the capability and resources of most vessel operators.

Each vessel operator should establish a data pathway whereby meteorological observations are transferred from the vessel to a national or international archive center. The pathway may be direct, with copies of all data sent by the operator to the archive center on digital media to a pre-defined schedule (e.g., after each cruise, quarterly, annually). Alternatively, the data can flow through a specialized data center (e.g., the SAMOS data center) which will ensure the observations arrive at an appropriate archive center. Establishing an archive protocol will ensure that the investment in time and money that goes into collecting the observations will not only benefit current scientists, but those 10, 20, or even 50 years in the future.

11. Bulk flux algorithms (and the atmospheric surface layer)

Bulk flux algorithms enable the turbulent air-sea fluxes (sensible heat H_s, latent heat H_l, and momentum τ) to be calculated from the measured difference between the values of the corresponding bulk meteorological variable (temperature t, humidity q, wind speed u) at height z and at the sea surface. The simple form of the bulk air-sea flux equation given in Section 2.1 is repeated here for convenience

$$F_x = C_x u(\delta_s - \delta_z) \qquad (11.1),$$

where F_x is the vertical flux of entity x (heat, moisture, momentum), u the wind speed, δ the value of the corresponding bulk meteorological variable (temperature, humidity, wind speed).

This equation suggests that C_x can be determined by measuring the surface fluxes, by whatever means possible, together with the mean physical variables. During the second half of the 1900s, many such determinations were made using profile, covariance and dissipation techniques for the fluxes. Many of these employed atmospheric boundary-layer relationships between the fluxes and the (stability-dependent) vertical profiles of each variable, which had been determined over uniform sites on land and were subsequently applied over the ocean. To compare observations taken in different situations, these relationships are used to reference all measured values to the "standard" height of 10m, and to define the transfer coefficient as a "neutral" value. The neutral value would give the same flux had the measurement been made at 10m height under conditions of neutral atmospheric stability, and is normally represented by C_{x10n}.

From this early work the exchange coefficient for momentum (or drag coefficient) was found to increase at higher wind speeds. A relationship suggested by Smith (1980), $C_{D10n}=(0.61+0.063U_{10n})\text{x}10^{-3}$, appears also to fit more modern data sets (Yelland et al. 1998, Drennan et al. 2005). The exchange coefficients for the "scalar" variables, sensible and latent heat, seemed to be fairly constant; for example, Large and Pond (1982) found for sensible heat $C_{H10n} = 1.13\text{x}10^{-3}$ (unstable conditions), 0.66 (stable conditions) and for moisture $C_{E10n} = 1.15\text{x}10^{-3}$. Reviews by Smith (1988,1989) concluded that $C_{H10n}=1.0\text{x}10^{-3}$ and $C_{E10n} = (1.2\pm0.1)\text{x}10^{-3}$ for winds between 4 and 14 ms^{-1}. At that stage there were few measurements below 4ms^{-1} or above 14ms^{-1}, and only recently has a clear increase of C_{E10n} as winds increase

been observed (Fairall et al. 2003). Values outside these limits were best regarded as extrapolations from the mid-range wind speeds where data was more plentiful. Further, as wind speed and atmospheric stability were usually the only variables considered, other variables such as sea state which might affect the air-sea exchange process were simply absorbed into the exchange coefficient.

The uncertainty in behaviour of the transfer coefficients, and the consequent limits to accuracy with which the fluxes could be calculated, became unacceptable as the sensitivity of climate models to the fluxes was recognised, particularly from efforts to couple ocean and atmospheric models. New bulk formulae were developed, incorporating better and more complete physical descriptions of the air-sea exchange process. The following is a brief, and by no means rigorous, account of the direction that these algorithms followed. Full details may be found in WCRP (2000) and standard texts (e.g. Kraus and Businger 1994)

The way in which the bulk meteorological variables (t, q, u) change with height above the sea surface depends on atmospheric stability, and is well known. The dimensionless profiles of the variables are given by Monin-Obhukov similarity theory (e.g. Businger et al. 1971)

$$\frac{\kappa z}{u_*}\frac{\partial \bar{u}}{\partial z}=\phi_m\,;\quad \frac{\kappa z}{t_*}\frac{\partial \bar{t}}{\partial z}=\phi_t\,;\quad \frac{\kappa z}{q_*}\frac{\partial \bar{q}}{\partial z}=\phi_q \qquad (11.2),$$

where κ (= 0.4) is von Karman's constant, and the scaling parameters (u_*, t_*, q_*) are defined with reference to the surface fluxes

$$-u_*^2=\frac{\tau}{\rho}\,,\quad -u_*t_*=\frac{H_s}{\rho C_p}\,,\quad -u_*q_*=\frac{H_l}{\rho\lambda} \qquad (11.3).$$

ρ and C_p are air density and specific heat respectively, and λ the latent heat of vaporisation. The dimensionless profiles φ_x are functions of the atmospheric stability ζ (= z/L), where

$$-L=\frac{T_v}{g\kappa}\frac{u_*^2}{\left[t_*\left(1+0.61q\right)+0.61tq_*\right]} \qquad (11.4)$$

is the Monin-Obhukov stability length (the height at which contributions to atmospheric turbulence by shear stress and buoyancy flux are roughly equal). The buoyancy flux is the quantity in square brackets, T_v [= $T(1+0.61q)$] is the virtual temperature of the air, and g the acceleration due to gravity. Over the ocean, particularly in the tropics, the contribution of moisture to buoyancy is significant. Experiments over land have established formulae for the dimensionless profiles of the form

$$\phi_m=(1-\alpha\varsigma)^{-\beta}\quad for\ \varsigma<0 \quad \text{unstable boundary layer} \qquad (11.5a)$$

$$\phi_m=(1+\gamma\varsigma)\quad for\ \varsigma>0 \quad \text{stable boundary layer} \qquad (11.5b),$$

where α, β and γ are empirically determined constants (see e.g. WCRP 2000). The observations also support the assumptions that

$$\phi_t=\phi_q=\phi_m^2\quad for\ \varsigma<0;\quad \phi_t=\phi_q=\phi_m\quad for\ \varsigma>0 \qquad (11.6)\,.$$

Both unstable and stable forms of the dimensionless profiles (11.2) can be integrated between the surface and measurement height z

$$u_z = u_0 + \frac{u_*}{\kappa}\left(\ln\frac{z_u}{z_o} - \psi_m\right); \quad t_z = t_0 + \frac{t_*}{\kappa}\left(\ln\frac{z_t}{z_{0t}} - \psi_t\right); \quad q_z = q_0 + \frac{q_*}{\kappa}\left(\ln\frac{z_q}{z_{oq}} - \psi_q\right) \quad (11.7),$$

where u_0, t_0, q_0 are the surface values, and the stability functions ψ_χ are integrals of the dimensionless profiles φ_χ. In neutral conditions the ψ_χ are zero and the profiles take the familiar logarithmic form. The heights for the wind and scalar measurements can be different; the denominators are the surface roughness lengths for each variable.

Certain aspects of these land-based equations differ when applied over the ocean. Over land $u_0 \equiv 0$, whereas the water surface is mobile. Physically, the correct wind velocity to use when calculating sea-air transfer is relative to the water surface, so when u_z is measured with respect to earth coordinates (e.g. using GPS) the surface current, u_0, should be subtracted vectorially (but see comments in section 2.5). Also, since the humidity at the air-sea interface, q_0, is calculated as the saturation vapour pressure (svp) over pure water at the SST (Clausius-Clapeyron relationship), it must be reduced by 2% to allow for the reduction of svp over saline water at 34psu (Kraus and Businger 1994).

Comparing equation (11.7) with the formal bulk flux equation (11.1) for the case of momentum,

$$\frac{-\tau}{\rho} = u_*^2 = C_D\left(u_0 - u_z\right)^2 \quad (11.8),$$

we see that the drag coefficient can be expressed as $C_D = \kappa^2\left(\ln\frac{z_u}{z_0} - \psi_m\right)^{-2}$ (11.9),

whence the 10m neutral value $C_{D10n} = \kappa^2\left(\ln\frac{10}{z_0}\right)^{-2}$ (11.10).

This emphasizes the important point that the neutral drag coefficient is directly related to the wind roughness length z_0 – the two are interchangeable. If the roughness of the sea surface can be specified, for example by a physically based wind/wave relationship or a well-founded empirical parameterization, the above equations can be solved to obtain the wind stress.

From classical studies in fluid mechanics, surface roughness and wind stress are related through the dimensionless roughness Reynolds number $R_r = u_* z_0 / \nu$, where ν is the kinematic viscosity of air. When $R_r > 2.0$ the surface wind regime is said to be aerodynamically "rough" and for $R_r < 0.13$ it is "smooth", with R_r approaching a constant value of about 0.11 as wind speed decreases. Over the ocean these limits on R_r correspond to 10m wind speeds of about 8ms^{-1} and 2ms^{-1} respectively; in between is a transition regime between rough and smooth flow.

On the basis that the ocean roughness results mainly from gravity waves generated by wind stress, Charnock (1955, 1958) proposed that $z_0 = \alpha_c u_*^2 / g$, where g is the acceleration due to gravity and α_c is Charnock's "constant". However, the wide range of values found for α_c signal that wind/wave characteristics are more complicated than this simple relation suggests. Smith (1988) proposed that the entire smooth to rough flow regime be written,

$$z_0 = \frac{\alpha_c u_*^2}{g} + 0.11\frac{\nu}{u_*} \qquad (11.11),$$

but this only fits the data if α_c is allowed to vary. The transfer coefficients for heat and moisture depend on both the momentum roughness length, and those for temperature and humidity, which can be similarly parameterized as $R_t = u_* z_{0t} / \nu$ and $R_q = u_* z_{0q} / \nu$. By considering physical transfer processes across the interface using surface renewal theory, in which small eddies transfer heat intermittently between the bulk and the ocean surface, Liu et al. (1979) determined empirical relationships between R_r, R_t, and R_q. This approach is the basis of some modern bulk algorithms, which solve equations for the fluxes, profiles and atmospheric stability iteratively. The bulk algorithm developed for community use in the TOGA-COARE experiment (Fairall et al. 1996b, 2003) is described in Appendix B.

In recent years, the imperatives of climate research which set the $10 \mathrm{Wm}^{-2}$ goal for net air-sea flux measurement has also led to greatly improved measurements, extending the wind speed range over which the exchange coefficients are valid. There remain difficulties at high winds (> ~$20 \mathrm{ms}^{-1}$) when spray droplets contribute to the transport of heat and water vapour, for which reliable parameterizations have yet to be developed. At very low winds, equation 11.1 predicts vanishing fluxes at zero mean wind. In reality, this limit is usually associated with variable, gusty winds which transport energy and stress even when the vector mean wind is zero (Bradley et al.1991). Godfrey and Beljaars (1991) avoid this problem by introducing a "gustiness" velocity, u_g, proportional to the convective scaling velocity for the atmospheric boundary layer W_*, (Deardorff 1970) where

$$W_*^3 = \frac{g}{T}\left[\frac{H_s}{\rho C_p} + 0.61 T \frac{H_l}{\rho \lambda}\right] z_i \qquad (11.12),$$

so that $u_g = \beta W_*$, the constant β to be determined empirically. (11.13).

The seastate (wave characteristics) and surface current also modify fluxes, the surface currents by changing the wind shear. A current moving in the same direction as the wind will result in smaller surface fluxes, while currents running counter to the wind will increase them. A situation can be imagined in which changing tidal currents cause variation in the fluxes under a constant wind. The magnitude of the vector difference of the wind and the surface current should replace wind speed in flux calculations, with the stress in the direction of the vector difference.

There have been many approaches to parameterize the influence of waves on surface stress. Most agree that the stress is larger when the wind waves (wave supported by the local winds) are relatively steep. This effect can be explained in terms of wave age (which has several different definitions), and usually parameterized through the drag coefficient. For example, short and sharp waves that initially form when there is sufficient wind over a smooth surface have a much larger drag coefficient than very tall, long and gently rolling waves. There is no convincing evidence that waves influence transfer coefficients for heat and moisture.

The influence of swell, waves produced by distant winds and not supported by the local winds, are more controversial. Wind waves tend to propagate in a direction parallel to the wind vector. Swell propagating in other directions has been observed to cause large variability in the traditional drag coefficient, which cannot be explained in terms of wave age. An alternative approach, which considers wave-related modifications in a similar manner to the current

modifications discussed above rather than the drag coefficient, has shown promise for both wind waves and swell, and is an area of ongoing research.

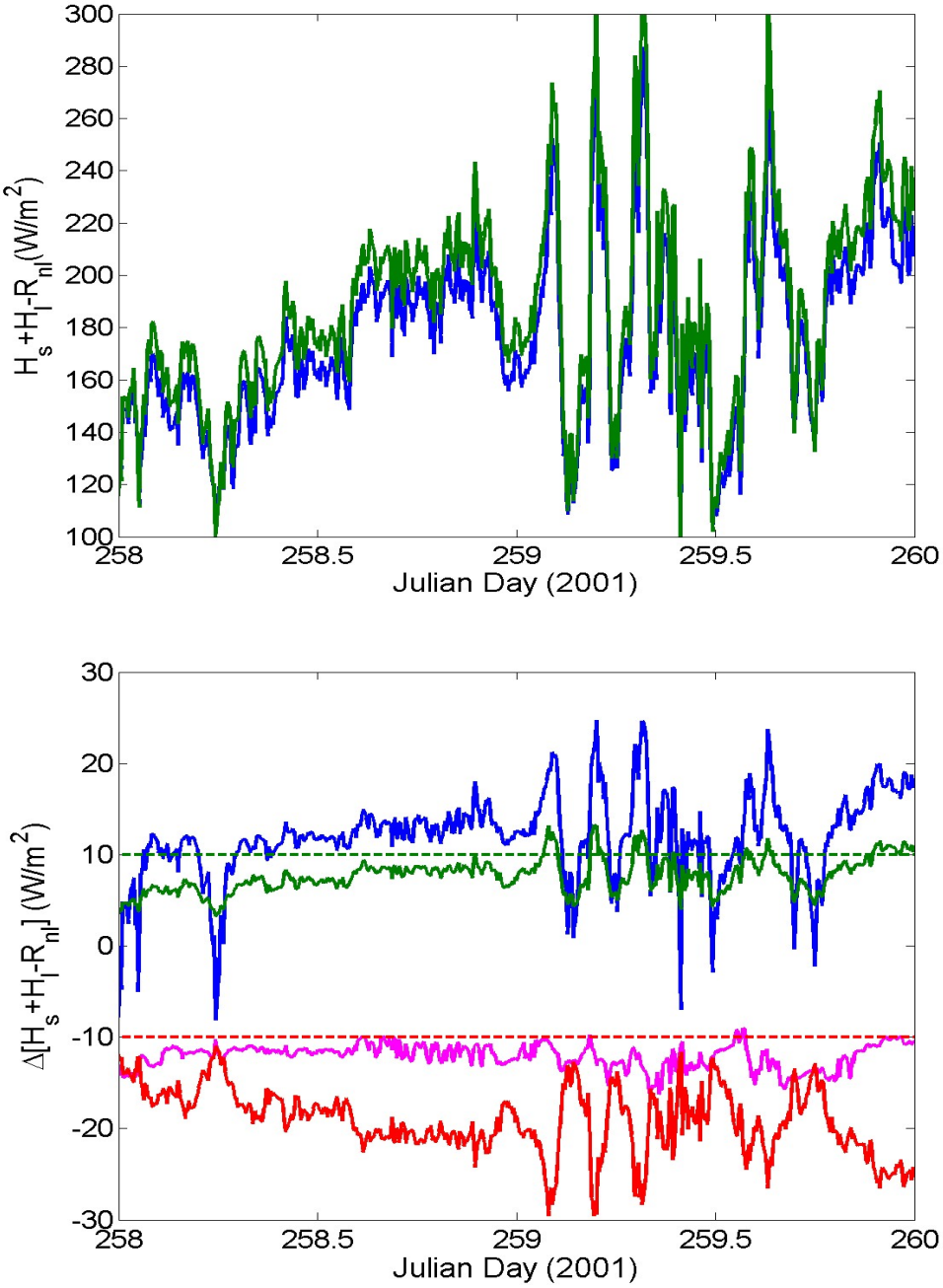

Figure 11.1. Sensitivity of bulk flux calculations to algorithm and input data; time series of sum of sensible, latent, and net longwave fluxes. Upper panel: COARE 3.0 (C3 blue) and Large and Pond (LP green). Lower panel: LP - C3 (blue), C3(Ts-0.5) - C3(Ts) (red), C3(qa-0.5) - C3(qa) (green), and C3(U - 0.5) – C3 (mauve).

Figure 11.1 looks at the **ocean heat loss terms** in equation 1.1 to examine the effect of different algorithms or small biases in the data. The upper panel is computed using two of the best known bulk flux algorithms, Large and Pond (1982; LP) and COARE3.0 (Fairall et al. 2003, C3). These are from different eras and contain different functions and assumptions, so this is not intended to evaluate them, but rather to provide natural differences in calculated fluxes. We consider the two consecutive but contrasting days of figures D1 and D2 with wind speeds in the range 3-6 ms^{-1}.

The lower panel shows the difference between LP and C3 (blue trace). LP produces greater ocean cooling, by around 10-15 Wm^{-2} on the steady day, but more variable and as much as 25 Wm^{-2} on the convective day. The other three traces indicate the effect of a realistic error (an electronic signal offset or calibration error for example) in the input data to the COARE3.0 flux algorithm. The ±10 Wm^{-2} target accuracy is indicated by the green and red dashed lines. An error in specific humidity of -0.5 gkg^{-1} (drier air) will increase latent heat flux and hence produce too much ocean cooling, by around 10 Wm^{-2} in this example (green trace); an error which reduces true wind speed by 0.5 ms^{-1} will reduce both latent and sensible heat loss totalling 10 Wm^{-2} (mauve trace); a -0.5ºC error in sea temperature affects sensible and latent heat, and also reduces the outgoing longwave radiation, the three effects together assigning around 20 Wm^{-2} too much warming of the ocean (red trace).

These figures assume that only one of the input variables is in error, while the other two are exact. In practice this is unlikely, hence the more stringent accuracy requirement given in Table 1. Note also that use of the routine ship weather observations, which Figure 3.2 showed can contain significant errors, will not produce air-sea fluxes of sufficient accuracy for climate studies without careful analysis and corrections to the observations.

.**Appendix A - useful formulae, parameters, and conversions**

Studies of the atmospheric and oceanic surface layers, and the transport of energy and matter across the interface between them, involve the dynamic and thermodynamic properties of the respective fluids, air and seawater. The following equations and values are frequently needed in the analysis following measurements of the state variables, air temperature, pressure, density, moisture content. In some cases they are not strictly rigorous - simplifications are made by neglecting small quantities, insignificant in the present context. More complete derivations are given in Andreas (2005). Comprehensive discussions of atmospheric thermodynamics can be found in standard texts, e.g. Garratt (1992), Bohren and Albrecht (1998).

Equations of State

Temperatures in degree Kelvin are denoted by T and in Celsius by t, where $T = t + 273.16$ K

Quantities relevant to the thermodynamic properties of moist air are:

The universal gas constant	$R = 8.3145$	(J mol^{-1} K^{-1})
Molecular mass of dry air	$m_a = 0.028965$	(kg mol^{-1})
Gas constant for dry air	$R_a = R/m_a = 287.05$	(J kg^{-1} K^{-1})
Molecular mass for water vapour	$m_v = 0.018015$	(kg mol^{-1})
Gas constant for water vapour	$R_v = R/m_v = 461.5305$	(J kg^{-1} K^{-1})

From the ideal gas law we obtain the density of dry air as:

$$\rho_a = (p - e)/R_a T \qquad \text{(kg m}^{-3}\text{)},$$

with temperature T in kelvins and (p - e) pressure in Pascals (100Pa=1mb). Note, to compute the *dry air* density we must remove the pressure contribution of water vapour from the pressure gauge reading. At standard temperature (273.15K = 0°C) and pressure (101325.0Pa = 1013.25mb) $\rho_a = 1.2922$ kg m^{-3}.

The behaviour of water vapour in the atmospheric surface layer approximates that of an ideal gas so that its *density* is given by

$$\rho_v = 100\, e / R_v T \qquad \text{(kg m}^{-3}\text{)},$$

where traditionally in meteorology e is the partial pressure of water vapour in millibars (mb). The vapour density is also referred to as the *absolute humidity*.

Other ways of specifying the water vapour content in a sample of moist air are:

Mixing ratio $\quad r = \rho_v / \rho_a = 0.622 e/(p - e)$ $\quad$ (kg kg^{-1} of dry air)

where the factor 0.622 = m_v/m_a , and the barometric pressure p and e are in the same units.

Specific humidity $\quad q = \rho_v / \rho = 0.622 e/(p - 0.378 e)$ $\quad$ (kg kg^{-1} of moist air)

where the factor 0.378 = (1 - m_v/m_a), and the density of moist air

$$\rho = \rho_a + \rho_v = 100\, p/(R_a T (1 + 0.61 q)) \text{ (kg m}^{-3}\text{)}.$$

The factor 100 converts from mb to Pa, and 0.61 = (m_d/m_v-1). The quantity $T(1+0.61q)$ is called the *virtual temperature* T_v , the temperature that air of given pressure and density would have if it were completely free of water vapour.

Saturation vapor pressure $e_s = 6.1121\,(1.0007 + 3.46x10^{-6}\,p)\,\exp(17.502\,t/(240.97 + t))$ (mb), with t (°C) air temperature**,** and p (mb) atmospheric pressure. This empirical expression is valid above pure water between -20° and 50°C (Buck, 1981)

Some relationships below require a value of the *saturation vapor pressure* (svp).

Above seawater the svp is depressed to $e_{sea} = e_s\,(1 - 0.000537S)$ (mb)

where S is salinity (psu). If S = 35 psu, $e_{sea} = 0.981e_s$ or roughly 2% less than over pure water.

Relative humidity $RH = 100(e/e_s)$ *as %* *or* (e/e_s) *as a fraction*

Dew point T_d : for given *e,* T_d may be obtained by inverting the *svp* equation. But most usually T_d is measured (see section 3.3) and *e* calculated by putting $t = Td$ (°C) in the *svp* equation.

Specific heat of dry air at constant pressure is given by the polynomial,

$$C_p = 1005.6 + 0.0172t + 0.000392t^2 \qquad (\text{J kg}^{-1}\ ^\circ\text{C}^{-1})$$

valid in the range ±40°C and for barometric pressures around one atmosphere. The temperature dependence is weak, and a constant value of 1006 J kg^{-1} °C^{-1} is usually adequate.

Latent heat of vaporization $\lambda_v = (2.501 - 0.00237t)\times 10^6$ (J kg^{-1}),

with the constant value 2.50×10^6 J kg^{-1} being accurate enough for most purposes in the surface layer.

Psychrometric equation $$e = e_s(t_w) - \frac{m_a}{m_v}\frac{C_p}{\lambda_v}(t - t_w)\,p \quad (\text{mb}),$$

where $e_s(t_w)$ is the *svp* at wet-bulb temperature t_w , $(t - t_w)$ is the *wet-bulb depression* and p the barometric pressure. The factors before the parenthesis are known as the *psychrometric constant*. Using the constant values quoted above, and combining with p = 1013.25 mb (the standard atmosphere at sea level), the practical psychrometer equation is usually written

$$e = e_s(t_w) - 0.66\,(t - t_w) \qquad (\text{mb}),$$

where t and t_w are referred to as dry-bulb and wet-bulb temperatures (°C) respectively.

Kinematic viscosity of dry air

$$\nu_a = 1.326\times 10^{-5}\,(1 + 6.542\times 10^{-3}t + 8.301\times 10^{-6}t^2 - 4.840\times 10^{-9}t^3)\ (\text{m}^2\ \text{s}^{-1})$$

valid for the temperature range t = ±50°C.

Dry adiabatic lapse rate $$\left(\frac{\partial t}{\partial z}\right)_{\Theta = const.} = -\frac{g}{C_p} = -\Gamma_d = -0.0098\ ^\circ\text{C m}^{-1}$$

where Θ is the potential temperature.

Ice-related expressions

Latent heat of fusion of ice $\lambda_f = 0.334 \times 10^6$ (J kg^{-1})

Saturation vapor pressure over ice (or snow)

$$e_s = 6.1115\,(1.0003 + 4.18x10^{-6}\,p)\exp(22.452\,t/(272.55 + t)) \quad \text{(mb)}$$

valid for $-50° \le t \le 0°$ (Buck, 1981)

Specific heat of ice $c_{pice} = -114.19 + 8.1288T + 3.421T\exp[-(T/125.1)^2]$ (J kg^{-1} K^{-1})

Radiometry

The following values of albedo and emissivity of the ocean surface were obtained during the TOGA-COARE campaign, and are broadband and isotropic.

Short-wave albedo of sea surface $\alpha = 0.055$

Long-wave emissivity of sea surface $\varepsilon = 0.97$

Stefan-Boltzmann constant $\sigma = 5.670 \times 10^{-8}$ (Wm^{-2}K^{-4})

Pyrgeometer equation $R_{l\downarrow} = V/s + \sigma T_c^4 + B\sigma(T_c^4 - T_d^4)$ (Wm^{-2})

with thermopile out put V (μV) and calibration factor s (μV/(Wm^{-2}), T_c and T_d temperatures (K) of the instrument case and dome respectively, and B a factor representing the IR transmission and absorption characteristics of the dome. For a given instrument, s will be given but B may not, in which case the value $B = 3.5$ is a fair average.

Outgoing long-wave radiation $R_{l\uparrow} = \varepsilon\sigma T_s^4 + (1-\varepsilon)R_{l\downarrow}$ Wm^{-2}

where T_s is the ocean surface temperature (K), ε (= 0.97) its emissivity and σ (= 5.67x10^{-8}) the Stefan-Boltzmann constant

Barometer correction

Near the surface, atmospheric pressure falls at about 0.12 mb m^{-1} as height increases. Since we need the value near the surface and the barometer is usually on the bridge, some tens of metres higher, we make a correction based on the hydrostatic equation for the atmosphere,

$$\frac{1}{\rho_a}\frac{\partial p}{\partial z} = -g$$ where z is height, p pressure and g the acceleration due to gravity.

Introducing the ideal gas law, integrating this expression from observation height to the surface and simplifying we have for the surface pressure

$$p_s = p\exp(gz/R_aT)$$

where p is the observed pressure at height z, R_a is the gas constant for dry air, and T (K) is a reference temperature (e.g. at z = 10m). For example, if the pressure at barometer height of 30m was 1000.0mb, with g = 9.81 ms^{-2}, R_a = 287.05 Jkg^{-1}K^{-1} and T = 290K, p_s = 1003.54 mb.

Conversions

1 nautical mile (nm) = 1.852 km by definition

1 knot = 1.852 kmhr^{-1}= 0.51444 ms^{-1}

1 standard atmosphere = 1013.25 mb

Standard gravity g = 9.80665 ms^{-2}

Latent heat flux of 100 Wm^{-2} evaporates 3.456 mm water per day

Gravity

Acceleration due to gravity, g (ms^{-2}) is calculated as a function of latitude at sea level by the expression

$$g = 9.78033(1 + (0.0053\sin^2\phi - 5.8\times10^{-6}\sin^2 2\phi))\ \text{(m s}^{-2}\text{)}$$

or by the polynomial

$$g = 9.7803267715\times(1 + c1\sin^2\phi + c2\sin^4\phi + c3\sin^6\phi + c4\sin^8\phi)\ \text{(m s}^{-2}\text{)}$$

where c1 = 0.0052790414
c2 = 0.0000232718
c3 = 0.0000001262
c4 = 0.0000000007

These two methods agree to four places of decimals. They give g = 9.7803 and 9.8322 ms^{-2} at the equator and the poles respectively. The standard value 9.80665 ms^{-2} is given at latitude ~ 45.5°

Relative wind conversions aboard ship

Conversion of Relative to True wind speed and direction

"True" wind and direction will be defined as being in earth-relative coordinates

Directions follow the meteorological convention – "northerly" winds are *from* the north, "easterly" *from* the east.

Then cog = ship's course over ground from GPS
sog = ship's speed over ground from GPS
head = gyrocompass heading, north=0° east=90°
rels = relative wind speed
reld = relative wind direction, 0° over bow 90° over starboard

relsn = rels.cos(head+reld) northerly component of relative wind
relse = rels.sin(head+reld) easterly component of relative wind

sogn = sog.cos(cog) north component of ship speed
soge = sog.sin(cog) east component of ship speed

un = relsn-sogn northerly component of true wind (-ve sign because wind dir. "from").
ue = relse-soge easterly component of true wind (-ve sign because wind dir. "from").

dirt = mod(atan2(ue,un)+360,360) true wind direction
ut = $(un^2 + ue^2)^{1/2}$ true wind speed

Notes. The above implies that angles are expressed in degrees. Some computer software requires that angles be expressed in radians, and entering degrees can generate bewildering results. – in this case angles should be multiplied by the factor rdcon = *pi*/180 (*pi* = 3.14159).

The atan2 function is commonly available in software such as Matlab, Fortran, Excel…. It computes, in our case, the arc tangent of *un/ue*, returning an angle in the range *–pi* to *+pi*, expressed in radians, using the signs of *un* and *ue* to compute the quadrant of the result. If the calculation is done by hand, care must be taken to resolve the ambiguity of the *arctan* function.

Conversion of Relative to Water-relative wind speed and direction

Certain applications, in particular air-sea flux calculation, require the wind speed relative to the surface water (see section 2.5 and equation 11.7 et seq.). We call this the "water-relative" wind. When the near-surface current speed and direction (earth-relative) are available (e.g from a surface mooring) this current can be resolved into north and east components cn and ce. These would normally be in the oceanographic convention "to". Then, having regard to this bizarre convention, the true wind components can be converted to water-relative, and the water-relative wind speed uw = $[(un+cn)^2 + (ue+ce)^2]^{1/2}$ which is equivalent to $(u_z - u_0)$ in equation 11.7.

Alternatively uw may be obtained by replacing *cog* and *sog* with course and speed from the ship's 2-axis Döppler-log and gyro-compass, as follows:

uf = forward speed from Döppler-log
us = side-slip to starboard (positive)
head = gyro-compass heading, north=0° east=90°
rels = relative wind speed
reld = relative wind direction, 0° over bow 90° over starboard

relsn = rels.cos(head+reld) northerly component of relative wind (as before)
relse = rels.sin(head+reld) easterly component of relative wind (as before)

sown = uf.cos(head)-us.sin(head) north component of ship speed
sowe = uf.sin(head)+us.cos(head) east component of ship speed

unw = relsn-sown northerly component of water-relative wind (-ve sign, wind dir. "from").
uew = relse-sowe easterly component of water-relative wind (-ve sign, wind dir. "from").

dirw = mod(atan2(uew,unw)+360,360) water-relative wind direction
uw = $(unw^2 + uew^2)^{1/2}$ water-relative wind speed

where again uw is equivalent to $(u_z - u_0)$ in equation 11.7.

The above comments regarding the mode of angles and use of atan2 apply.

These issues and other aspects of the reporting of true wind are discussed in considerable detail by Smith et al. (1999).

Appendix B – the TOGA-COARE Bulk Flux Algorithm

B1. History and features

In 1993, as part of the TOGA-COARE Air-Sea Interaction (Flux) Working Group activity, Chris Fairall, Frank Bradley and David Rogers began development of a bulk air-sea flux algorithm for use by the COARE community. The purpose was to ensure that the bulk flux results from every measuring platform were derived from identical assumptions, physical functions and computational methods. Faced with the challenging net heat flux accuracy target of 10 Wm^{-2}, any disagreements would be due to the basic observations, not differences in the bulk algorithm. In some respects, the same situation applies to the SAMOS initiative.

The COARE algorithm had to take account of the light wind, strongly convective conditions found in the region of the tropical Pacific warm pool. It was based on the model of Liu, Katsaros and Businger (1979, LKB), which used the formalism of Monin-Obhukov similarity theory for the atmospheric surface layer, solving equations (11.2) to (11.7) iteratively for the surface fluxes. The velocity roughness was specified by the Charnock/Smith expression (11.11), and the scalar roughness lengths from relationships between the velocity and scalar roughness Reynolds numbers given by LKB. Independent estimates of α_c (=0.011) and the gustiness parameter, β (=1.20) in equation (11.13) were made from covariance and dissipation flux measurements made during COARE. The *unstable* profile functions were a blend of the Kansas functions, ψ_k, near neutral (Businger et al., 1971) with a form, ψ_c, that obeys the theoretical scaling limit in highly convective conditions (Fairall et al., 1996b). The *stable* forms were as determined for Kansas.

At version 2.5b the COARE bulk flux algorithm was made generally available (Fairall et al. 1996b). Its major shortcomings were that the exchange coefficients were based on less than 1000 hours of directly measured fluxes and solely on COARE data, so was effectively "tuned" to tropical conditions with few wind speed observations greater than 10ms^{-1}. Clearly the algorithm needed to be generalized for more global applications, and tested against a much broader dataset. By 1999 Fairall's group at NOAA/ETL had undertaken cruises in all ocean basins (Fairall et al., 1997). From these a flux database of over 7200 h was assembled, including 800 h with wind speeds in excess of 10 ms^{-1}, and 2200 h at high latitudes. It was augmented with 94 h of high wind data from the HEXMAX experiment (De Cosmo et al.,1996). A subset of this data was used to refine the algorithm as version COARE 3.0, and it was tested against the entire database (Fairall et al., 2003).

Codes are available at ftp://ftp.etl.noaa.gov/user/cfairall/bulkalg/cor3_0/ and accompanied by a "readme" description. Inputs required are time series of the meteorological variables, together with the height (or depth) of measurement; i.e. date, time, wind speed, air temperature and humidity, sea temperature, downward short and long-wave radiation, rainfall, latitude, longitude. The radiation data is required for the calculation of ocean surface warming, and the ship's position for gravity and the solar time.

Features of version 3.0 are as follows:

1. Below 10 ms^{-1} the Charnock parameter in equation (11.11) retains the value ($\alpha_c = 0.011$), but above 10 ms^{-1} takes a simple wind-speed dependence based on data from various sources (e.g. Hare et al., 1999).

2. The Liu et al. (1979) scalar roughness relationship has been replaced with a much simpler one that fits both the COARE and HEXMAX data bases, $z_{0t} = z_{0q} = 5.5 \times 10^{-5} R_r^{-0.6}$.

3. A gustiness factor (equations 11.12 and 11.13) is calculated in the flux loop, using $\beta = 1.25$ determined from COARE measurements, and applied as $\sqrt{(u^2 + u_g^2)}$ to avoid singularity as u→0.

4. An empirical constant in the *convective* portion of the scalar profile function has been optimized to match direct profile observations (Grachev et al., 2000).

5. The Kansas *stable* profile functions (Businger et al., 1971) have been replaced by those from Beljaars and Holtslag (1991) which compare well with new profile data taken over the Arctic ice cap (Persson et al., 2002) and appear to be a better fit at extreme stability.

6. The stability iteration loop uses a bulk Richardson number parameterization as a first guess (Grachev and Fairall, 1997), thus reducing calculation time and making the algorithm more attractive for use in numerical models.

7. SST (skin temperature) can be obtained from measurements at depth, using models of the diurnal warm layer and cool skin (see section 2.6, Fairall et al., 1996a and Wick et al., 2005). The models require downwelling long- and short-wave radiation data; values for broadband surface albedo and ocean emissivity are taken as 0.055 and 0.97 respectively (from COARE observations). These optional models are not used if SST is obtained using an infra-red or microwave radiometer.

8. An option has been included to allow the velocity roughness to be calculated from wave parameters. We have taken two models from the recent literature that are wave age and/or wave slope based. Oost et al. (2000) requires the wave period to be specified, and Taylor and Yelland (2001) need both wave period and significant wave height. However, these schemes have not been tested with reliable wave measurements.

9. The so-called Webb correction (Webb et al. 1980) to latent heat flux arises from the requirement that the net dry mass flux be zero. The latent heat flux is therefore formulated in terms of mixing ratio, the fundamentally conserved quantity, instead of specific humidity. However, the model returns the mean Webb velocity, which can be used to compute Webb corrections for any trace gas or particle fluxes measured simultaneously.

10. The momentum and sensible heat fluxes due to rainfall are calculated (Caldwell and Elliott, 1971; Gosnell et al. 1995).

B2. Examples of COARE3.0 performance

The essence of the bulk flux scheme is the specification of roughness lengths or, equivalently, of the 10-m neutral transfer coefficients. Version 3.0 is based on averaging thousands of data points; in Figure B1 the actual data are shown with the model. An example of the model's ability to yield the correct values, on average, for fluxes is shown in Figure B2 where both model-derived and measured latent heat fluxes have been composited in wind speed bins (the lines denote means and the symbols denote medians). The agreement is excellent from 0 to 20 m/s. Another way to view the state of the transfer coefficients is to ratio with the Version 3.0 specifications (Figure B3). Here the ETL data are shown as points with statistical uncertainties in the mean quantity. The dashed lines are the transfer coefficients used by the two major operational weather forecast centers (NCEP and ECMWF). NCEP recently replaced their model (labeled 'old' in the figure) with a derivative of the COARE 2.5 model. The operational parameterizations are now within 10% of the ETL data and the COARE algorithm for wind speeds from 0 to 20 m/s.

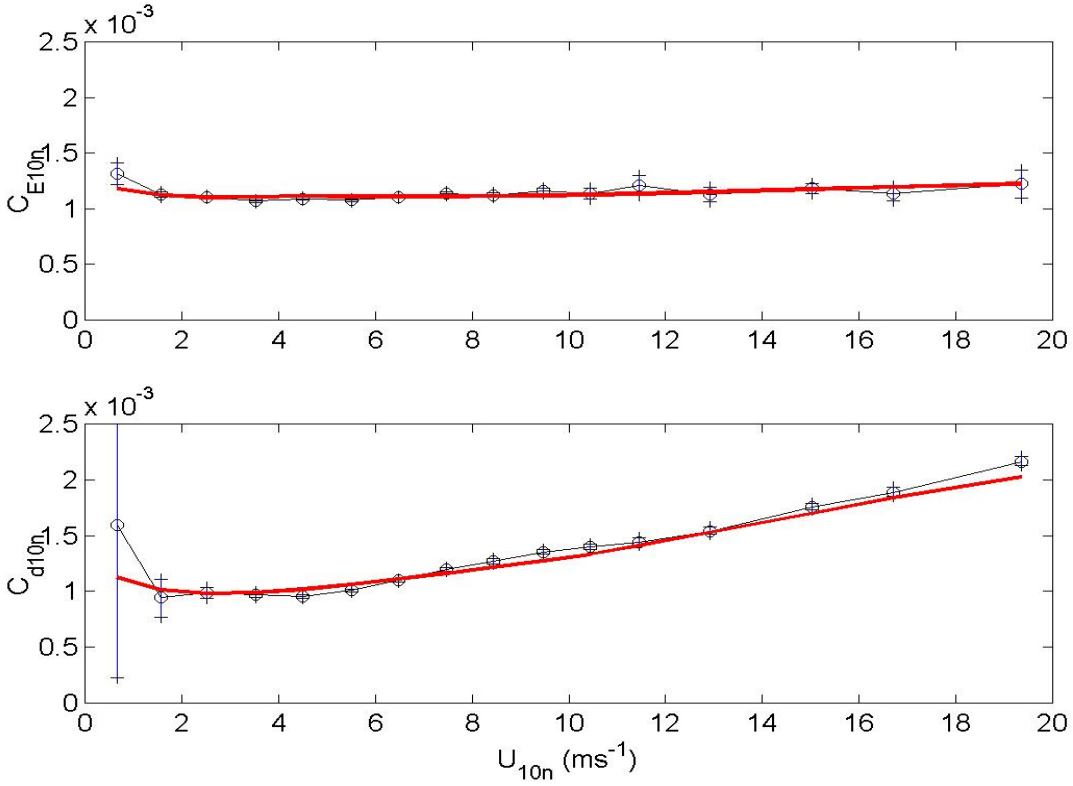

Fig. B1. Wind speed dependence of the momentum (lower panel) and scalar transfer (upper panel) coefficients for COARE versions 3.0 (solid line) and measurements (thin line with circles)

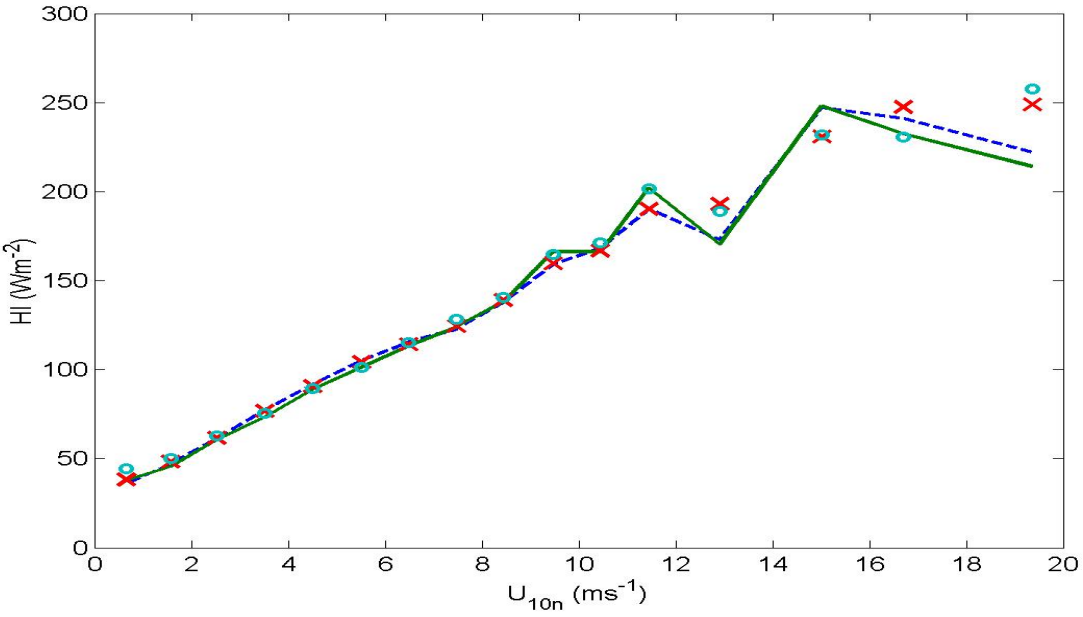

Fig. B2. The average of covariance and ID latent heat fluxes computed in 10-m neutral wind speed bins. Mean values are shown by lines and medians by symbols: the solid line and circles are measured fluxes, and the broken line and crosses are calculated with COARE 3.0.

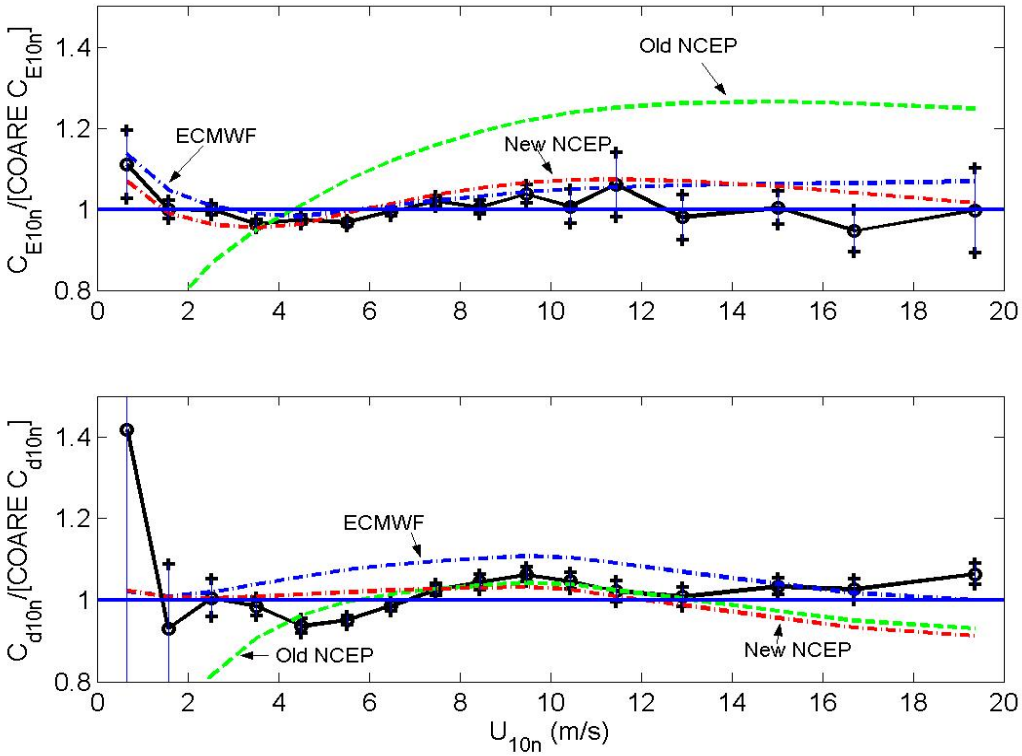

Fig. B3. The average wind speed dependence of 10-m neutral transfer coefficients divided by the COARE 3.0 values [Upper panel, C_{e10n}; lower panel C_{d10n}]. The dashed lines are NCEP and ECMWF formulae (as labeled); the solid line with symbols is the average ETL data.

Appendix C - IR radiative flux errors caused by objects in the field of view.

Calculations of errors in standard PIR radiative flux radiometers (pyrgeometer) begins with the relationship of the radiance (radiant flux from a particular location in the sky), I, to the irradiance (total flux normal to a horizontal plane), R (W/m^2)

$$R = \iint I(\theta,\varphi)\cos(\theta)d\Omega\,.$$

where φ is the azimuth angle, θ the zenith angle, and $d\Omega=\cos(\theta)d\theta d\varphi$ the incremental solid angle.

A pyrgeometer measures the downwelling IR radiation integrated over the hemisphere of the sky. If we assume the downwelling IR is isotropic (independent of φ and θ), the integral for a PIR with an unobstructed view of the sky becomes

$$R = I_0 \int_{-\pi}^{\pi} d\varphi \int_{0}^{\pi/2} \cos^2(\theta)d\theta = \pi^2/2I_0 = \sigma T_{sky}^4$$

where σ is the Stefan-Boltzmann constant, and T_{sky} an effective radiative temperature for the sky.

In fact, the IR radiation is somewhat anisotropic. At low elevation angles, the radiation temperature is close to the air temperature and at zenith it is lower than T_{sky}. The approximation used here will overestimate the effect of objects near the horizon and underestimate for objects near zenith.

We can also compute this integral for the energy received by the PIR from an object of intensity I_x in the field of view defined by some width w and some height h with its bottom some distance d away. In this case, we do the integral from $\pm\delta\varphi$ and 0 to $\delta\theta$ where the angles depend on h

$$\delta\varphi = atn(w/2/d)$$
$$\delta\theta = atn(h/d)$$

where δθ describes the elevation angle of the object above the horizon. This yields

$$R = I_1 \int_{-\varphi}^{+\varphi} d\varphi \int_{\pi/2-\delta\theta}^{\pi/2} \cos^2(\theta)d\theta = I_1\delta\varphi[\delta\theta + \cos(\delta\theta)\sin(\delta\theta)] = f\sigma T_x^4$$

where T_x is the temperature of the object in question and

$$f = \frac{2}{\pi^2}\delta\varphi[\delta\theta + \cos(\delta\theta)\sin(\delta\theta)]$$

It now follows that the flux error (i.e., additional flux sensed by the PIR) is simply

$$\Delta R = f\sigma(T_x^4 - T_{sky}^4)$$

We show two figures of examples of estimated errors for a 10-m tall pole of width 10 cm, a 10-m mast of width 30 cm, and a nearby ship bulkhead that is 6 m wide and 3 m high. The examples are for typical mid-latitude clear sky conditions (T_{sky}=0ºC). One figure is for the object at roughly ambient air temperature, the other for an object warmed considerably by bright sun. In each case, the height given describes the height of the object that is higher than the PIR (i.e., it is in the field of view). The results are given as a function of distance of the object from the PIR.

In the case of the pole, the correction might be useful for a PIR mounted on the side of the pole or mounted on a forward rail where there are antennas or GPS receiver poles nearby. The mast example might be useful when mounting a PIR on the side of a mast. The bulkhead example describes the situation where a PIR is mounted on a lower deck some distance from higher parts of the ship (e.g., the bridge deck). Finally, note that the effects described here are functions of the angular size of the object (distance does not enter in to it except as it relates to the angle). Thus, a 10 m tall 10 cm wide pole 10 m away has the same effect as a 5 m tall 5 cm wide pole 5 m away (because $\delta\varphi$ and $\delta\theta$ are the same). Also, the temperature effects scale almost linearly.

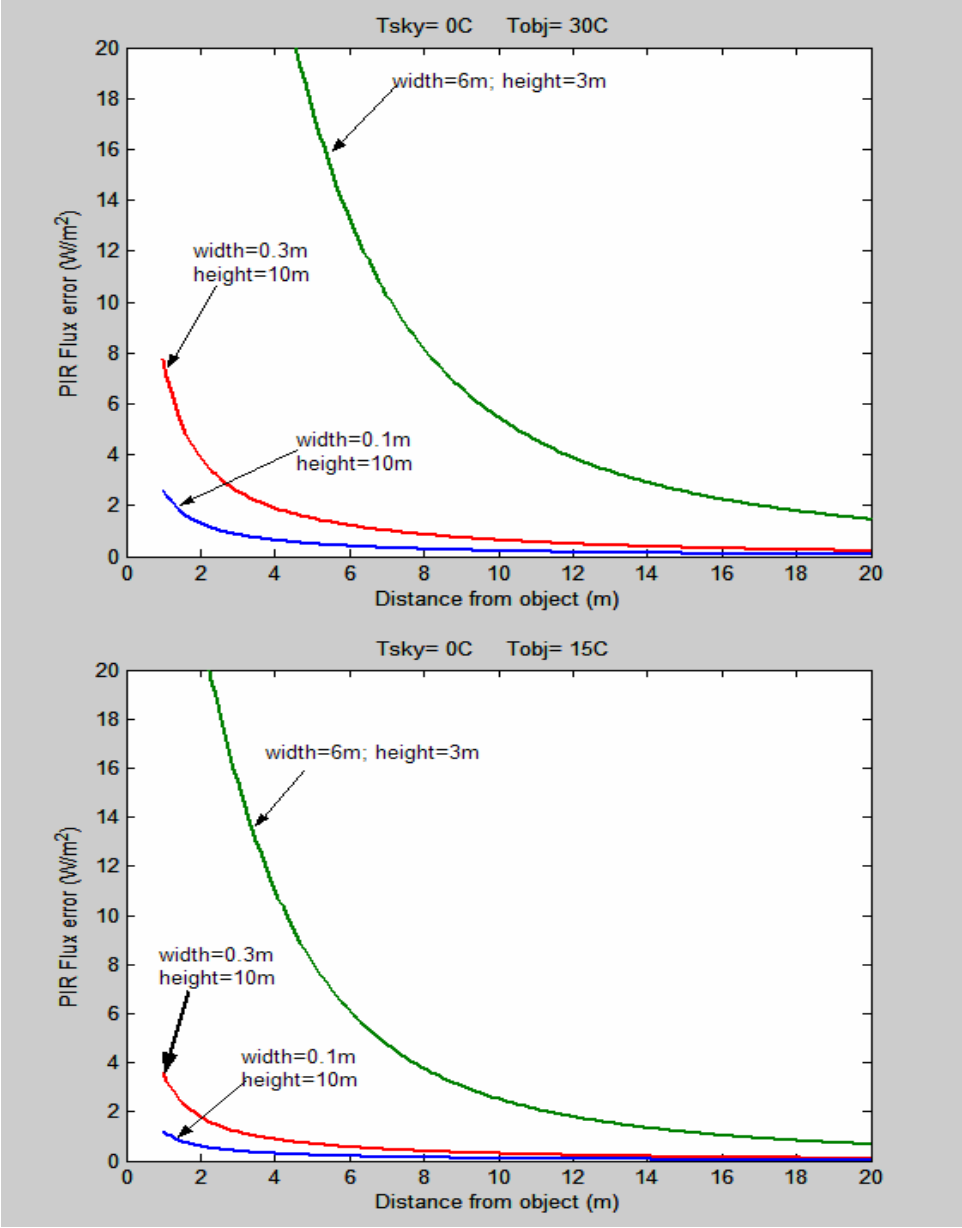

Figure C1. Longwave flux errors caused by shipboard objects in the field of view of a pyrgeometer; a tubular pole (blue), a mast (red), and a bulkhead (green). The assumed radiative sky temperature 0ºC is typical of mid-latitude clear sky conditions. The lower panel is for an object at roughly ambient temperature; the upper panel is for an object warmed considerably by strong sun.

Appendix D – Examples of meteorological observations and fluxes

The magnitude and behaviour of the meteorological variables, and the resulting bulk air-sea fluxes is illustrated in the following figures. We give two contrasting cases in tropical waters, on consecutive days from EPIC2001, and one from a mid-latitude cruise (Stratus-5, 2005).

Figure D1 shows that conditions on Day 258 were fairly steady with no sign of convective activity. There was no rain, although the solar trace R_s indicates broken cloud. The wind steadily increased from around 2 to 5 ms^{-1} during the course of the day. During the daylight hours, the wind was probably strong enough to prevent the formation of a warm layer, and the air-sea temperature difference was remarkably steady. Consequently the sensible and latent heat fluxes increased modestly, without major fluctuations. The fairly high 420 Wm^{-2} of downward longwave radiation was mainly due to the high humidity typical of the atmospheric boundary layer over the tropical ocean; at a temperature of 30ºC the ocean surface emits about 465 Wm^{-2} of thermal energy so that R_{nl} is a loss of 45 Wm^{-2}. So the net energy is a loss to the ocean at night, and a gain due to solar absorption during the day.

In contrast (Figure D2), Day 259 was convectively active, with a series of rainstorms throughout the night. These were accompanied by increasing wind speed and humidity, while the air cooled through several degrees from the associated downdrafts. Over this period the sea surface temperature decreased only slightly (~ 1ºC) so the air-sea temperature difference varied considerably, reflected in variability of the turbulent heat fluxes. Note that the rain produced more ocean cooling than any other flux component at the time of the storm. The solar trace indicates considerable cloudiness, although the solar energy still peaked at over 1000 Wm^{-2}. However, the cloud caused much greater variability and larger values in downward longwave radiation than on the previous day.

The Stratus cruises study the climatology of the stratus cloud deck off the west coast of Ecuador, Peru and Chile. Day 287 of the 2005 cruise (Figure D3), contrasts markedly with the tropical examples; stronger winds (consistently around 9 ms^{-1}) sea temperature lower by about 10ºC, lower humidity, and the persistent stratus cloud cover. The air-sea temperature difference varied somewhat but, as with the tropical examples, H_s was very small. The drier air had two consequences for fluxes, tending to increase H_l and decrease R_l . However, because of the lower sea temperature, outgoing longwave radiation was only about 400 Wm^{-2} so **net** longwave was small until breaks in the cloud cover late in the day. Despite the persistent cloud, shortwave radiation is substantial and the net heat input to the ocean is as in the other two examples; a small loss throughout the night and a gain during the day.

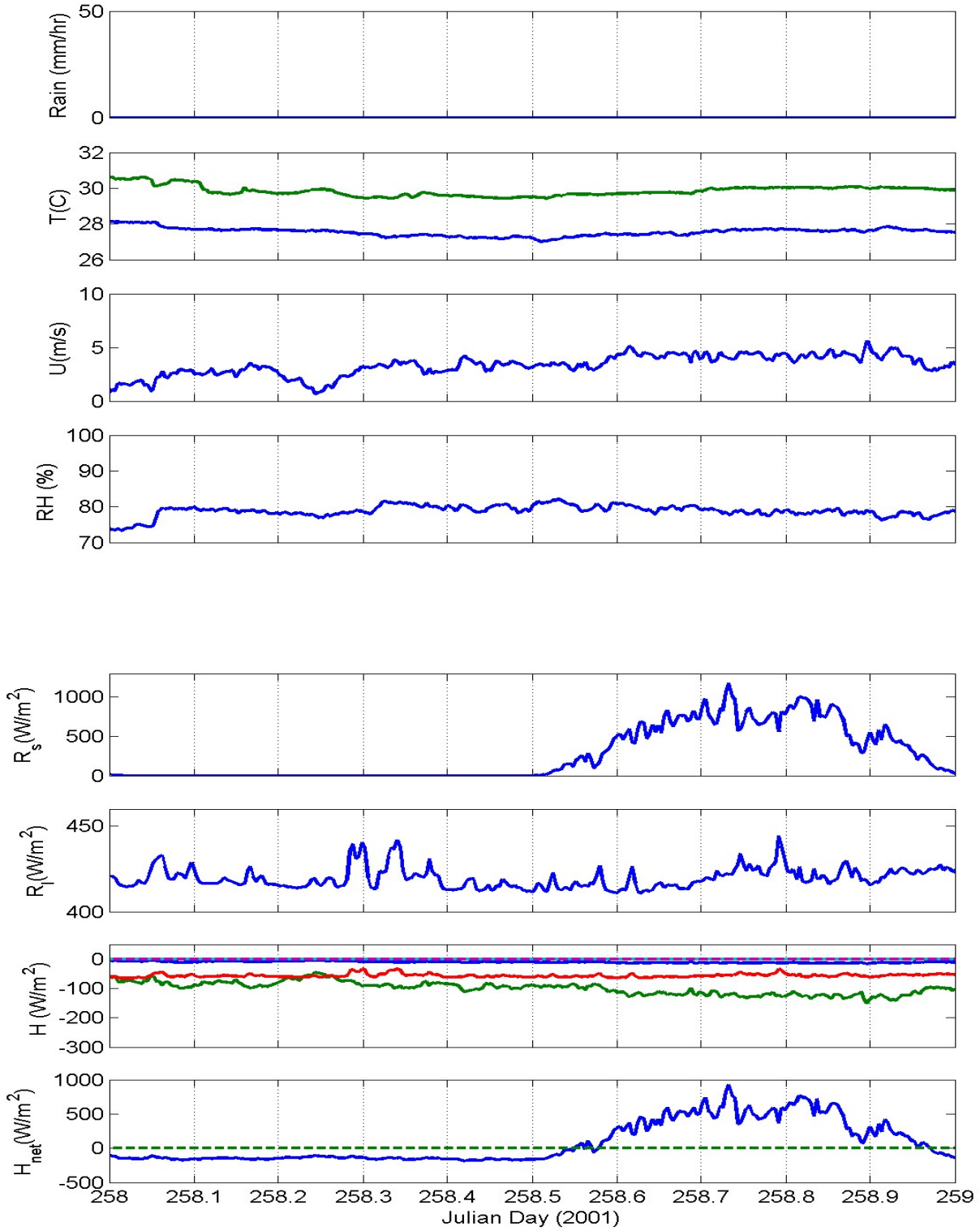

Figure D1. Bulk meteorology and flux variables from a typical clearish day in the tropics. Reading down from the upper panel the variables are: rain rate; water (green line) and air temperature (blue line); wind speed; relative humidity; downward solar flux; downward IR flux; heat flux components [$-H_s$ (blue), $-H_l$,(green), R_{nl} (red), $-H_{rain}$ (cyan)]; and net heat flux.

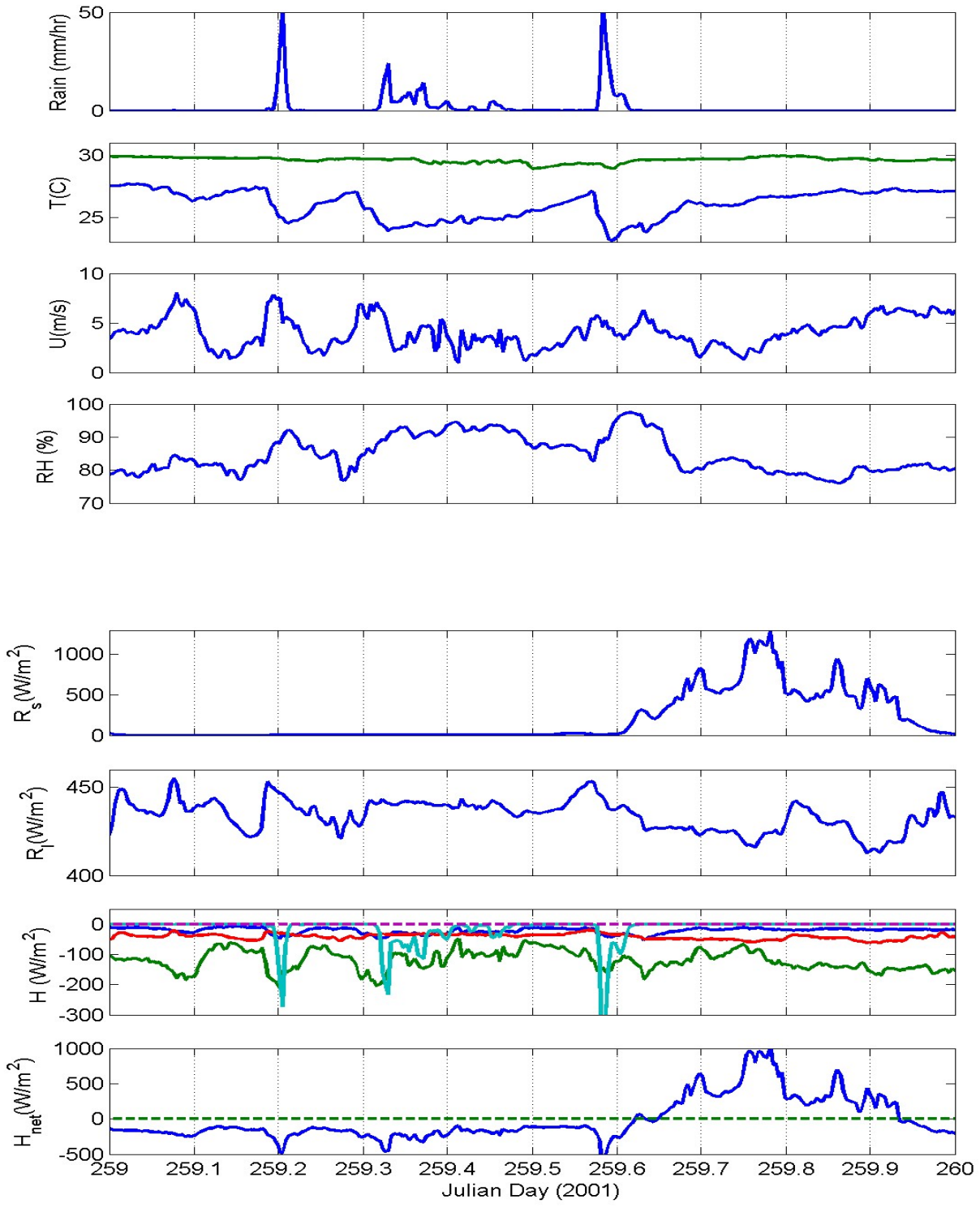

Figure D2. Bulk meteorology and flux variables for a convectively active day in the tropics. Reading down from the upper panel the variables are: rain rate; water (green line) and air temperature (blue line); wind speed; relative humidity; downward solar flux; downward IR flux; heat flux components [$-H_s$ (blue), $-H_l$ (green), R_{nl} (red), $-H_{rain}$ (cyan)]; and net heat flux.

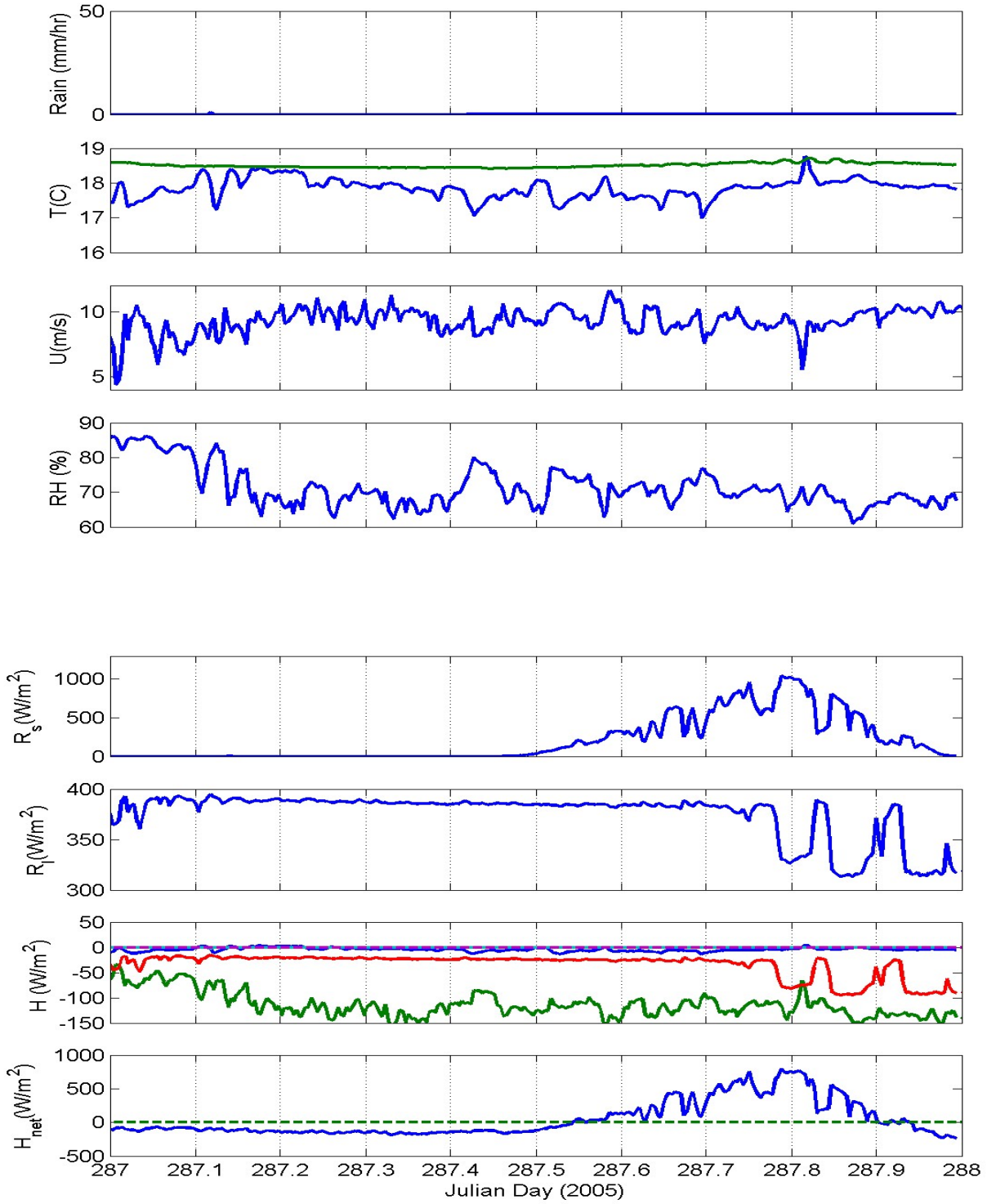

Figure D3. As for Figures D1 and D2, but for a region of ocean with quite different climatology; higher wind speeds, much lower sea and air temperatures, and lower humidity. Reading down from the upper panel the variables are: rain rate; water (green line) and air temperature (blue line); wind speed; relative humidity; downward solar flux; downward IR flux; heat flux components [$-H_s$ (blue), $-H_l$ (green), R_{nl} (red), $-H_{rain}$ (cyan]; and net heat flux.

Appendix E: The Beaufort wind scale

In the early nineteenth century, Admiral Sir Francis Beaufort developed a wind scale based on the behavior of sailing ships (Huler 2004). In 1838, the British Admiralty adopted this scale as a method for unifying the reporting of winds at sea. But not until the early twentieth century did that scale emerge as the descriptive list of wind effects on both land and seat that we now know as the Beaufort Scale (Huler 2004).

The Beaufort number or force B is related to the wind speed (in m s^{-1}) at a standard reference height of 10 m, U_{10}, through (List 1984, p. 119; Strangeways 2001)

$$U_{10} = 0.836 B^{3/2} . \quad \text{(B1.1)}$$

But the key feature of the Beaufort Scale is that it associates U_{10} and B with a description of wind, sea state, and wind effects on land and, thus, provides an estimate of U_{10} from visual observations alone (e.g., Bowditch 1977, p. 1059; List 1984, p. 119).

Table E1. Beaufort Scale, with the associated wind speed ranges for each Beaufort force in meters per second, knots, and miles per hour. $H_{1/3}$ is the significant wave height, the average height of the highest one-third of all waves occurring during a period (Kinsman 1965).

Force	Wind Description	U_{10}			$H_{1/3}$	Over the sea
		(m s^{-1})	(knots)	(mph)	(m)	
0	Calm	0.0–0.2	<1	<1	0	Sea like a mirror
1	Light air	0.3–1.5	1–3	1–3	0.1–0.2	Ripples with appearance of scales; no foam crests
2	Light breeze	1.6–3.3	4–6	4–7	0.3–0.5	Small wavelets; crests have glassy appearance but do not break
3	Gentle breeze	3.4–5.4	7–10	8–12	0.6–1.0	Large wavelets; crests begin to break; scattered whitecaps
4	Moderate breeze	5.5–7.9	11–16	13–18	1.5	Small waves becoming longer; numerous whitecaps
5	Fresh breeze	8.0–10.7	17–21	19–24	2.0	Moderate waves taking longer form; many whitecaps and chance of some spray
6	Strong breeze	10.8–13.8	22–27	25–31	3.5	Large waves forming; white foam crests extensive, and spray probable
7	Moderate gale	13.9–17.1	28–33	32–38	5.0	Sea heaps up, and white foam from breaking waves begins to be blown in streaks; spindrift appears
8	Fresh gale	17.2–20.7	34–40	39–46	7.5	Moderately high waves of greater length; edges of crests break into spindrift; foam is blown in well marked streaks
9	Strong gale	20.8–24.4	41–47	47–54	9.5	High waves; dense streaks of foam; sea begins to roll; spray may reduce visibility
10	Whole gale	24.5–28.4	48–55	55–63	12	Very high waves with overhanging crests; sea surface takes on white appearance as foam in great patches is blown in very dense streaks; rolling sea is heavy; visibility reduced
11	Storm	28.5–32.6	56–63	64–72	15	Exceptionally high waves; sea covered with long white patches of foam; small and medium sized ships might be lost to view behind waves; visibility further reduced
12	Hurricane	>32.7	>64	>73	>15	Air filled with foam and spray; sea completely white with driving spray; visibility greatly reduced

Appendix F – Useful web-sites

http://www.etl.noaa.gov/et6/wgsf/

http://www.gfdi.fsu.edu/SEAFLUX/

http://uop.whoi.edu/projects/projects.htm

http://woodshole.er.usgs.gov/operations/sea-mat/air_sea-html/index.html

http://oaflux.whoi.edu/

http://www.ncdc.noaa.gov/oa/climate/vosclim/vosclim.html

http://woodshole.er.usgs.gov/operations/sea-mat/

http://www.pmel.noaa.gov/home/data.shtml

http://www.ifremer.fr/ird/soopip/

http://www.meteo-technology.com/

http://seaboard.ndbc.noaa.gov/index.shtml

http://daac.gsfc.nasa.gov/CAMPAIGN_DOCS/hydrology/TRMM_analysis.html

http://www.researchvessels.org/

http://las.ngdc.noaa.gov/las/servlets/dataset?catitem=9

Appendix G – Data stewardship example: SAMOS Initiative

F1 Introduction

This appendix contains detailed information on metadata documentation and a sample data format used by the Shipboard Automated Meteorological and Oceanographic System (SAMOS) initiative. The metadata discussion and forms provide a good foundation to the documentation that is necessary to ensure that the meteorological data collected by a ship are useful for climate studies well after they are collected. The data format described, is a prototype and is one of several examples of a well documented format that could be employed.

F2 SAMOS metadata

This section provides guidance on completing the metadata forms (Figures F1, F2) used in the SAMOS initiative. Collecting detailed metadata from participating vessels is essential to achieve the scientific and data stewardship goals outline by the SAMOS initiative. The forms have been designed to be filled out when a vessel is recruited to participate in SAMOS data exchange. These forms could be used by ship operators as a guide to the wide array of metadata that are needed to ensure future applicability of collected observations for climate research.

F2.1 Vessel Metadata

The vessel metadata (Figure F1) is required to uniquely identify the vessel collecting and providing data to the SAMOS Initiative.

Vessel Name†

The registered name of the vessel (e.g., Melville)

Call Sign

Alpha-numeric call sign used to identify the vessel (e.g., WECB).

IMO Number†

The number issued by the International Maritime Organization (e.g. 8717283) to uniquely identify the vessel. This number stays with the vessel even if the name and call sign are changed.

Recruiting Country (if participating in VOS program)†

The International Organization for Standardization (ISO) code for the country whose

Meteorological Service recruited the vessel (This will be a 2-character code, e.g. AU).

Vessel Type

A 2-letter code defining the type of vessel (Appendix 1).

Operating Country

The country operating the research vessel or responsible for installing and maintaining the SAMOS on a merchant vessel.

Home Port (optional)

The home port of the vessel or a commonly visited port, if no home port exists.

Date of Recruitment

Calendar date (YYYYMMDD) when a vessel agrees to participate in the SAMOS data exchange.

Data Reporting Interval

Typical temporal interval (in seconds) between reported values. Ideally the reporting interval should be the same duration for each desired navigation, meteorological, and oceanographic parameter. (e.g., SAMOS seeks 60 second interval, if possible).

Participation in other data exchanges (optional)

The SAMOS initiative would like to know if the vessel is participating in other routine data exchange programs (e.g., VOS, VOSClim, SOOP, ASAP, SEAS, GOSUD, etc.).

F2.2 Contact metadata

The contact metadata (Figure F1) are essential to maintain the open exchange of data, metadata, and data quality information with the vessel and the vessel's home institution. Two-way communication is essential to provide data quality feedback while the vessel is at sea; thus, reliable contact information (emails) is needed either for persons aboard each vessel or at each home institution.

Home Institution

Name and postal address of the institution that operates the vessel. For merchant ships, this would be the name and address of the institution that installs and maintains the SAMOS.

Contact Person

Name, email, phone, and fax for the primary SAMOS data contact at the home institution. This person should have overall knowledge of the SAMOS installation and data management procedures for the vessel. The person will serve as the primary point of contact for the SAMOS data center.

Vessel Home Page (if available)

The URL for the vessel's home page. A link from the SAMOS data center web page will be made to each participating vessel's home page.

Technician Name(s)

Name of marine technician(s) responsible for meteorological data collection and SAMOS service while at sea. For vessels lacking an onboard technician, please fill field with "no tech onboard".

Technician Email(s)

General or specific email address(es) that will allow the SAMOS data center to reach the marine technician while the vessel is at sea. Along with the Alternate Contacts, this (these) email(s) will be used to provide data quality feedback to the vessel while it is underway. This field is only applicable to vessels with onboard technicians.

Alternate contact(s)

Alternate email(s) which will be used for real-time communication with the vessel for the purpose of data quality feedback. Contact points should be decided by vessel operators and could include a generic email for the chief scientist or a contact at the vessel's home institution when no onboard technician is available.

F2.3 Vessel layout

Metadata describing the overall dimensions and design of the vessel (Figure F1) are valuable to the scientific data quality evaluation. Knowing the position of the instruments relative to upstream obstacles to the wind or in relation to the vessel exhaust stack can aid in the identification of suspect data values.

Dimensions†

The dimensions of the vessel expressed in meters to the nearest 1/10 m. These parametersare defined in WMO publication number 47, Annex V:

a. Length

The length over all (LOA) of the vessel (e.g. 94.9 m),

b. Breadth

The molded breadth (beam) of the vessel (e.g. 20.3 m),

c. Freeboard

The average freeboard of the vessel as measured from the maximum summer loadline (e.g. 2.6 m),

d. Draught

The average vertical distance between the vessel's keel and the maximum summer loadline (e.g. 7.9 m),

e. Cargo ht.

The average height of the cargo above the maximum summer load line on the particular route where observations are made (e.g. 6.5 m). If the cargo is below the main deck (e.g. the vessel is traveling in ballast or is a bulk tanker), report the height of the main deck itself. *Note: may not be applicable to research vessels.*

Digital Photography and Vessel Schematics

Digital photos (.jpg format) and scanned schematics (.pdf format) of vessels and/or sensor locations provide a wide range of information for data quality assurance and applications.

Requested photos include (1) a side view of the entire vessel and (2) one or more photos of the masts or sites that house the SAMOS instrumentation. Mast or instrument photos are most useful when taken at a distance sufficient to show the sensor's environment and possible obstacles to air-flow around the sensor.

Desired schematics include a top, side, and bow or stern view of the vessel. Marking the location of the meteorological and oceanographic sensors on the schematics would be helpful, but is not required.

Please send any available digital images or schematics to samos@coaps.fsu.edu and provide the date submitted on the metadata form.

The naming convention† for the digital file(s) is in the following format:

xxxxxxxxxyyyymmddaaa...aaa.jpg where

xxxxxxxxx	IMO number (a nine digit number, include leading zeros if applicable)
yyyymmdd	year, month, day
aaa...aaa	short description of the photo or schematic
Example:	000851245200202 14anemometer_port_side.jpg
	000851245200202 14aft_view_schematic.pdf

Examples of requested files can be viewed on the SAMOS web page under the "digital imagery" button on the metadata portal (http://samos.coaps.fsu.edu/html/meta.php).

F2.4 Data File Specification

SAMOS data exchange is designed around daily email attachments containing the SAMOS observations collected over the previous day. The data file specification (Figure F1) provides information needed by the DAC to uncompress and process each attached file. This specification is designed for SAMOS, but the principles would apply to any data exchange or archiving program. The user must provide a format, version, information on compression, and a provider contact for any files sent to a data or archive center.

File Format

Name of the format used for emailed data file attachments. The format must be self-describing (what variables are where in the file), have a known delimiter between values, and have a known missing value. (E.g., SAMOS data exchange format).

Format Version

Version number of the file format (e.g., 001 for SAMOS format).

File Compression

If files provided to the SAMOS DAC are compressed, please indicate the compression algorithm used (e.g., zip, gzip, etc.)

Email Data Sent From

The email address that originated the SAMOS data message. This is used to verify that the files originate from a known provider.

F2.5 Primary Instrument Metadata

Figure F2 outlines metadata related to the individual parameters typically observed by a SAMOS and would be most relevant to anyone designing an observing system to conduct turbulent flux studies. The information is critical for both the data quality evaluation and for the future scientific application of the data. Gray areas in Figure F2 denote metadata that are not applicable to the listed parameter.

Logging System Name

Name or acronym identifies the combined instrument and data logging system used on the vessel (e.g., NOAA SCS, WHOI IMET).

System Version

Version number of data logging software.

Wind Direction Convention

Identify whether wind direction measurements represent the direction **to** which or **from** which the wind is blowing.

Anemometer Zero-line Reference

The installed orientation of the zero reference on the anemometer compass in degrees measured clockwise from the bow.

0˚ – reference pointed toward bow

90˚ – reference pointed toward starboard

180˚ – reference pointed toward stern

270˚ – reference pointed toward port

Having this reference will aid in the quality control of reported true winds.

Pressure Adjusted to Sea Level

Please state whether or not the measured atmospheric pressure has been adjusted to mean sea level.

Designator for SAMOS

Specific to SAMOS, but shows the importance of a unique way to identify each measured parameter in a data storage format. For SAMOS, a short alphanumeric tag is used to identify the type of data value within each record. For SAMOS version 001 data exchange format (Section F3) this designator appears in each line before the data value. The designator may also be column heading for a fixed format tabular file. Note that the time designator(s) should also be provided (e.g., HMS for hour, minute, seconds; YMD for year, month, day; etc.)

Instrument Make

Manufacturer of the instrument (e.g., R. M. Young).

Instrument Model

Model or series number of instrument (e.g., 5103).

Units

Original units for each parameter (e.g., Deg. +East, knots, ˚C, etc.) SI units are preferred, but as long as the DAC knows the original units, we can convert the values to SI units.

Instrument Location

The instrument locations are defined using a three dimensional set of measurements (to the nearest 1/10 m) that include:

a. **From Bow** - distance from the foremost point of the vessel above the mean water line (bow) back to the instrument on a line parallel to the vessel center line (positive value);

b. **From Center Line** - distance to port (P indicator or negative value) or starboard (S indicator or positive value) on a line perpendicular to the center line;

c. **Height/Depth** - height above (depth below) the mean water line (positive above the water, negative for a depth measurement).

Measured vs. Calculated

An indicator designating that the parameter was either directly measured (M) or was calculated (C) based on other measured parameters. An example of a calculated value is the true winds which must be derived from the vessel-relative winds, course, heading, and speed of the vessel. When possible, please provide (via email or an attached document) the formula used for each calculated value.

Data Averaging

a. **Spot vs. Average Value** – Indicate whether the parameter represents an instantaneous (spot) versus a time averaged value.

b. **Value Time Center** – When the value is time averaged, indicate whether the time stamp associated with the value represents the start, center, or end of the averaging period.

c. **Length** – When the value is time averaged, please provide the length of the averaging period (in seconds)

Sampling Rate

The typical sampling rate from each individual instrument (in Hertz).

Data Precision

The fractional value (decimal) to which the sensor can resolve changes in the measured parameter. This may be the manufacturer's precision, but preferable value would be the expected precision of the instrument as deployed in the field.

Date In or Last Calibration

At the minimum, SAMOS plans to record the installation date or the last date of calibration for each sensor. Please use a YYMMDD format.

Radiation direction convention

For each radiation measurement, indicate whether the sensor is measuring downwelling (dn) or upwelling (up) radiation.

2/2/06 SAMOS Vessel Metadata form Version 01

Vessel Information

Vessel Name	Call Sign	IMO Number	Recruiting Country	Vessel Type

Operating Country	Home Port	Date of Recruitment	Data Reporting Interval (sec.)	Participation in other data exchanges

Contact Information

Home Institution		Aboard Vessel	
Name		Technician Name(s)	
Address		1	2
		Technician Email(s)	
		1	
Contact Person		2	
Name		Alternate Contact email(s)	
Email		1	
Phone	Fax	2	
Vessel Home Page			

Vessel Layout

Dimensions		Digital Imagery and Schematics	Date Submitted
Length	m	Photo – Vessel side view	
Breadth	m	Photo(s) – Instrument Mast(s) / Site(s)	
Freeboard	m	Schematic – Top View	
Draught	m	Schematic – Side View	
Cargo height*	m	Schematic – Bow / Stern View(s)	
*If applicable		Submit electronic imagery to: samos@coaps.fsu.edu	

Data File Specification

File Format	Format Version	File Compression (zip, gzip, etc.)	Email Data Sent From
Submit Files as Email Attachments to: samos_data@coaps.fsu.edu			

Figure F1. Vessel metadata form used in SAMOS initiative.

2/2/06 SAMOS Instrument Metadata form Version 01

Primary Instrument Metadata		Vessel Name		Use this form to provide primary sensor information for each available parameter.
Logging System Name		System Version		
Wind direction convention (to/from)		Anemometer zero-line reference (deg)		Pressure adjusted to sea level (yes/no)	

Parameter	Designator for SAMOS	Instrument		Distance (nearest 0.1 m)				Data Averaging					
		Make	Model	Units	From bow	P/S from center line	Height /depth	Measured/ Calculated	Spot vs. Average Value	Value Time Center	Length (sec)	Sampl-ing rate (Hz)	Data precision (decimal)	Date in/last calibration (YYMMDD)
Time														
Latitude														
Longitude														
Heading														
Course over ground														
Speed over ground														
Speed over water														
Vessel-relative wind direction														
Vessel-relative wind speed														
Earth-relative wind direction														
Earth-relative wind speed														
Atm. pressure														
Air temperature														
Wet-bulb temperature														
Dewpoint temperature														
Relative humidity														
Specific humidity														
Precipitation														
Shortwave radiation (up/dn)														
Longwave radiation (up/dn)														
Visibility														
Ceiling height														
Sea temperature														
Salinity														
Conductivity														

Figure F2. Instrument metadata form used in SAMOS initiative.

F3 SAMOS data format

The important considerations for a data storage format are that it provides unique identifiers for each data element. These identifiers can be in a header line at the top of the file or, in the case of SAMOS, be imbedded within the individual data records. The advantage of the SAMOS format is that data pairs (identifier:value) can drop out when the value is missing. The disadvantage is the repeated identifiers result in longer data lines. Using a header is a good option; however, when a data value is missing, a place holder (missing value) must exist in the data record or the format will be difficult if not impossible for a computer to read.

F3.1 SAMOS requirements for all data

1. Observation times must be reported in the Universal Time Coordinate (UTC)
2. Time format: YYYYMMDDhhmmss (We recommend a 4 digit year and a yr, mon, day order for the date. Date and time portions can be separated as long as unique designators are used, e.g., YMD and HMS.)

3. Original units must be supplied (SI units preferred). It is important to include latitude and longitude (e.g., +E, -W) and wind direction (to which, from which wind is blowing) conventions.

2. SAMOS data exchange format

The exchange format uses two separators, one between tagged pairs "," and one between the designator and the data value ":". Each tagged pair consists of an alphanumeric designator and the data value associated with the designator. An example of the format:

$SAMOS:001,CS:KAOU,YMD:20030907,HMS:000011,AT:17.40,BP:1010.27,…,

WSP:5.6,WDP:354.4,TWP:5.4,TIP:278.3,WSS:6.7,WDS:350.5,TWS:6.6,TIS:274.4,...,

LA:44.66956,LO:-130.35859,COG:149.5,SOG:0.9,GY:284.7,CS8:23

- Note 1: The format is designed to have all values for a single observation time (YMD, HMS) in a single line. The line breaks in the example are just to improve readability in this document.
- Note 2: The $SAMOS:001 represents the first version of the SAMOS data format. In the future, additional format designators and versions are possible.
- Note 3: The $SAMOS:001 tagged pair is followed with the ship call sign pair (CS:call_sign). Beyond these first two tagged pairs, the order of the data does not matter as the designators uniquely identify each tagged pair and their data values.
- Note 4: Each institute can decide whether or not to include an 8 bit checksum for each line in the file (at the end of each line). If you do plan to have a CS8, please provide us with details on how the number is calculated so we can decode the value.

References

Andreas, E.L., 2005

Beljaars, A. C. M., and A. A. M. Holtslag, 1991: Flux parameterization over land surfaces for atmospheric models. *J. Appl. Meteor.*, **30**, 327-341.

Bohren, C. F., and B. A. Albrecht, 1998: *Atmospheric Thermodynamics*. Oxford University Press, 402 pp.

Bowditch, N., 1977: *American Practical Navigator.* Vol. 1. Publication No. 9, Defense Mapping Agency Hydrographic Center, Washington, D.C., 1386 pp.

Bradley, E. F., P. A. Coppin, and J. S. Godfrey, 1991: Measurements of sensible and latent heat flux in the western tropical Pacific Ocean, *J. Geophys. Res.*, **96**, 3375-3389

Brunt, D., 1932: Notes on radiation in the atmosphere. *Quart. J. Roy. Meteor. Soc.*, **58**, 389-420.

Buck, A. L., 1981: New equations for computing vapor pressure and enhancement factor. *J. Appl. Meteor.*, **20**, 1527–1532.

Businger, J. A., J. C. Wyngaard, Y. Izumi, and E. F. Bradley, 1971: Flux profile relationships in the atmospheric surface layer, *J. Atmos. Sci.* **28**, 181-189.

Caldwell, D.R. and W.P. Elliott, 1971: Surface stresses produced by rainfall. *J. Phys. Oceanog.*, **1**, 145-148

Charnock, H., 1955: Wind stress on a water surface. *Quart. J. Roy.Meteor. Soc.,* **81,** 639–640.

Charnock, H., 1958: A note on empirical wind-wave formulae. *Quart. J. Roy.Meteor. Soc.,* **84,** 443–447

COAPS, 2003. Report 03-0? 1st Workshop on High Resolution Marine Meteorology, ??? March 2003, Shawn R. Smith (Ed.), Centre for Ocean-Atmosphere Prediction Studies, Florida State University, Tallahassee, FL, 32306, USA.

COAPS, 2004. Report 04-01 2nd Workshop on High Resolution Marine Meteorology, 14-15 April 2004, Silver Spring, MD, USA, Shawn R. Smith (Ed.), Centre for Ocean-Atmosphere Prediction Studies, Florida State University, Tallahassee, FL, 32306, USA.

Deardorff, J.W, 1970: Convective velocity and temperature scale for the unstable planetary boundary layer and for Rayleigh convection. *J. Atmos. Sci.* **27**, 1211.

DeCosmo, J., K. B. Katsaros, S. D. Smith, R. J. Anderson, W. A. Oost, K. Bumke, and H.Chadwick, 1996: Air-sea exchange of water vapor and sensible heat: The HumidityExchange Over the Sea (HEXOS) results. *J. Geophys. Res.*, **101**, 12001-12016.

Drennan , W.M., P.K. Taylor, and M.J. Yelland, 2005: Parameterizing the sea surface roughness. J. Phys. Oceanog., **35,** 835-848.

Fairall, C.W., E.F. Bradley, J.S. Godfrey, G.A. Wick, J.B. Edson, and G.S. Young, 1996a: The cool skin and the warm layer in bulk flux calculations. *J. Geophys. Res*., **101**, 1295-1308.

Fairall, C.W., E.F. Bradley, D.P. Rogers, J.B. Edson, G.S. Young, 1996b: Bulk parameterization of air-sea fluxes for TOGA COARE. *J. Geophys. Res.,* **101**, 3747-3764.

Fairall, C.W., A.B. White, J.B. Edson, and J.E. Hare, 1997: Integrated shipboard measurements of the marine boundary layer. *J. Atmos. Oceanic Tech.,* **14**, 338-359.

Fairall, C. W., P. O. G. Persson, E. F. Bradley, R. E. Payne, and S. Anderson, 1998: A new look at calibration and use of Eppley Precision Infrared radiometers: Part I theory and application. *J. Atmos. Oceanic Tech*., **15**, 1230-1243.

Fairall, C. W., E. F. Bradley, J. E. Hare, A. A. Grachev, and J. B. Edson, 2003: Bulk parameterization of air-sea fluxes: Updates and verification for the COARE Algorithm. *J. Clim.*, **16**, 571-591.

Fairall, C. W., J. E. Hare, A. A. Grachev, E. F. Bradley, and J. B. Edson, 2001: Preliminary results from the ETL open ocean air-sea flux database. *Proc. 11th Conf. On Interaction of the Sea and Air.* AMS. San Diego, CA, 14-18 May, 5-8.

Garratt, J. R., 1992: *The Atmospheric Boundary Layer.* Cambridge University Press, Cambridge, Mass., 316 pp.

Godfrey, J. S., and A. C. M. Beljaars, 1991: On the turbulent fluxes of buoyancy, heat, and moisture at the air-sea interface at low wind speeds. *J. Geophys. Res.*, *96*, 22,043-22,048.

Gosnell, R., C.W. Fairall and P.J. Webster, 1995: The sensible heat of rainfall in the tropical ocean. *J. Geophys. Res.*, **100**, 18437-18442

Grachev, A.A., and C.W. Fairall, 1997: Dependence of the Monin-Obukhov stability parameter on the bulk Richardson number over the ocean. *J. Appl. Meteorol.*, **36**, 406-414.

Grachev, A. A., C. W. Fairall, and E. F. Bradley, 2000: Convective profile constants revisited. *Bound.-Layer Meteorol*., **94**, 495-515.

Hare, J. E., P. O. G. Persson, C. W. Fairall, and J. B. Edson, 1999: Behavior of Charnock's relationship for high wind conditions. *Proc. 13th Symposium of Boundary Layers and Turbulence.* AMS. Dallas, TX, Jan. 15-20, paper 5B.8.

Hare, J. E., C. Fairall, T. Uttal, D. Hazen, M.F. Cronin, N. Bond, and D. Veron, 2005: Cloud, radiation, and surface forcing in the equatorial eastern Pacific. *NOAA Technical Memorandum OAR PSD-307.* US Dept. of Commerce, 59 pp.

Hasse, L., M. Grossklaus, K. Uhlg and P. Timm, 1998: A ship raingauge for use in high winds. *J. Atmos. Oceanic. Tech.*, **15**, 380-386.

Huler, S., 2004: *Defining the Wind.* Three Rivers Press, 290 pp.

Kinsman, B., 1965: *Wind Waves.* Prentice-Hall, 676 pp.

Kraus, E. B. and J. A. Businger, 1994: *Atmosphere-Ocean Interaction*. Oxford University Press, New York, NY. 352 pp.

Large, W.G. and S. Pond, 1982: Sensible and latent heat flux measurements over the ocean. *J. Phys. Oceanog.*, **12**, 464-482

Liu, W. T., K. B. Katsaros, and J. A. Businger, 1979: Bulk parameterization of the air-sea exchange of heat and water vapor including the molecular constraints at the interface. *J. Atmos. Sci*., **36**, 2052-2062.

List, R. J., 1984: *Smithsonian Meteorological Tables*. Sixth ed. Smithsonian Institution Press, 527 pp.

Minnett, P. J., K. A. Maillet, J. A. Hanafin and B. J. Osborne. 2005: Infrared Interferometric Measurements of the Near-Surface Air Temperature over the Oceans. *J. Atmos. Oceanic Tech.*, **22**, 1019–1032.

Oost, W. A., G. J. Komen, C. M. J. Jacobs, and C. van Oort, 2002: New evidence for a relation between wind stress and wave age from measurements during ASGAMAGE. *Boundary-Layer Meteorol.*, **103**, 409-438.

Persson, O. G. P., C. W. Fairall, E. L Andreas, P. S. Guest, and D.K. Perovich, 2002: Measurements near the Atmospheric Surface Flux Group tower at SHEBA: Near-surface conditions and surface energy budget. *J. Geophys. Res.,* **107**, 8045.

Price, J.F., R.A. Weller and R. Pinkel, 1986: Diurnal cycling: observations and models of the upper ocean response to diurnal heating, cooling and wind mixing. *J. Geophys. Res*., **91**, 8411-8427.

Smith, S. D., 1980: Wind stress and heat flux over the ocean in gale force winds. *J. Phys. Oceanogr*., **10**, 709-726.

Smith, S. D., 1988: Coefficients for sea surface wind stress, heat flux, and wind profiles as a function of wind speed and temperature. *J. Geophys. Res.*, **93**, 15,467-15,472.

Smith, S. D., 1989: Water vapor flux at the sea surface. *Boundary-Layer Meteorol.*, **47**, 277-293.

Smith, S.R, M.A. Bourassa, and R.J. Sharpe, 1999: Establishing more truth in true winds. *J. Atmos. Oceanic Tech.*, **16**, 939-952.

Strangeways, I., 2001: Back to basics: The 'met enclosure:' Part 6–Wind. *Weather*, **56**, 154–161.

Taylor, P. K., and M. A. Yelland, 2001: The dependence of sea surface roughness on the height and steepness of the waves. *J. Phys. Oceanogr*., **31**, 572-590.

WCRP, 1985: Scientific Plan for the Tropical Ocean and Global Atmosphere Programme. WCRP Publications Series, No. 3, WMO Tech. Doc. 64, Geneva, 146pp.

WCRP, 1989: WOCE Surface Flux Determinations – A strategy for in situ measurements. Working Group on *in situ* measurements for Fluxes WCRP-23 (WMO/TD No.304), WMO, Geneva.

WCRP, 2000: World Climate Research Programme, Final report of the Joint WCRP/SCOR Working Group on Air-Sea Fluxes (SCOR Working Group 110): Intercomparison and Validation of Ocean-Atmosphere Energy Flux Fields. WCRP-112, WMO/TD-No. 1036, Case Postale No. 2300, CH-1211 Geneva 2, Switzerland. 362 pp.

WCRP, 2001: World Climate Research Programme, Proceedings of the Workshop on Intercomparison and Validation of Ocean-Atmosphere Flux Fields, Potomac, MD, USA, 21-24 May 2001. WCRP-115, WMO/TD-No. 1083, Case Postale No. 2300, CH-1211 Geneva 2, Switzerland. 362pp.

Webb, E. K., G. I. Pearman, and R. Leuning, 1980: Correction of flux measurements for density effects due to heat and water vapour transfer. *Q. J. Roy. Met. Soc.*, **106**, 85-100.

Webster, P.J., and R. Lukas, 1992: TOGA-COARE: The Coupled Ocean-Atmosphere Response Experiment. *Bull. Amer. Meteor. Soc.*, **73**, 1377-1416.

Weller, R.A., E.F. Bradley, and R. Lukas, 2004: The Interface or Air-Sea Flux Component of the TOGA Coupled Ocean-Atmosphere Response Experiment and its Impact on Subsequent Air-Sea Interaction Studies. *J. Atmos. Oceanic Tech.*, **21**, 223-257.

Wick, Gary A., J. Carter Ohlmann, Christopher W. Fairall, and Andrew T. Jessup, 2005: Improved oceanic cool-skin corrections using a refined solar penetration model. *J. Phys. Oceanogr.*, **35**, 1986-1996.

Yelland, M. J., B. I. Moat, P. K. Taylor, R. W. Pascal, J. Hutchings and V. C. Cornell, 1998: Wind stress measurements from the open ocean corrected for air flow distortion by the ship. Journal of Physical Oceanography, 28 (7), 1511 - 1526.

Bibliography (some topics to be populated)

Applications

Atmospheric boundary layer and structure

Businger, J. A., J. C. Wyngaard, Y. Izumi, and E. F. Bradley, 1971: Flux profile relationships in the atmospheric surface layer, *J. Atmos. Sci.* 28, 181-189.

Edson, J. B., C. W. Fairall, P. G. Mestayer, and S. E. Larsen, 1991: A study of the inertial-dissipation method for computing air-sea fluxes, *J. Geophys. Res.*, 96, 10,689-10,711.

Edson, J.B., A. A. Hinton, K. E. Prada, J.E. Hare, and C.W. Fairall, 1998: Direct covariance flux estimates from moving platforms at sea. *J. Atmos. Oceanic Tech.*, 15, 547-562.

Garratt, J. R., 1992: *The Atmospheric Boundary Layer.* Cambridge University Press, Cambridge, Mass., 316 pp.

Grachev, A.A., and C.W. Fairall, 1997: Dependence of the Monin-Obukhov stability parameter on the bulk Richardson number over the ocean. *J. Appl. Meteorol.*, **36**, 406-414.

Kraus, E. B. and J. A. Businger, 1994: *Atmosphere-Ocean Interaction*. Oxford University Press, New York, NY. 352 pp.

Webb, E. K., G. I. Pearman, and R. Leuning, 1980: Correction of flux measurements for density effects due to heat and water vapour transfer. *Q. J. Roy. Met. Soc.*, **106**, 85-100.

Bulk algorithms

Beljaars, A. C. M., 1994: The parameterization of surface fluxes in large-scale models under free convection. *Quart. J. Roy. Met. Soc.*, **121**, 255-270.

Blanc, T. V., 1985: Variation of bulk-derived surface flux, stability, and roughness results due to the use of different transfer coefficient schemes, *J. Phys. Oceanogr.*, **15**, 650-669.

Brunke, M. A., C W. Fairall, and X. Zeng, 2003: Which bulk aerodynamic algorithms are least problematic in computing ocean surface turbulent fluxes? *J. Clim*., **16**, 619-635.

Fairall, C.W., E.F. Bradley, D.P. Rogers, J.B. Edson, G.S. Young, 1996: Bulk parameterization of air-sea fluxes for TOGA COARE. J. Geophys. Res. 101, 3747-3764.

Fairall, C. W., E. F. Bradley, J. E. Hare, A. A. Grachev, and J. B. Edson, 2003: Bulk parameterization of air-sea fluxes: Updates and verification for the COARE Algorithm. *J. Clim.*, **16**, 571-591.

Corrections to ship observations, and quality control

Berry, D. I. and E. C. Kent, 2005: The Effect of Instrument Exposure on Marine Air Temperatures: An Assessment Using VOSClim Data. *International Journal of Climatology.* **25**, 1007-1022.

Berry, D. I., E. C. Kent and P. K. Taylor, 2004: An analytical model of heating errors in marine air temperatures from ships. J. Atmos. Ocean. Tech., 21(8), 1198 - 1215.

Bourassa, M. A., D. M. Legler, J. J. O'Brien, and S. R. Smith, 2003: SeaWinds Validation with Research Vessels, J. Geophys. Res., 108, DOI 10.1029/2001JC001081

Dobson, F. W., 1981: Review of Reference Height for and Averaging Time of Surface Wind Measurements at Sea, Marine Meteorology and Related Oceanographic Activities Report No. 25, WMO, Geneva, 64 pp.

Kent, E. C., and D. I. Berry, 2005: Quantifying random measurement errors in Voluntary Observing Ships meteorological observations. Int. J. Climatol., 25(7), 843-856.

Kent, E. C. and P. G. Challenor, 2006: Towards estimating climatic trends in SST data, part 2: Random errors. *J. Atmos. Oceanic Technol.*, in press.

Kent, E. C. and A. Kaplan, 2006: Towards estimating climatic trends in SST data, part 3: Systematic errors. *J. Atmos. Oceanic Technol.*, in press.

Kent, E. C. and P. K. Taylor, 2006: Towards estimating climatic trends in SST data, part 1: Methods of measurement. *J. Atmos. Oceanic Technol*., in press.

Kent, E. C., P. K. Taylor and P. G. Challenor, 1998: A comparison of ship and scatterometer-derived wind speed data in open ocean and coastal areas. *Int. J. Remote Sensing*, **19**, 3361-3381.

Kent, E. C., P. K. Taylor, B. S. Truscott and J. S. Hopkins, 1993a: The accuracy of voluntary observing ship's meteorological observations - Results of the VSOP-NA. *J. Atmos. Oceanic Technol.*, 10(4), 591-608.

Kent, E. C., S. D. Woodruff and D. I. Berry, 2006: WMO Publication No. 47 Metadata and an Assessment of Voluntary Observing Ships Observation Heights in ICOADS. Submitted to the Journal of Atmospheric and Oceanic Technology.

Met Office, 1995: Marine Observers Handbook. Met. O. 1016, Eleventh Edition, HMSO, 227pp.

Moat, B. I., M. J. Yelland, R. W. Pascal and A. F. Molland, 2005: An overview of the airflow distortion at anemometer sites on ships. *Int. J. Climatol.*, **25**, 997-1006, DOI: 10.1002/joc.1177.

Moat, B. I., M. J. Yelland, R. W. Pascal and A. F. Molland, 2006a: Quantifying the airflow distortion over merchant ships, part I: validation of a CFD model. *J. Atmos. Oceanic Technol.*, in press.

Moat, B. I., M. J. Yelland and A. F. Molland, 2006b: Quantifying the airflow distortion over merchant ships, part II: application of model results. *J. Atmos. Oceanic Technol.*, in press.

Smith, S. R., M. A. Bourassa and R. J. Sharp, 1999: Establishing more truth in true winds. *J. Atmos. Oceanic Technol.*.**16**, 939–952.

Yelland, M. J., B. I. Moat, P. K. Taylor, R. W. Pascal, J. Hutchings and V. C. Cornell, 1998: Wind stress measurements from the open ocean corrected for air flow distortion by the ship. *Journal of Physical Oceanography*, **28**, 1511 - 1526.

Yelland, M. J., B. I. Moat, R. W. Pascal and D. I Berry, 2002: CFD model estimates of the airflow distortion over research ships and the impact on momentum flux measurements. J. Atmos. & Oceanic Tech., 19 (10), 1477-1499.

Field Campaigns (BAMS descriptions)

Curry, J. A., and 18 coauthors, 2004: SEAFLUX. *Bull. Am. Met. Soc.,* **85**, 409-424.

Persson, P. O. G., J. E. Hare, C. W. Fairall, W. D. Otto, 2005: Air-sea interaction processes in warm and cold sectors of extratropical cyclonic storms observed during FASTEX. Q. *J. Roy. Met. Soc.*, **131**, 877-912.

Yu, L., R. A. Weller, and B. Sun, 2004: Mean and variability of the WHOI daily latent and sensible heat fluxes at in situ flux measurement sites in the Atlantic Ocean. J. Clim. In press.

Flux measurement

Finkelstein, P. L., and P. F. Sims, 2001: Sampling error in eddy correlation flux measurements. *J.Geophys. Res.*, **106**, 3503-3509.

Godfrey, J. S., and A. C. M. Beljaars, 1991: On the turbulent fluxes of buoyancy, heat, and moisture at the air-sea interface at low wind speeds. *J. Geophys. Res.*, *96*, 22,043-22,048.

Gosnell, R., P.J. Webster, and C.W. Fairall, 1995: The sensible heat flux due to rain in TOGA COARE. *J. Geophys. Res.*,**100**, 1843718442.

Smith, S. D., 1988: Coefficients for sea surface wind stress, heat flux, and wind profiles as a function of wind speed and temperature. *J. Geophys. Res.*, **93**, 15,467-15,472.

Smith, S. D., C. W. Fairall, G. L. Geernaert, and L. Hasse, 1996: Air-sea fluxes: 25 years of progress. *Bound.-Layer Meteorol.*, **78**, 247-290.

Taylor, P. K., and M. A. Yelland, 2001: The dependence of sea surface roughness on the height and steepness of the waves. *J. Phys. Oceanogr.*, **31**, 572-590.

Yelland, M. and P. K. Taylor, 1996: Wind stress measurements from the open ocean. *J. Phys. Oceanogr.*, **26**, 541-558.

Yelland, M., B. I. Moat, P. K. Taylor, R. W. Pascal, J. Hutchings, and V. C. Cornell, 1998: Measurements of the open ocean drag coefficient corrected for air flow disturbance by the ship. *J. Phys. Oceanogr.*, **28**, 1511-1526.

Instrument and data comparisons

Burns, Sean P. and 13 coauthors, 1999: Comparisons of aircraft, ship, and buoy meteorological measurements from TOGA COARE. *J. Geophys. Res.*, **104**, 30853-30884.

Burns, Sean P. and 14 coauthors, 2000: Comparisons of aircraft, ship, and buoy radiation and SST measurements from TOGA COARE. *J. Geophys. Res.*, **105**, 15627-15652.

Cronin, M., C. W. Fairall, and M. J. McPhaden, 2006: Accuracy of buoy-derived and NWP surface heat fluxes in the Tropical Pacific. *J. Geophys. Res.*, accepted.

Gulev, S. K., D. Cotton, and A. Sterl, 1998: Intercomparison of the North Atlantic wave

climatology from voluntary observing ships, satellite data, and modelling. *Phys. Chem.*

Earth, **23**, 587-592.

Oncley, S. P., L. K. Kristensen, J. Mann, and J. C. Wyngaard, 1997: How close is close enough when measuring scalar fluxes with displaced sensors. *J. Atmos. Oceanic Tech.*,

Smith, S.R., D. M. Legler, K. V. Verzone, 2001: Quantifying uncertainties in NCEP reanalyses using high-quality research vessel observations. J. Climate 14 (20): 4062-4072.

Sun, B., L. Yu, and R. A. Weller, 2003: Comparisons of surface meteorology and turbulent heat fluxes over the Atlantic: NWP model analyses versus moored buoy observations. J. Clim., 16, 679-695.

Sea surface temperature and ocean mixing

Donlon, C. J., P. Minnett, C. Gentemann, T. J. Nightingale, I. J. Barton, B. Ward and J. Murray, 2002: Towards improved validation of satellite sea surface skin temperature measurements for climate research. *J. Clim.*, **15**, 353-369.

Fairall, C.W., E.F. Bradley, J.S. Godfrey, G.A. Wick, J.B. Edson, and G.S. Young, 1996a: The cool skin and the warm layer in bulk flux calculations. *J. Geophys. Res*., **101**, 1295-1308.

Price, J.F., R.A. Weller and R. Pinkel, 1986: Diurnal cycling: observations and models of the upper ocean response to diurnal heating, cooling and wind mixing. *J. Geophys. Res*., **91**, 8411-8427.

Webster, P. J., C. A. Clayson, and J. A. Curry, .1996: Clouds, radiation and the diurnal cycle of sea surface temperature in the tropical Western Pacific. *J. Clim*., **9**, 1712-1730.

Wick, Gary A., J. Carter Ohlmann, Christopher W. Fairall, and Andrew T. Jessup, 2005: Improved oceanic cool-skin corrections using a refined solar penetration model. *J. Phys. Oceanogr.*, **35**, 1986-1996.

Technology (e.g. JTech articles)

Fairall, C.W., A.B. White, J.B. Edson, and J.E. Hare, 1997: Integrated shipboard measurements of the marine boundary layer. *J. Atmos. Oceanic Tech.,* **14**, 338-359.

Fairall, C. W., O.P.G. Persson, R. E. Payne, and E. F. Bradley, 1998: A new look at calibration and use of Eppley precision infrared radiometers. *J. Atmos. Oceanic Tech.*, **15**, 1230-1243.

Kent, E. C. and P. K. Taylor, 1997: Choice of a Beaufort Equivalent Scale. J. Atmos. Oceanic Technol., 14(2), 228-242.

Payne, R.E., 2002: Recognising problems in shipboard logging meteorology systems. Woods Hole Oceanog. Inst. Tech. Rept. WHOI-2002-05, Woods Hole, MA 02543, USA

Tanner, C. B. and G. W. Thurtell, 1969: Anemoclinometer measurements of Reynolds stress and heat transport in then atmospheric surface layer. University of Wisconsin Technical Report ECOM-66-G22-F, 82pp. [Available from US Army Electronic Command, Atmospheric Sciences Laboratory, Ft. Huachuca, AZ 85613.]

Glossary of meteorological and oceanographic terms and Acronyms